Republic of Iraq

Ministry of Higher Education

and Scientific Research

University of Babylon

College of Engineering

Design and Performance Analysis of Orthogonal Time Frequency Space in Communication Networks

A Thesis

Submitted to the College of Engineering\ University of Babylon in Partial Fulfillment of the Requirements for the Degree of Doctorate Ph.D. of Science in Electrical Engineering\ Electronic & Communication.

By

Musaddak Maher Abdul Zahra

Supervised by

Prof. Dr. Laith Ali Abdul Rahaim

2023 A.D **1444 A.H**

بِسْمِ اللَّهِ الرَّحْمَنِ الرَّحِيمِ

﴿يَرْفَعِ اللَّهُ الَّذِينَ آمَنُوا مِنْكُمْ وَ
الَّذِينَ
أُوتُوا الْعِلْمَ دَرَجَاتٍ وَاللَّهُ بِمَا تَ
عْمَلُونَ خَبِيرٌ﴾

(صَدَقَ اللَّهُ الْعَلِيّ الْعَظِيم)

سورة المجادلة/ الأية (11)

DEDICATION

To My Father and Mother

To My Supervisor

To My family

To My friends

Abstract

The wireless communication system is called the core of the Internet managing networks for telecommunications. For growing transmitting capability over fixed bandwidth, there are many potential techniques that had been developed in the recent years. One of the most effective methods that can offer achieving more information is orthogonal frequency division multiplexing (OFDM). From other side, using massive multi-input multi-output (massive MIMO) techniques in the modern wireless transmission links offers highest performance and best spectral efficiency among all the recent techniques.

On the other hand, one of the most attractive modern modulation techniques is orthogonal time frequency space (OTFS) technology which is considered as a new modulation's generation that overcome the challenges of fifth generation (5G).

In this thesis, three main complementary systems had been proposed. The first designed simulation is massive MIMO (mMIMO-OTFS) system between user and base station based on OTFS modulation system for both uplink and downlink scenarios.

The system performance for massive MIMO-OTFS system shows a great advantages among ordinary MIMO systems by achieving better spectral efficiency and energy efficiency of the designed systems. By using 256 subcarrier OTFS system, the best achieved transmission rate achieved for both uplink and downlink scenarios with acceptable bit error rate (BER) of around (10^{-5}). A second system of powerful simulation framework for a backhaul RoF-MMW optical transmission system had been designed between main base station and remote antenna unit based on multi-carrier OFDM modulation.

The powerful simulation of beyond 5G optical MC-OFDM transportation along radio over fiber-mille meter wave (RoF-mmW) long transmission system had been successfully implemented.

By using 50 Gb/s default bit rate and 128 QAM (quadrature amplitude modulation) format for OFDM-RoF-MMW system along 50 km, the best achievement of overall bit rate obtained (11.2 Tb/s) with accepted BER to get ultra-high-capacity transmission system. By using python DSP and the losses compensators used in the simulation framework, the peak average power ratio (PAPR) losses and drift in the receiver section had been compensated and many values of OFDM carriers (16, and 32 OFDM carriers) achieved for ultra-high-capacity transmission system.

Then, the powerful simulation of next generation all optical-OFDM (AO OFDM) transmission system had been implemented by using optical FFT based on MMI couplers to achieve highest capacity transmission system. A successful transmission of 16 AO-OFDM had been achieved with an ultra-high capacity system with a long distance reach to (1000 Km). While a distance reach to (480 Km) achieved for 32 OA OFDM.

The optimum input power for 16 AO OFDM system to give less symbol error rate (SER) is (-8 dBm) and the optimum input power for 32 AO OFDM system is (-4 dBm). The total achieved data rate from 16 AO OFDM system is 32 Tb/s and the total achieved data rate from 32 AO OFDM is approximately 64 Tb/s which is considered as the best achieved transmission capacity system among all recent works. The combination between massive MIMO techniques and backhaul RoF-MMW systems offers a new generation for ultra-high-capacity communication systems with best performance among the recent developed systems.

List of Abbreviations

3GPP	Third Generation Partnership Project
3D	Three Dimension
3D-SOMP	Three Dimension Sparse Orthogonal Matching Pursuit
4G	Fourth Generation
5G	Fifth Generation
ADC	Analogue to Digital Converter
AWG	Array Waveguide Grating
AWGN	Additive White Gaussian Noise
ASE	Amplified Spontaneous Emission
BS	Base Station
BER	Bit Error Rate
B5G	Beyond 5G
B-SMF	Bundled-Single Mode Fiber
BPSK	Binary Phase Shift Keying
CD	Chromatic Dispersion
CS	Compressed Sensing
CSI	Channel State Information
CP	Cyclic Prefix
CMA	Constant Modulus Algorithm
CDM	Code Division Multiplexing
DA-LMS	Data-Aided Least-Mean-Square
DD-LMS	Decision-Directed Least-Mean-Square (LMS)
DEMUX	Demultiplexer
DFL	Distributed Feedback Laser
DFT	Discrete Forrier Transform
DP	Dual Polarized
DD	Delay Doppler
DD-MZM	Dual-Drive Mach–Zehnder Modulation
DP-MZM	Dual-Parallel Mach–Zehnder modulation
DSP	Digital Signal Processing
DWDM	Dense Wavelength Division Multiplexing
DPP	Dirty Paper Precoding
EDFA	Erbium-Doped Fiber Amplifier
FDM	Frequency Division Multiplexing
FF	Far-Field
FFT	Fast Fourier Transform
FMF	Few-Mode Fiber
FWM	Four Wave Mixing
FPR	Free Propagation Range

FSR	Free Spectral Range
GPS	Global Positioning System
GM-LAMP	Gaussian Mixture Approximate Message Passing Learned
GI	Guard Interval
HF	Hybrid Field
IEEE	Institute of Electrical and Electronics Engineers
IFFT	Inverse Fast Fourier Transform
ISI	Inter-Symbol Interference
IMDD	Intensity-Modulated Direct Detection
LO	Local Oscillator
NMSE	Normalized Mean Square Error
NF	Near Field
MZM	Mach–Zehnder Modulation
MCF	Multi-Core Fiber
MDM	Mode Division Multiplexing
MIMO	Multiple-Input-Multiple-Output
MMA	Multiple Modulus Algorithm
MMF	Multi-Mode Fiber
MUX	Multiplexer
MMW	Milli-Meter Wave
MMSE	Maximum Mean Square Error
MU MIMO	Multi User Multiple Input Multiple Output
MRC	Maximal Ratio Combining
MLP	Multi-Layered Perceptron
MISO	Multi Input Single Output
MSP	Modified Subspace Pursuit
MSMCE	Modified-Sensing-Matrix-Based Channel Estimation
mMIMO	Massive Multi-Input Multi-Output
OSNR	Optical Signal-to-Noise Ratio
OFDM	Orthogonal Frequency Division Multiplexing
OTFS	Orthogonal Time Frequency Space
OMP	Orthogonal Matching Pursuit
OSTBC	Orthogonal Space Time Block Code
PAPR	Peak to Average Power Ratio
PD	Photo Diode
PDM	Polarization Division Multiplexing
PSK	Phase Shift Keying
PON	Passive Optical Networks
QoS	Quality of Service
RAU	Remote Antenna Unit

RoF	Radio over Fiber
RF	Radio Frequency
LAN	Local Area Networks
LTE	Long-Term Evolution
LTE-A	Long-Term Evolution Advanced
QAM	Quadrature Amplitude Modulation
QPSK	Quadrature Phase Shift Keying
SDM	Space Division Multiplexing
SNR	Signal-to-Noise Ratio
SMF	Single-Mode Fiber
SISO	Single Input Single Output
SIMO	Single Input Multiple Outputs
SSMF	Standard Single Mode Fiber
TDE	Time Domain Equalizer
TDM	Time Division Multiplexing
UWB	Ultra-Wide Bands
UE	User Equipment
VP	Vector Perturbation
WDM	Wavelength Division Multiplexing
WLAN	Wireless Local Area Network
XL-mMIMO	Extreme Large massive MIMO
ZF	Zero Forcing

List of Tables

List of Figures

List of Contents

f_k	Frequency of the kth subcarrier
F_0	Frequency space between two subcarriers
n_{eff}	The effective index
λ	Wavelength in vacuum
T	length of the OFDM symbol
x_k	k th complex data symbol
$\hat{x}_k$	retrieve estimated function
N_{ch}	free spectral ranging
λo	the center wavelength
R	slab region radius
ns	an effective index in slab region
τ	the time variance between neighboring stations
$A_i(t)$	$i$the port optical carrier in the input slab zone
θn	phase shift
θi	input slab zone of the phase delay
θo	output slab zone of the phase delay
θ	Azimuthal angle
$\delta(t)$	Dirac delta
$h(\tau, v)$	Delay-Doppler impulse response
$h[n, m]$	Time Frequency impulse response
Λ	M×N time-frequency symbol plane
Γ	resource element in the Delay-Doppler plane
Δf	resolution for frequency
$1/(M\Delta f)$	Delay resolution
N	is an additive receptor noise
W_{ZF}	weight matrix of zero forcing
$\mathbf{u}^H$	received pilots are represented
$\mathbf{T}^H$	transmitted pilot signals are represented
σ^2	power of noise
D	aperture of the array
$(\mathbf{r}, \theta)$	r and θ are polar coordinates
$E_y(r, \theta)$	transverse-field (E) within the mode
$\theta(k)$	Term of phase resulting noise on the k^{th} symbol
$v(k)$	AWGN variable
$\sigma(k)$	Noise variance
d^q	depicts the vector of the transmission symbol
v^q	represent the qth antenna's additive white Gaussian noise

$\boldsymbol{\tau_i}$	Propagation delay
$\boldsymbol{\hat{a}}$	Polarization vector
$\boldsymbol{A_x}$	Polarization x component
$\boldsymbol{A_y}$	Polarization y component
$\boldsymbol{P_x}$	Power of polarization x component
$\boldsymbol{P_y}$	Power of polarization y component
$\boldsymbol{\Phi_x}$	Phase of polarization x component
$\boldsymbol{\Phi_y}$	Phase of polarization y component
$\boldsymbol{Rb}$	Bit rate
$\boldsymbol{R_s}$	Symbol rate
$\mathbf{C_{QPSK}}$	Constellation of QPSK
$\mathbf{C_{PM-QPSK}}$	Constellation of PM-QPSK
$\mathbf{C_{PM-16QAM}}$	Constellation of PM-16QAM
$\boldsymbol{N}$	Dimensions number
$\boldsymbol{E_s}$	Average energy of constellation
$\boldsymbol{\Delta L}$	length-difference of optical medium between neighboring waveguides
$\boldsymbol{N_{max}}$	I/O signals max. number on the FSR
$\boldsymbol{n_g}$	AWG group-refractive-index
$\boldsymbol{m}$	Integer number
$\boldsymbol{n_c}$	AWG effective index
V	pre-coding matrix

Chapter One

Introduction to Modern Communication Systems

1.1 Background

Living human styles and communication have led to wireless communications being feasible and flexible [1]. There is a growing need for improved wireless communications systems for quicker data transmission, high quality information, multimedia communication, live video streaming and content share [2-5]. Although wireless systems have overcome various problems from wireless techniques, some elements cause issues to develop an effective wireless communication system [6,7]. The design of an efficient communication system is hampered by two important elements [8].

First, is fading which is a phenomenon that results in changes of the channel strength due to small-scale impacts of the multipath. Second are Huge-scale fluctuations might come from the loss of track caused by attenuation or the shade caused by large barriers. Wireless communication is carried out on the open air in which systems are subjected to various transmission problems that leading to signal loss [9]. The primary goal of study is to learn how to overcome these problems so as to improve the efficiency of a communication system.

The characteristics of such wireless communication are [10,11]:

- Cost efficiency: Wired communication networks are cheaper and require no comprehensive maintenance or infrastructure. Time investment for preparation and work is not necessary with wireless communication. Even if wireless communication involves wireless cabling, the cost of wireless communication is quite cheap.
- Flexibility: Wireless communication allows people to stay for sending and receiving messages in a desk or phone booth. Every Wireless Transmitter can accept a number of receivers that are restricted to physical connections of the equipment via the wireless communication System.

- Comfort: Wireless devices like mobile phones are easy to operate. It allows everyone to use the phone regardless of where they are located. Physical interaction is not required to transmit messages. The ongoing contact guarantees that people are able to react promptly to catastrophes.

With its effective qualities, the development of wireless systems has produced various advances.

- Transmission: The distance conveyed using wireless system can be anywhere from a few metres (e.g. remote control) to thousands of kilometres (e.g. radio communication).
- Applications: Include GPS devices, door openers, wireless computer mice, headboards, radio reception, satellite, wireless television and cable telephones. Figure below shows recent application areas of wireless technology [12].

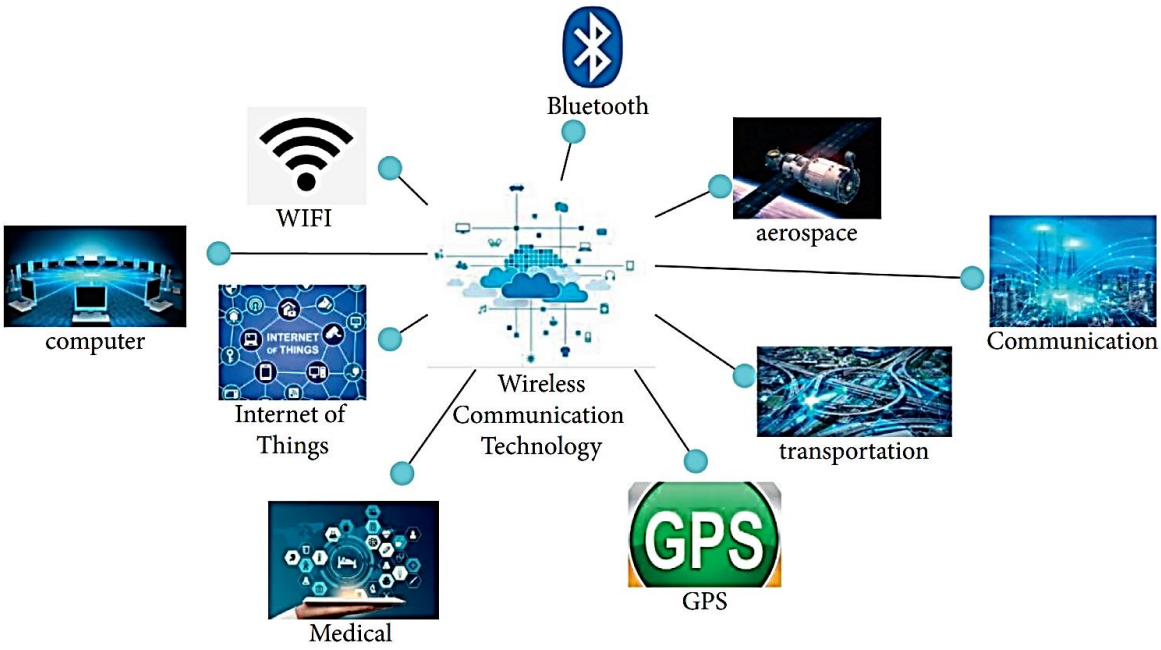

Fig.(1.1): Applications areas of Wireless Communications Technology [12]

The role of wireless communication in our lives has been identified with radio communication and television broadcasting [13]. Both applications leverage technology to be used with the same channel and several signals [13]. This approach is called frequency division multiplexing (FDM).

FDM was widely utilised to establish voice communication for wireless systems in the first generation [14]. Time division multiplexing (TDM) was employed for the efficient use of the communication channel in second generation systems in which data processing is also enabled [15]. In order to develop third generation systems, data transfer, multimedia traffic and an integrated voice were needed [16]. The ability of the channel is restricted. Fourth generation is the stage of broadband mobile network that supersedes third generation and is the predecessor of fifth generation (5G) [17-19].

5G is described as the next generation mobile network, however, it is not projected as a modest improvement over 4G but as a new network [20].

5G has some challenges that must be overcome [20]. Multiple antennas per device will be common, so the beamforming and steering is very important to enhance the performance, the efficiency and reduce the interferences [21]. Studies talk about employing higher frequencies, in the range of microwaves [22]. Besides, it is very important to improve the efficiency of overall system. Figure (1.2) shows the generations evolution of wireless communication systems.

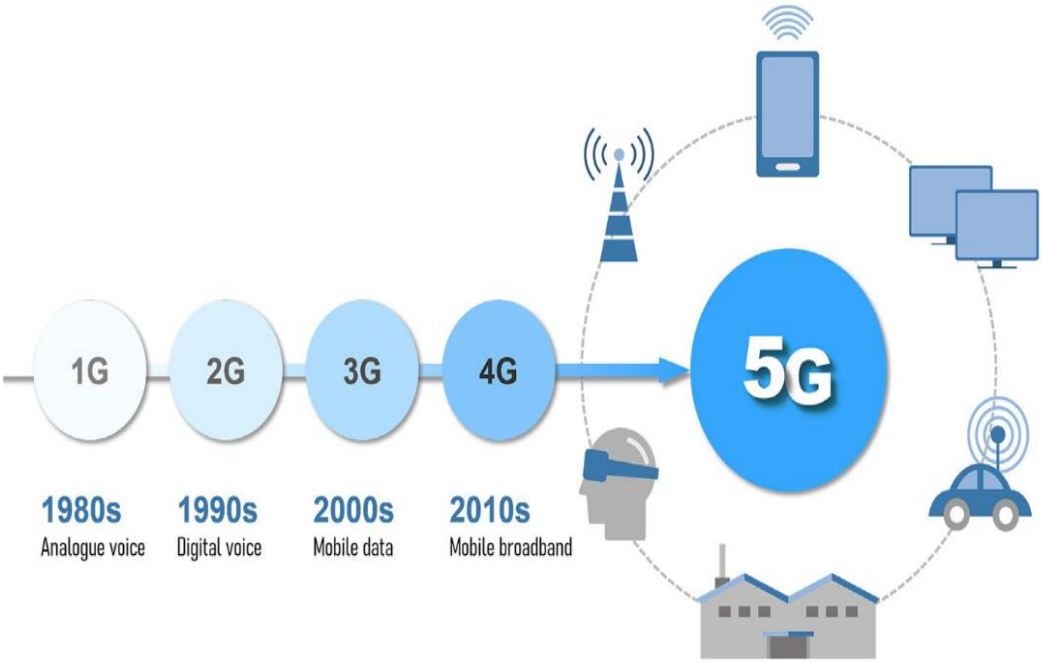

Fig. (1.2): Evolution of wireless communication systems [23]

1.2 MIMO Systems

The MIMO systems were induced as technologies that offer high mobility data rates [24-26]. High transfer rate, spatial diversity and a greater coverage are provided by MIMO systems [26]. They also offer better connection stability with no visible change in the strength and bandwidth of the transmission [27]. MIMO decoding and data detection systems are subject to Channel State Information (CSI) [28]. The MIMO system grows in linear terms with its performance when considering a flat fading channel and is known to the receiver [29].

The MIMO system is rapidly gaining in importance in wireless communications, as opposed to the single input multiple outputs (SIMO), single input single output (SISO), and the multi input single output (MISO) systems [30]. A multiple antenna transmission will be employed, together with a MIMO communication system, to produce a Massive MIMO system as shown in figure (1.3) [31]. Such system can achieve enhanced antenna gain and increase the signal to noise (S/N) ratio. Also, combining massive MIMO technique with orthogonal frequency division multiplexing (OFDM) modulation can produce high spectral efficiency and higher data rates [32-33].

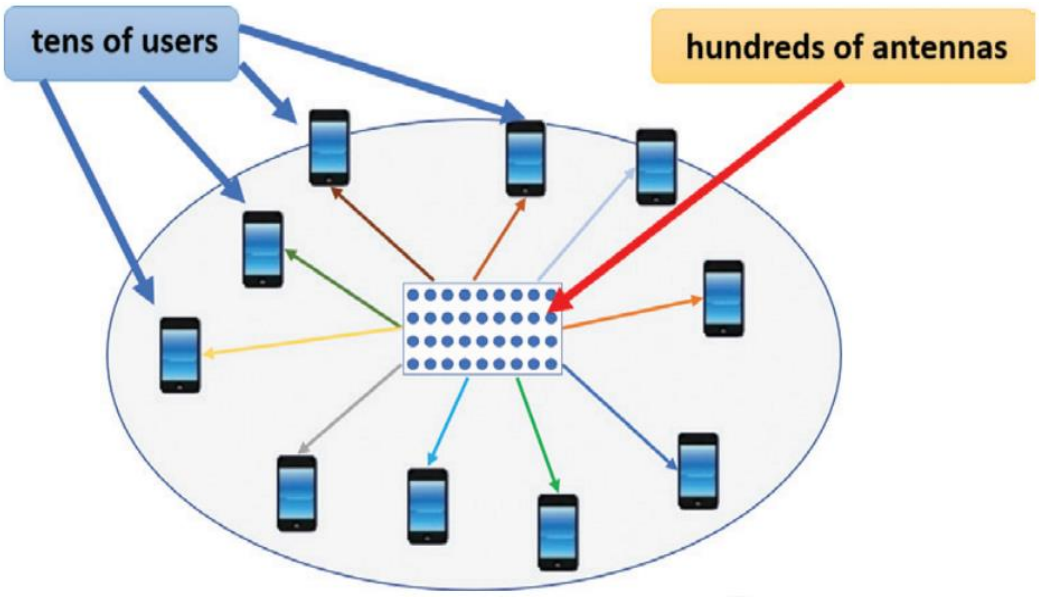

Fig. (1.3): Operation principle of Massive MIMO [31]

1.3 Millimetre Wave Technology

There are need for new technologies to provide larger data transmission rates for users at business data centres with higher bandwidth smartphones, thus, the demand is more than before for users of business data centres [34].

There are a large number of technologies available for the delivery of high fibre optic cabling. Millimetre wave technology delivers bandwidth equivalent with fibre optics, but without the logistical and economical disadvantages of applications [35].

With a wavelength of between 1 –10 millimetres, the RF signal spectrum is between 30GHz and 300GHz [36]. The term of the Millimetre Wave mainly relates to a few radars frequency bands that are 38, 60 and, more recently, 70 and 90 GHz wavelengths [36]. Commercial millimetre waves (MMW) Cable-Free links are high performing, reliable, high capabilities, and offer latest-generation wireless networking. As a result of their advantages, Millimetre waves had been used widely in modern wireless systems to enhance system capabilities and performance. Figure below shows the frequency range of cellular and millimetre waves [37].

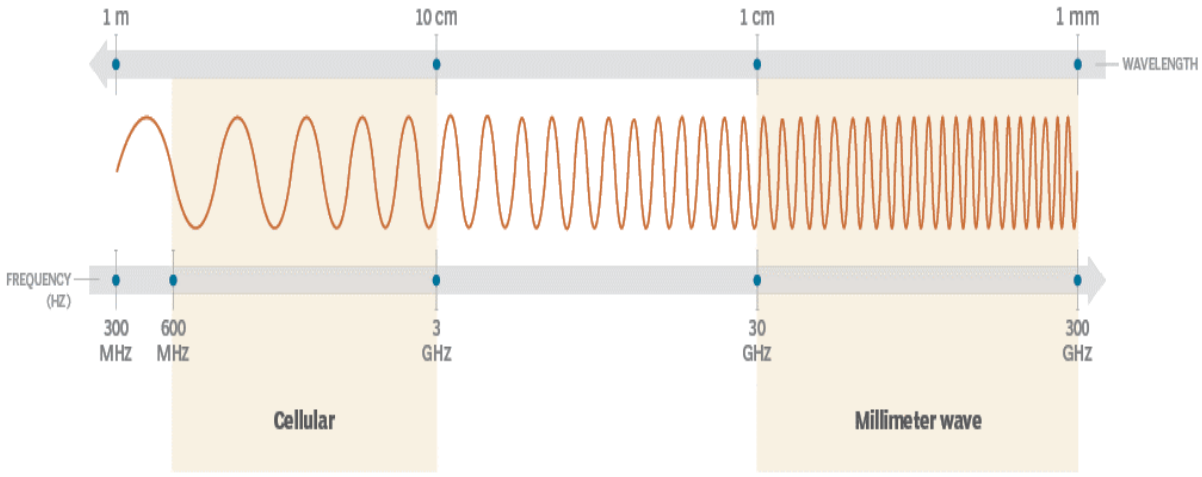

Fig(1.4): Cellular wave vs Millimetre wave [37]

1.4 Radio over Fiber systems (ROF)

The term "Radio over Fiber" (RoF) refers to a technique that permits radio frequency (RF) signals to be transmitted over an optical fiber link with only a slight loss in performance of RF [38]. Although distributed antenna systems are already using RoF systems, most of them use single mode fiber links powered by distributed feedback laser (DFB) or Fabry-Perot laser diodes [38]. Many studies investigate the feasibility of using a cheap laser diode fibre link to transmit radio frequency (RF) signals, such as those used in ultra-wide bands (UWB) and local area networks (LAN). This contained building a system of RF fiber optic by modeling, characterizing, and simulating the optical link components such as single mode fiber (SMF), laser diode, and PIN photo diode alongside the components of RF [39].

RoF links are comparable to digital fiber optic links, with the exception that they are typically operated at the linear region of the laser diode [39]. Further, the signals that would be responsible for propelling these links would largely be of the small signal variety, consequently, modest signal models would be sufficient to describe these links [39]. Then, links of RoF were began getting applied widely for remoting of antenna for wireless cellular networks and satellite earth stations [38]. These fiber links often used intensity-modulated direct detection (IMDD) technology. Figure (1.5) explain the general concept of RoF [38].

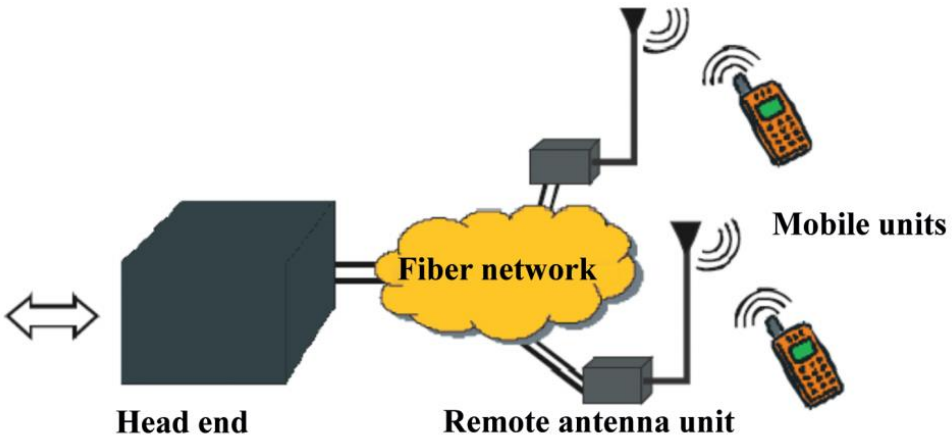

Fig.(1.5): : General Concept of RoF [38]

1.5 Literature survey

With optical carriers in the environment, RoF technology can transmit radio frequency communications simply. In modern mobile communication, on the other hand, massive MIMO transmission systems has often been used in some researches in modern transmission systems to increase energy and efficiency. Several studies and systems implemented in the fields of modern wireless and optical communication technologies.

Many methods had been obtained by researchers in Millimeter Waves-RoF of passive optical networks (PON) to develop communication system's generation, transmission, and detection.

This thesis presents a hybrid transmission system that combines massive-MIMO uplink and downlink systems with backhaul RoF-MMW technologies to improve mobile forward flexibility and increase overall communication system performance. The following related works will be illustrated to be compared with our proposed systems. At first, the following related works will be presented for uplink wireless transmission systems based on MIMO techniques between user and base station.

Yuyu Yan et al in (2012) [40] implemented the uplink multi user MIMO technology in the Advanced Long-Term Evolution (LTE) networks. Based on the simulated results and according to their findings, the joint-pairing method outperforms the other pairing strategies as it is crucial to concurrently take user channel orthogonally and scheduling priority into account when choosing an uplink MU-MIMO coupling. With more receive antennas higher gain of uplink Multi User MIMO achieved in terms of configuration for receive antenna. When the distance between the receiving antennas is reduced, there is a greater variation in the orthogonality of the user channels that have been scheduled, which favors a pairing strategy that takes into account channel orthogonality, like the scheme of maximal and joint orthogonality pairing.

Fredrik Rusek et and colleagues (2013) [41] described a large MIMO system with tens of antennas that offers unique opportunities in wireless communication while conserving transmit power. Their uplink MIMO system has the potential to bring about a radical change in this area of technology. Their research concluded that large MIMO systems necessitate a reduction in the spacing between the antennas. They set up a small simulation framework using an indoor 128-antenna base station and six users with single antenna with ideal environment. In the reality, channels are not ideal and thus, there is a loss in their systems performance compared to ideal channels.

Muhammet N Seyman and Necmi Taspınar in (2013) [42] proposed neural network of feed-forward (MLP) multilayered perceptron implemented with the algorithm of Levenberg–Marquardt for channel estimation factors in uplink MIMO–OFDM system. Mean square error (MSE) and Bit Error Rate (BER) performances of Least Mean Square error (LMS) and least square (LS) algorithms are also compared to their suggested neural network to achieve the performances. Channel estimator using neural network has got much better assessment than LMS and LS algorithms.

Junho Lee (2016) [43] used millimeter wave (mm-wave) hybrid MIMO far-field (FF) system using massive arrays of RF (Radio Frequency) beam formers followed by a baseband processor of MIMO, and suggested an efficient open-loop channel estimator for this system. They had noticed that by randomly permuting the RF beam forming matrix, the estimation accuracy may be greatly increased. Simulation results showed that their suggested far-field orthogonal matching pursuit (OMP) method might get better results than the state-of-the-art methods such as the LS method depend on the model of virtual channel.

Yu Han et al in (2019) [44] introduced a new channel modelling to create a near-field non-stationary uplink massive MIMO system. In order to locate the scatterers, two channel estimate techniques were suggested and identify the

mapping between scatterers and subarrays. The visible scatterers of each subarray were strategically placed using a method developed for subarray-based transceivers that made use of stationarity on the subarray. The outcomes showed good NMSE performance for the low-complexity subarray-wise technique, whereas it can find almost all the mappings and accurately position the scatterers.

Xiuhong Wei et al in (2020) [45] designed a MIMO system depend on proposed prior-aided Gaussian mixture approximate message passing learned (GM-LAMP) channel estimation scheme. In particular, they started by deriving a new function to improve the AMP method based on the established fact that beam-space channel elements can be described by the Gaussian mixture distribution. Simulation results by using both the ray-tracing and theoretical channel model depend data of channel offered that, the suggested network of GM-LAMP can produce better accuracy of channel estimation.

Mingyao Cui and Linglong Dai in (2022) [46] provided the first Near Field (NF) channel estimate algorithm for uplink XL-MIMO systems employing hybrid precoding to account for the property of NF channels. They have suggested modelling the NF channel of XL-MIMO in the domain of polar and built the distance and angular rules of sampling for the matrix of domain of polar transform. Results from their simulations demonstrated that, in the NF region, the suggested NF channel estimation techniques outperformed the state-of-the-art FF channel estimation schemes in terms of NMSE. Additionally, the FF region can make advantage of the suggested NF channel estimation properties separately.

From other side, many studies had been made to develop the backhaul transmission link between certain base station and other base station. The following related works will be presented to be compared with our hybrid backhaul OFDM-RoF-MMW system.

Z. Wang, "Optical FFT/IFFT circuit realization using arrayed waveguide gratings and the applications in all-optical OFDM system", Optics Express, Vol. 19, No. 5, pp. 4501-4512, 2011

Pham T Dat et al in (2014) [47] successfully modeled and demonstrated all the signal's models known by IEEE 802.11 and third generation partnership

project (3GPP) for LTE, WLAN, and LTE-A signals over RoF system based on MMW technique. They also achieved the possibility of developing the convergence of the system for an uplink-backhaul networks and estimated its range of transmission. Their simulated results confirmed the potential to use the system in broadband wireless access networks and in future high capacity and speed small-cell mobile networks.

Jaswinder Kaur and Vishal Sharma in (2019) [48] investigated the impetus and aptness systems of interated multi-carrier radio over fiber to achieve a spectrally and reliable effective framework and suggested an orthogonal space time block code (OSTBC) supplied to OFDM-MIMO-RoF framework by combining Quadrature Amplitude Modulation (QAM) schemes with higher order spatial diversity. The suggested work is implemented for scenarios of line of sight (LOS) and NLOS (non-line of sight). Furthermore, the described work elucidated a related exploration of quality of service (QoS) for 9^{th} order spatial diversity (package of 3×3 antenna), 6^{th} (3×2 package of antenna), and recommended the optimal antenna package.

Muhammad Usman Hadi et al in (2019) [49] offered of digital 20 MHz LTE signal transmission across 70 km of SSMF (Standard Single Mode Fiber) with 64 QAM for broadband wireless signal distribution and transportation applications. It has been demonstrated that digital optical links can handle transmission up to 70 km while attenuating the flaws in A-RoF links. The measured values are all in the acceptable range for LTE, making this a viable option for the upcoming generation of wireless networks.

Moussa El Yahyaoui in (2019) [50] used an efficient local-oscillator (LO) at 15 GHz to suggest a novel method for the transmission and generation of a MIMO OFDM channel via optical fiber link. This method is depended on optical carrier suppress (OCS) and subcarrier multiplexing modulation applying both dual-drive Mach–Zehnder Modulation (DD-MZM) and dual-parallel Mach–Zehnder modulation (DP-MZM). Their proposed method is capable of 70 Gb/s data rate on

50 km single mode fiber (SMF) connected by 3 m wireless transmitted system. The increase in optical power created as a result of this performance enhancement.

Mehtab Singh et al in (2021) [51] proposed new design under the dust effect depend on transceiver of radio over free-space-optical (RoFSO), that was known as OFDM-mode division multiplexer (OFDM-MDM). Over two distinctive Hermite-Gaussian modes, two separate 40 GHz-20 Gbps- 4QAM dataset bearing optical beams are transported; HG01 and HG00, of a single-frequency laser to realize a single-channel 80 GHz- 5G system. They calculated the greatest link distance possible while still meeting acceptable assessment standards, i.e., 20 dB SNR for every condition of desert weather.

T. H. Dahawi In (2021) [52] proposed a novel RoF-PON system setup that makes use of two 60 GHz MIMO based on a wired signal employing OFDM and a 5G universal filtered multicarrier waveform. Signals of MIMO are integrated as the lower and upper sidebands of the wired signal of OFDM at the optical line terminal. The 60 GHz millimeter wave is also up-converted and down converted using modern methods, being self-heterodyning and remote optical heterodyning, respectively. When a downstream link is used across a conventional PON network with a 20 km spread, simulation results showed highly excellent network performance.

At last, there are many modern studies to explore and implement advanced techniques for downlink wireless transmission frameworks depend on OTFS modulation as illustrated below.

M. Kollengode Ramachandran and A. Chockalingam in (2018) [53] proposed a solution for MIMO-OTFS channel estimation and signal detection in high-Doppler channels. They created a vectorized formulation of the for MIMO-OTFS in input-output relationship, allowing for the use of various detection methods for detection of MIMO-OTFS signal. They introduced a message-passing-based iterative algorithm with low complexity for detecting MIMO-OTFS. They were able to attain high BER performance in their simulations, even at high Doppler

frequencies (e.g., 1880 Hz) in a framework of 2×2 MIMO as compared with performance of MIMO-OFDM. Additionally, they provided a delay-Doppler domain channel estimation system that employs delay-Doppler impulses as pilots.

Changyoung An and Heung-Gyoon Ryu1 in (2019) [54] proposed a system of mobile communication with a high throughput that capable of functioning even when operating at high speeds. They built system of OTFS and system of (2×2 MIMO-OTFS) and ability of channel of proposed systems is analyzed and evaluated in the channel of spreading for delay-Doppler. As a results of simulation, it is verified that the data stream's channel capacity is assigned to an (2×2 MIMO-OTFS) antenna of system is similar to that capacity of channel for system of 1×1 OTFS. As a result, it can be assured that a system of 2×2 MIMO-OTFS is nearly twice as capable as system of 1×1 OTFS.

Rasheed O K et al in **(2020)** [55] presented a novel estimation of channel for OTFS-massive MIMO downlink transmission systems. In light of the fact that the representation of Delay Doppler (DD) of time-varying channels is inherently sparse, The DD estimation of channel issue was represented in this work as a sparse signal recovery issue. Compressed sensing (CS) based estimate approaches were used to find an answer to this issue. Specifically, they offered modified subspace pursuit (MSP) and orthogonal matching pursuit (OMP) depend algorithms for DD estimation of channel in system of OTFS-Massive MIMO. The designed CS-based algorithms produced a superior NMSE and performance of BER compared to those of the scheme of impulse-depend estimation of channel.

Mohammadali Mohammadi et al in (2021) [56] examined how well cell-free massive MIMO using modulation OTFS performed in terms of spectral efficiency (SE) performance, considering the impact of channel estimation. The typical downlink and uplink SE were expressed as closed-form expressions. According to their findings, OTFS outperforms OFDM in high-mobility conditions to increase the throughput of cell-free systems of massive MIMO. Moreover, the increase in 0.95-likely per-user throughput with embedded pilot-depend

estimation of channel in correlated shadowing is almost 5.1 times higher than in the scenarios of uncorrelated fading.

Ding Shi et al in (2021) [57] developed a downlink channel state information (CSI) acquisition strategy for massive systems of MIMO-OTFS in the presence of the fractional Doppler, containing algorithm of channel estimation and design of deterministic pilot. It began with an analysis of the relationship of input-output of systems of SISO OTFS, which takes into account the fractional Doppler in real-world applications depend on the OFDM system and developed it to systems of massive MIMO-OTFS. Then, the deterministic pilot was created using the model of downlink CSI acquisition, and the algorithm of modified-sensing-matrix-based channel estimation (MSMCE) was offered to reconstruct the delay-Doppler-beam domain.

A comprehensive review for designing and describing massive MIMO techniques and hybrid OFDM backhaul Millimeter Waves-RoF-PON systems are presented in the following table.

Table (1.1): Next Generation Communication Systems: Technologies, advantages and limitations

Reference	Features	Limitations
[40]	-Uplink MU-MIMO technology in the Advanced Long-Term Evolution (A-LTE) -Obtained joint-pairing for better performance	-Only single MIMO antenna used at receiver
[41]	-Designed a large MIMO system with tens of antennas -Allow multi user MIMO transmission	-Ideal channel, so fading not taken into account
[42]	-Efficient channel estimation parameters in uplink MIMO–OFDM using neural network - MP method achieve Better BER than LMS and LS methods	- Low order of only 4×4 MIMO–OFDM proposed -Single user used for the proposed system
[43]	-Efficient channel estimator for a mm-wave hybrid MIMO. -Consisting of RF beam formers with large antenna arrays	- Not enough values of BER and MSE using proposed OMP -Not enough number of transmitted antennas of 32 used

[44]	-Presented a new channel modeling to obtain a near-field non-stationary system in an extremely large-scale uplink massive MIMO	-Used for only near field environments - Used OMP for only near field channel estimation - Small number of base station antennas, so Nr=16.
[45]	- Designed a Millimeter-wave-mMIMO system based on proposed efficient GM-LAMP channel estimation. - Better MSE performance of GM-LAMP among OMP and AMP channel estimation	- Very complex system with high computational complexity - Work for only near field environments - Not enough number of base station antennas, so Nr=256.
[46]	-Presented the near-field channel estimation algorithm in uplink systems of XL-MIMO using hybrid precoding for near field channel property for the first time - Can support nearfield or far-field separately	- Only the near-field channel property was considered. -Can use Far-field property separately -Only polar domain used for near field representation
[47]	-Successfully modeled and demonstrated all the signal's models known 3GPP and IEEE 802.11 for LTE, WLAN, and LTE-A signals over RoF system based on MMW technique.	- OFDM transmission not supported -Short transmission reach
[48]	- integrated systems of multicarrier RoF to achieve a spectrally and reliable efficient system and suggested an OSTBC equipped system of MIMO-OFDM-RoF	-Only 3×3 antenna package supported -MMW not supported for this system
[49]	- presented a digitized 20 MHz LTE signal transmission across 70 km of SSMF with 64 QAM - Impairments in Analogue-RoF links can be reduced with the use of digital optical links.	- Short reach -Low data rate - Only support LTE signals
[50]	-Transmit a OFDM-MIMO channel across optical- fiber by a single local oscillator at 15 GHz -2×2 MIMO OFDM-RoF used	-Low data rate -Short reach -MMW not supported
[51]	-Propose a novel design of OFDM-MDM based RoFSO	-Very complex MDM design and cost -MMW not supported
[52]	- With the use of UFMC and wired OFDM, a pair of 5G MIMO-RoF signals has been developed for use over a regular PON.	-Small data rates -Short distances -Only two MIMO signals used

	- Two MIMO-RoFs were combined in a high spectrally efficient manner using the SSB-FT technology. - As effective convergence was demonstrated, along with good spectral efficiency and low-cost deployment.	
[53]	-Proposed channel estimation and signal detection methods of MIMO-OTFS in high Doppler conditions.	- Massive MIMO not supported - Need more efficient channel estimation
[54]	-Designed OTFS and 2×2 OTFS-MIMO systems - The delay Doppler spreading channels are used to test the channel capacity of these systems.	-Only 2×2 OTFS-MIMO used -Massive MIMO not supported --Small data rates
[55]	-Designed a new channel estimation for OTFS-massive MIMO systems for downlink transmission system. -Proposed OMP and MSP channel estimation	-Little number of base stations antennas used, N=16 -Need more efficient channel estimation for better MSE and BER.
[56]	-Designed a cell-free massive systems of MIMO with modulation of OTFS. - Good SE achieved	-Little number of base stations antennas used, N=16 -Support only uplink transmission -Need more efficient channel estimation for better MSE and BER.
[57]	-Proposed for massive MIMO-OTFS, a scheme of downlink CSI acquisition. - The MSMCE algorithm for re-creating the domain of delay-Doppler-beam was introduced.	-Very complex modeling and channel estimation -Only single user supported for the proposed simulation. -Need more efficient channel estimation to achieve better MSE
Our Proposed Systems	-Contributed XL-mMIMO uplink transmission system proposed for best performance -Both near-field and far-field supported at the same time in uplink mMIMO system. -Highest spectral efficiency (SE) using downlink Massive MIMO-OTFS transmission systems between base station and user achieved. -Many Advance precoding techniques for Massive MIMO-OFDM and Massive MIMO-OTFS systems had been proposed.	

	-Ultra-high capacity RoF-MMW transmission systems between base stations enabling many modern modulation formats. -Use many OFDM carriers of 8,16 and 32 had been proposed to increase the overall system bit rate -The use of Python algorithm for phase shift correction at the receiver compensate the drift	

1.6 Objective of Thesis

The combination between different technologies and achieving the highest rates for transmission systems with best performance are most required goals for the beyond 5G radio access networks which is extremely important for the usage of huge channel bandwidths and big channel multiplexing in the recent days. The main goals of thesis are:

1. Study the main advanced technologies in wireless communication systems to be used for beyond 5G system.
2. Design a suitable and efficient technology to obtain high spectral energy and efficiency between user and base station for both uplink and downlink scenarios.
3. Design and implement hybrid wireless and optical transmission system to enable high data rate and long distances.
4. Integrate the designed systems to achieve efficient wireless transmission between user and base station and high-capacity backhaul transmission system between two base stations.

1.7 The Main Contributions of the Thesis

1. Increased network capacity and coverage using massive MIMO technology with huge antennas at base station to cover multi users spontaneously and increase the spectral and energy efficiencies.
2. Design a contributed downlink OTFS-mMIMO wireless transmission system using large number of antennas at the BS under different Doppler effects.
3. Novel method for designing OTFS-mMIMO channel estimation based on modified 3D-SOMP algorithm to achieve highest spectral and energy efficiencies among all OTFS recent algorithms.
4. Ultra-High data rates have been achieved using high order multi carrier OFDM channels multiplexed/ demultiplexed using a low-complexity and low-cost comb generation technique and wide bandwidth.
5. Long transmission distances and ultra-high capacity achieved using all optical OFDM backhaul systems.
6. Integrated system obtained including novel OTFS-Massive MIMO system between user and tower with very high spectral efficiency and hybrid OFDM-RoF-MMW backhaul transmission between base station and remote station enabling ultra-high capacity and long-distance transmission system.

1.8 Organization of Thesis

This thesis is divided into five chapters. Chapter 1 explains the introduction about the wireless systems, MIMO systems, mobile communications, millimeter wave technology, different multiplexing techniques, RoF links, and literature survey. The second chapter explains the theory and Mathematical Modeling of the principle of OFDM modulation and massive MIMO system using precoding techniques of massive MIMO. Also, the principle of OTFS modulation for

massive MIMO will be presented. Finally, the principle of optical OFDM transportation along RoF-MMW will be illustrated.

Chapter three explains the system description for the massive MIMO systems and OFDM-RoF-MMW systems which are the proposed works for our thesis. Chapter 4 gives the simulation result details for designing uplink and downlink massive MIMO-OTFS system using many precoding techniques. Then, MMW generation over RoF channel based on OFDM overall results will be illustrated. Finally, chapter 5 presents the conclusion and future work of this thesis.

Chapter Two

Theory of Modern Communication Systems

2.1 Introduction

This chapter presents the theory and modeling of modern communications systems and optical networks that related to our work. There are many modern technologies developed to obtain highest capacity and best performance in the wireless communication field. Among of them, the use of MIMO applications for both uplink and downlink transmission links in the modern base station to support beyond 5G (B5G) systems. From other side, using optical techniques in modern backhaul transmission systems between two base stations offers the most favorable capacity and distance. The following sections illustrates the most effective techniques to be used in the modern communication systems.

2.2 Multiplexing Techniques

The phrase "multiplexing" is a technique of combining several signals, such as analogue or digital, in one signal across a channel [58]. This technology applies to both telecommunications and computer networks [58]. For example, a cable is utilised for carrying various telephone calls in telecommunications [59]. The multiplexed signal is carried via a cable or channel and the channel is separated into many channels [59].

Computer network multiplexing is a type of approach used to mix and transmit many data streams across a single media [60]. Multiplexing is the main part of hardware, such as multiplexer or MUX [60]. For the production of a single output line, multiplexer merges *'n'* input lines.

This technology generally follows the principle of many-to-one, meaning *n*-input lines and 1-output line [60].

A device such as demultiplexer or DEMUX is employed in order to separate a signal into numerous at the receiving end [61]. This technique follows the principle of one-to-many lines and *n*-output lines [61]. This process separates a medium from a low-power medium and then is transferred from a medium with high-power to a low-capacity via several streams [62]. Once numerous senders try to broadcast the signals by a single channel, the physical channel will be separated and allocated by a tool like Multiplexer [62].

2.2.1 Types of Multiplexing Techniques

- **Frequency Division Multiplexing (FDM):** In the 20th century the FDM was employed by a coaxial cable system in telephone companies for multiplexing several voice streams [63]. For restricted distances, low-cost cable systems like *K* or *N* carriers, however, do not allow high bandwidths [63]. The analogue multiplexing of analogue signals is used for integration. This kind of process is important if the network's bandwidth is better than the communications' unified bandwidth [64].
- **Wavelength Division Multiplexing (WDM):** WDM is a form of technology that uses fibre. In high-throughput systems, this is the single most useful concept. A multiplexer is used to combine signals at the end of the transmitter portion, while a de-multiplexer is used to separate signals separately at the conclusion of the destination portion [65]. WDM's major role on the multiplexer is to connect different light sources to only light sources, and the de-multiplexer can translate this light into several light sources [65].

- **Time Division Multiplexing (TDM):** The TDM is one way to deliver a signal across a certain channel by separating the time edge into slots [66]. For each message signal, the same as a single slot is used. TDM is mostly beneficial for digital and analogue communications, which multiply a number of low-speed channels into high-speed transmission channels [67]. Each low-speed channel, depending on the time, will be given an exact position, no matter where it is in the synchronisation mode. Both MUX and DEMUX ends are syncing on time and switching to the next channel at the same time [67].
- **Code Division Multiplexing:** The abbreviation (CDM) refers to multiplexing code division. It's a technique that works with communication between the spread spectrum [68]. A narrowband signal may be conveyed through a split over numerous channels or through a broad frequency band in this sort of communication. It does not otherwise compress digital signal bandwidths for frequencies. It is less susceptible to intrusion and hence offers greater ability to communicate and a safer private connection. When multiplexing the code division to allow a common communication channel to be transmitted by various signals from different users, the technology is represented to as CDMA or Code Division Multiple Access [69].
- **Space Division Multiplexing:** Multiplexing of space division is a type of method where radio, metal transmission medium is physically separated by means of isolation and where space or waveguides retain channel separations [70]. Many channels can be reached by time, frequency, or WDM on each physically different channel. Some POV (Passive Optical Network) systems use SDM by downstream transmitting on one of the FOCs, while upstream transmitting on the rest of the fibre occurs [71].

- **Orthogonal Frequency Division Multiplexing:** The word OFDM refers to " Orthogonal Frequency Division Multiplexing," and otherwise it's a kind of signal modulation that delivers substantial benefits to the connection of data. So, OFDM is mainly employed for numerous latest broadband & WLAN systems, such as cellular telephony, wireless internet connection, etc [72]. OFDM employs a lot of carriers with low bit rate data, which means that the carriers are very flexible and provide high spectrum effectiveness for preferred fading, incursion and multi-track impacts. The processing necessary to the signal format has been found rather high by OFDM-based early systems, although technological advancement means that this kind of technology has little to do with the required process [73].

2.3 OFDM Modulation

OFDM is a multi-carrier transport technique for communication system with high data-rate transmission [74]. To ensure the orthogonality of subcontractor's careful control of the relationship between all the operators is necessary [74]. The initial OFDM is therefore produced by selecting the needed range, depending on the modulation system and the input data [75]. Any carrier's production requires the same transmission dates to be allocated. For the basis of the modulation scheme, the required amplitude and phase are computed [75]. Then the appropriate spectrum is transformed to its time domain signal using an inverse Fourier transformation [76]. Inverse Fast Fourier Transform is used for various applications where efficient transformations are performed and also orthogonal signals are guaranteed. The FFT is the outcome of the identification of equivalent waveforms resulting from a sum of the orthogonal sinusoidal component, A time domain signal converted into its corresponding frequency spectrum. The amplitude

and stage of the sinusoidal component act the spectrum of the signal of time domain [77].

The OFDM principle is the division and transmission of a high-rate data stream in low-rate streams by several subcarrier. It divides the basic bandwidth into narrow parallel orthogonal sub channels. OFDM signals are generated at the transmitter by IFFT, which yields orthogonal carriers as shown in figure below [77].

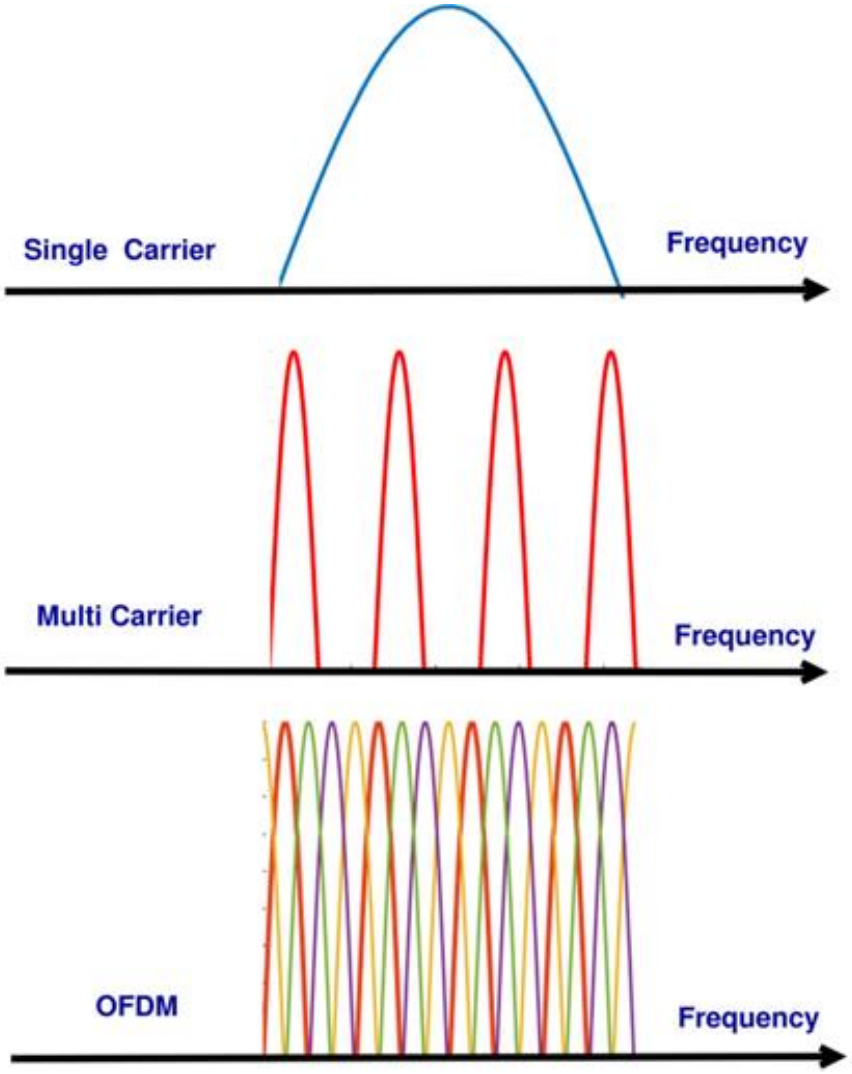

Fig 2.1: Frequency spectrum for different multicarrier transmission

Figure (2.2) shows the idea in the frequency field [78]. Due to its rectangular form of pulse in the temporal area the spectrum of each modulated carrier is $sin(k\,f)/\,f$. Although the spectrum of several modular carriers overlaps, each operator lies in the spectral nulls of all other carriers [78].

Therefore, no interference in the data streams for two subcarriers until the recipient makes the proper demodulation.

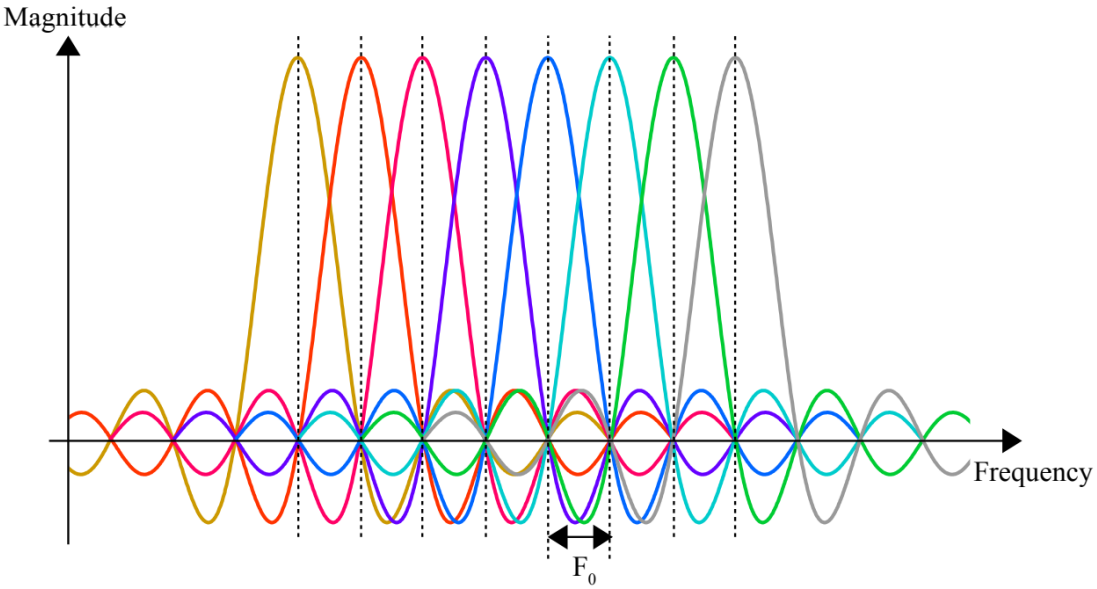

Fig. (2.2): Multi- Carriers OFDM signal [78]

Where F_0 is frequency space between two subcarriers. Modulation is the method through which a certain parameter of the peripheral waveform may be changed to use this signal to transmit a message. Usually a high-frequency sinusoidal waveform is a carrier signal used. Therefore, the method of modulation is called analogue modulation. The carrier parameter is constantly changing and is called analogue signal.

Upon converting the analogue signal into a digital sample signal, several types of digital modulation techniques can be achieved by

distinguishing the carrier signal parameter [79]. The Binary Amplitude Shift keying (BASK) varies by amplitude, and changing phase outcomes are achieved using the Binary (BPSK) [79]. The digital modulation techniques are categorised on the basis of detection or bandwidth compaction properties [80]. Based on the principle of ASK and PSK modulations, quadrature amplitude modulation (QAM) can be obtained [80]. QAM modulation have many advantages among the recent modulation formats so it had been used widely with OFDM applications [80]. Principle of QPSK and QAM will be shown in Appendix A.

As can be observed in Figure 2.3, the line signal's spectrum is similar to that of N independent signals of QAM, where the signaling rate between N frequencies [81]. One of the complex integers from the initial input is carried by each QAM signal.

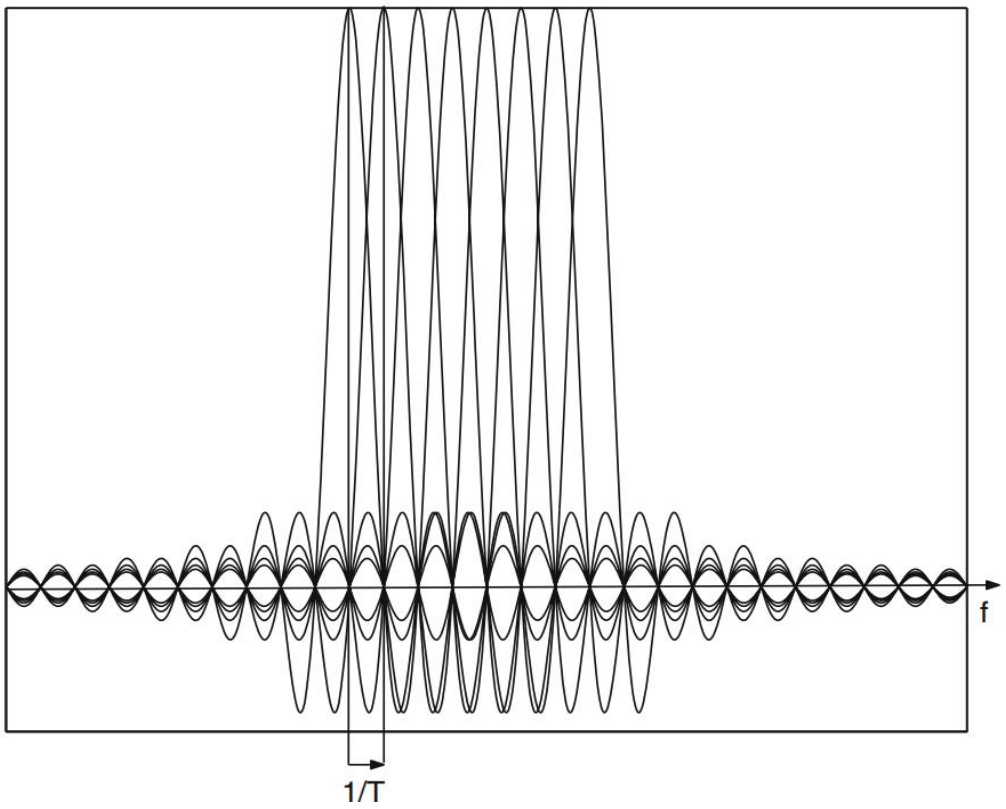

Fig. (2.3): Spectrum of OFDM for every signal of QAM

Each QAM signal′s spectrum is of the following form $sin(k\ f)/\ f$, as can be seen in Figure (2.3), the other subcarriers all have central nulls. This guarantees the subcarriers' orthogonally.

This approach modulates a binary code for the analogue carrier signal. Digital modulator devices are the interfaces between transmitters and channels. The digital modulation system is characterised according to its capacity for detection or compression of bandwidth. The key criteria for optimum modulation are cost-efficiency, bandwidth, power efficiency, signal to noise ratio (SNR), higher service quality and the BER.

In accordance with this methodology, each modulation scheme is evaluated for its performance by measuring its chance of error, named additive white Gaussian noise (AWGN). The modulation approaches, which can send more bits/symbol, are immune to noise-induced mistakes and channel interferences. Delay distortion may be a significant parameter for the determination of any modulation scheme for digital radio [81].

2.3.1 Cyclic Prefix for OFDM

To remove inter-symbol interference**,** Cyclic Prefix (CP) has been established. Cyclic prefix means that a part of the end of the main symbol body is copied and the first part of the symbol is added [82]. Since the signal contains the same set of frequency domain components, the frequency content of the signal does not change. The interval between symbols to prevent ISI is termed Guard Interval/Time (GI). It is implemented as a CP to eliminate ISI and preserve orthogonality among OFDM subcontractors, till the time of the guard extends beyond the channel delay as shown in figure below [83].

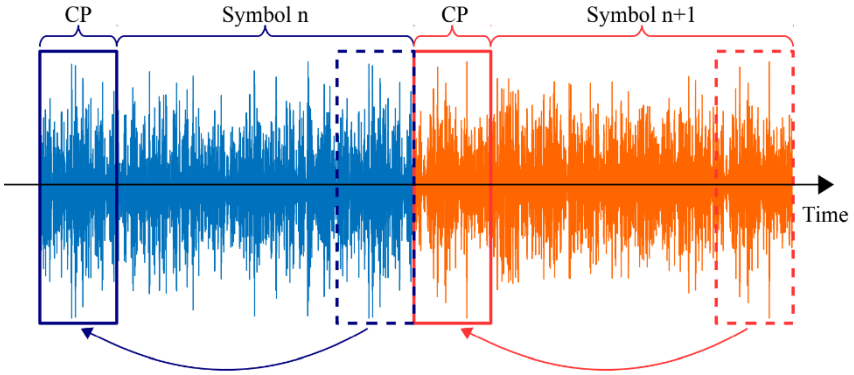

Fig. (2.4): Principle of the Cyclic Prefix

Figure (2.4) shows the construction of cyclic prefix. Cyclic Prefix (CP) was designed to eliminate inter-symbol interferences. Cyclic prefixes indicate copying a part of the end of the body of the sign and adding the first part of the symbol. The frequency content of a signal does not vary as the signal comprises the same set of components for the frequency domain. The gap between ISI prevention symbols is called the time interval of the guard (GI). It is used as a CP in order to eliminate ISI and preserve OFDM subcontractors' orthogonalities till the time the guard expires over the channel delay [83]. Averages for minimising the noise of the channel estimation are the channel values obtained with the pilot symbols. Finally, the initial set of pilot symbols equalises half of the frame and the remaining half of the frame is equalised with the second set of pilot symbols [83].

2.3.2 Modelling of OFDM system

To comprehend the workings of the OFDM system, let's use Figure (2.5) as a diagram [84]. A serial-to-parallel conversion is performed, and the data is then grouped into individual bits to create a complex-number (x) after QAM or PSK modulator so that be sent over *N* low rate information stream. Subcarriers of the form are assigned to each low-rate data stream [85]:

$$\phi_k(t) = e^{j2\pi f_k t} \qquad (2.1)$$

where f_k is the frequency of the k th subcarrier.

Respectively, one symbol of base-band for OFDM with N subcarrier is:

$$s(t) = \frac{1}{\sqrt{N}} \sum_{k=0}^{N-1} x_k \phi_k(t),\ 0 < t < T \qquad (2.2)$$

where T is the length of the OFDM symbol and x_k is the k th complex data symbol. Let's now examine the built-in OFDM symbol in more detail in order to examine the orthogonal sub-carriers [84].

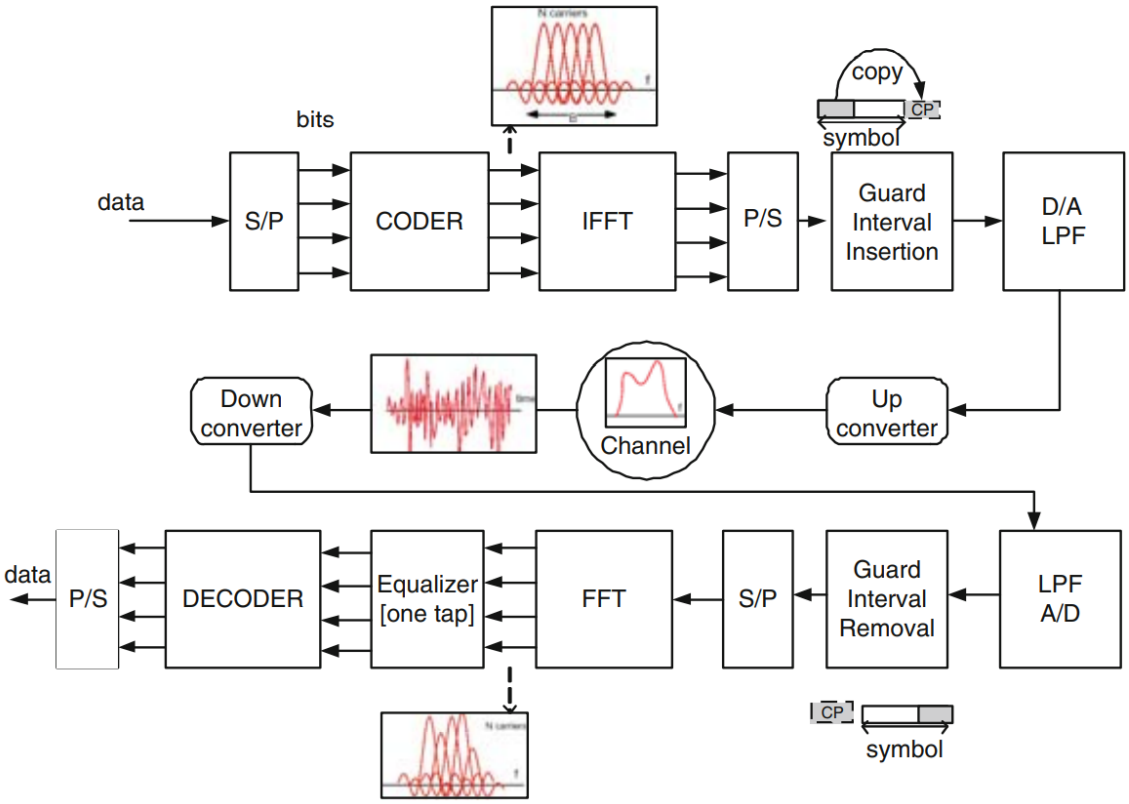

Fig. (2.5): Schematic of OFDM system

OFDM frequency-domain orthogonality is achieved by convolving Dirac pulses with $\text{sinc}\,(\pi f T)$. Since in time-domain a rectangle $(T)$is multiplied with a subcarrier ϕ_k, which is a convolution in frequency-domain between $\text{sinc}(\pi f T)\ and\ \delta(f - f_k)$. This is basically $1/T$ shifted version of

sinc (f) for every f_k and sinc (πfT) has zero values for all frequency bands that are integer multiple of $1/T$.

It is important to keep in mind that the time domain can also be used to prove the orthogonality of OFDM subcarriers. The symbol interval has an integer cycle's number within a symbol-time (T), and the difference in exactly one cycle between neighboring subcarriers. While demodulating it at the receiver, down transformed, and has an integration with a frequency j/T, then the x_j is received since any other subcarrier when it is down transformed with a frequency $(i-j)/T$ generates zero after integration because $(i-j)/T$ generates integer number of cycles during the integration-interval (T).

Channel dispersion breaks down the orthogonality of the sub-carries and leads to ICI when a signal is sent through a channel, and ISI is caused by delay dispersion between subsequent OFDM symbols. It was previously mentioned that CP is employed to maintain orthogonality and prevent ISI. As we can see, this makes equalization at the receiver is very easy. Points in the constellation of the modulation become warped if multipath exceeded the CP. As seen in Figure (2.5), the sub-carriers are no longer guaranteed to remain orthogonal when multipath delay exceeded the CP, because modulation points might be anywhere along the corresponding contour. The radius of the contour increases and crosses the other contours as delay spread becomes more severe. Therefore, this leads to a mistake.

The CP is created by the cyclic expansion of the symbol of OFDM and is used in the guard interval between subsequent blocks over a period [86]:

$$s(t) = \frac{1}{\sqrt{N}} \sum_{k=0}^{N-1} x_k \phi_k(t), \ -\tau < t < NT \qquad (2.3)$$

For an ISI to be avoided, it is necessary that τ be larger than the channel length τ_h. The CP lowers the bit rate to $(\mathrm{Nb}/NT + \tau)$, more power to transmit is required where b is the bits that a subcarrier can send. The transformation of a discrete time linear convolution into a discrete time circular convolution is done via the CP. Therefore, the data block and channel impulse response being communicated can be modelled as a convolution in a cyclic fashion to account for the transmitted data This is a DFT of point-wise multiplication samples in the frequency domain. The received signal then changes into [84]:

$$y(t) = s(t) * h(t) = \frac{1}{\sqrt{N}} \sum_{k=0}^{N-1} H_k x_k \phi_k(t),\ 0 < t < NT \qquad (2.4)$$

Where:

$$H_k = \int_0^{\tau_h} h(t) e^{j2\pi f_k t}\, \mathrm{d}t \qquad (2.5)$$

Hence, k th subcarrier now has a content of channel H_k, which is the FT of $h(t)$ at the frequency f_k.

The symbol of OFDM is sampled $(t = nT$ and $f_k = k/NT)$ in the receiver and demodulated with an FFT. Respectively, here is the format of the data that was sent in [86]:

$$y_k = H_k x_k,\ k = 0, \ldots, N-1 \qquad (2.6)$$

By using *N* equalizers with parallel one tap, the detected actual information can be recovered. Just the estimated channel contents are used by the one-tap equalization $\left(\hat{H}_k\right)$ and apply it to retrieve estimated $\hat{x}_k$ as the fallowing [84]:

$$\hat{x}_k = \frac{y_k}{\hat{H}_k} = \frac{H_k}{\hat{H}_k} x_k \qquad (2.7)$$

2.3.3 Advantages and disadvantages of OFDM

The principal advantages of OFDM include the easier overlap, OFDM uses spectrum efficiently, exhibiting great resilience to selective fading by dividing the conduit in a narrow band fading subchannel, compared to the single carrier system [87]. It is possible to recover lost symbols using the appropriate channel coding. The canals that are interlinked are frequency selective channels. Adaptation to harsh channel conditions is achievable without complicated time-domain equalization [87].

The main disadvantage of OFDM on the other hand is that OFDM needs RF-power amplifier with a big peak to average power ratio (PAPR) as they have the variation of amplitude with an extensive dynamic range. It demands low power efficiency for the linear transmitter circuitry [87]. In comparison to a single carrier OFDM has a higher sensitivity to carrier frequency offset and drift. It is susceptible to the change of Doppler [87].

2.4 Principle of All Optical-OFDM depending on AWG geometry conversion

An Arrayed Waveguide Grating (AWG) MUX / DeMUX is a planar system with imaging and dispersion properties. It consists of I/O waveguides, usually equal to the number of transmitted channels [88]. A typical (AWG) consists of two free-space planar star couples and a set of arrayed planar waveguides with lengths gradually increase, connected as illustrated in Figure (2.6). In practice, however, AWG design is generally complicated by adding other functional elements to compensate for polarization and temperature dependencies and to maximize the flatness of the channel passband or minimize insertion losses and inter-channel crosstalk [89].

AWG is used as the IFFT / FFT Orthogonal Frequency Division Multiplexing transmission circuits. The channels' number in a free spectral ranging Nch [90] as follows:

$$N_{ch} = \frac{\lambda_o R}{n_s dD}, \tau = \frac{N_c \Delta L}{c} \qquad (2.8)$$

Where λo is the center wavelength, R slab region radius, ns is an effective index in slab region, τ is the time variance between neighboring stations, and Nc is the group index of effective index nc. Next, IFFT can be accomplished by AWG circuits. The Optical IFFT circuits are paired with optical phase shifters and delaying time. It could be concluded that the expression of i th subcarrier after IFFT in one OFDM symbol time [90]:

$$A_i(t) = \sum_{n=0}^{N-1} \exp(-j\theta_n) \cdot a_i(t - n\tau) \qquad (2.9)$$

Where $A_i(t)$ is $i$the port optical carrier in the input slab zone and θn is the phase shift. In AWG, the increase ΔL of the arrayed waveguide causes time delay, and the region of the input/output slab causes phase shift.

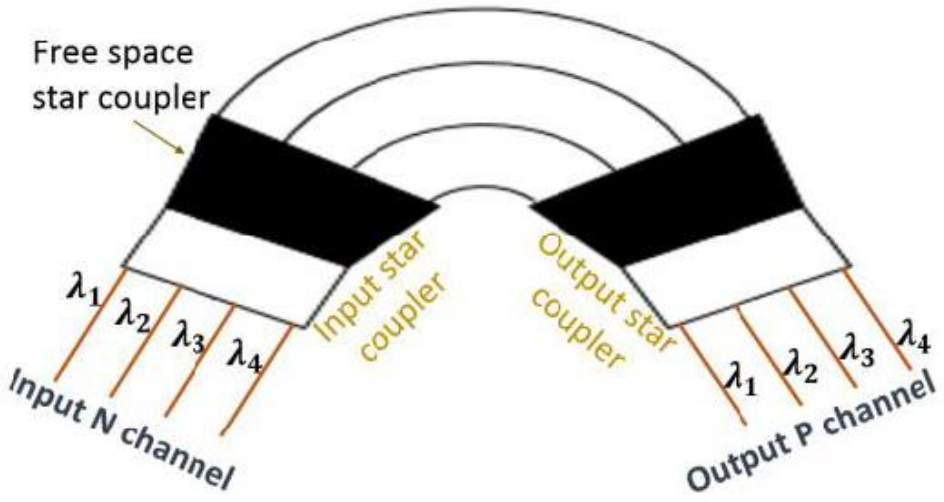

Fig. (2.6): Schematic views of the simplest AWG design [90]

For AWG, the response expresses between p output and i input as a filter is:

$$h_{ip}(t) = \sum_{m=0}^{N-1} \exp\left(-j2\pi m \frac{n_s d}{\lambda_o}(\sin\theta_i + \sin\theta_o)\right)\delta(t - m\tau) \qquad (2.10)$$

where θi and θo is the input and output slab zone of the phase delay, and $\delta(t)$ is the Dirac delta. The input/output port of the phase factor can express as:

$$\sin\ \theta_i = i\frac{D}{R} \sin\ \theta_o = p\frac{D_1}{R} \qquad (2.11)$$

Therefore, Eq. (3) can be express from Eqs. (2) and (5):

$$h_{ip}(t) = \sum_{m=0}^{N-1} \exp\ \left(-\frac{j2\pi m}{N_{ch}}(i + p)\right) \cdot \delta(t - mt) \qquad (2.12)$$

Then converting Eq. (5) by Fourier transformer, in spectral domain we can get the AWG transfer function:

$$H_{ip}(f) = \sum_{m=0}^{N-1} \exp\ \left(-\frac{j2\pi m}{N_{ch}}(i + p)\right) \cdot \delta(-2\pi f_m \Delta\tau) \qquad (2.13)$$

Then we can use the AWG as IFFT / FFT circuits. As signals pass through the AWG as IFFT to achieve modulation of OFDM, the express is:

$$A_p(t) = \sum_{m=0}^{N-1} \exp\left(-j\frac{2\pi m}{N_{ch}}(i + p)\right) \cdot a_i(t - m\tau) \qquad (2.14)$$

The output slab area contains only one port, since the signal after IFFT is the N subcarrier overlay. Therefore, it can select the output port where the phase shifts in the output area are equal. So, the impact of θo in optical IFFT can be neglect.

$$A_p(t) = \sum_{m=0}^{N-1} \exp\left(-j\frac{2\pi m}{N_{ch}}\right) \cdot a_i(t - m\tau) \qquad (2.15)$$

Also, the optical FFT is similar in form, so, the OFDM signal can be expressed after p th OFFT module.

$$S_i(t) = \sum_{m=0}^{N-1} \sum_{n=0}^{N-1} \exp\left(-j2\pi i \frac{(m+n)}{N_{ch}}\right) \cdot a_i(t - (\mathrm{m} + \mathrm{n}).\tau) \qquad (2.16)$$

The authentic signal forms OFDM after the OFFT module.

2.5 OTFS Modulation

Recently, it has been suggested that OTFS modulation can withstand the Doppler shift introduced by channels in highly mobile wireless networks [91]. QAM symbols are established on the Delay-Doppler (2D) plane for OTFS modulation in order to be sent across the channel, $\mathrm{h}(\tau, \mathrm{v})$ is the Delay-Doppler impulse response of a complicated channel [92]. The ZAK Transform serves as a link between the Time-Frequency domain and the domain of Delay-Doppler, which is determined as the following [93]:

$$h[n,m] = \iint h(\tau, v) e^{-j2\pi(mv-\tau n)} dv d\tau \qquad (2.17)$$

$$H[n,m] = \iint h(\tau, v) e^{j2\pi(mv-\tau n)} dv d\tau \qquad (2.18)$$

Delay-Doppler and Time-frequency transformations are defined in a single array of building blocks, as shown in Figure (2.7), in which the time duration is NT and bandwidth Bw $= M\Delta f$ [91].

The array, defined on the M×N time-frequency symbol plane, is [92]:

$$\Lambda = \{(\mathrm{nT}, \mathrm{m}\Delta f), n = 0, \dots, N-1, m = 0 \dots, M-1\} \qquad (2.19)$$

The following resource element is described in the Delay-Doppler plane [92]:

$$\Gamma = \left\{\left(\frac{k}{NT}, \frac{l}{M\Delta f}\right), k = 0, \dots, N-1, l = 0 \dots, M-1, \right\} \quad (2.20)$$

Where, Δf represent subcarrier spacing and T represent length of OFDM symbol. Consequently, we are able to obtain the time resolution T, the resolution for frequency is Δf, $1/(M\Delta f)$ is the Delay resolution, and $1/NT$ is the Doppler resolution.

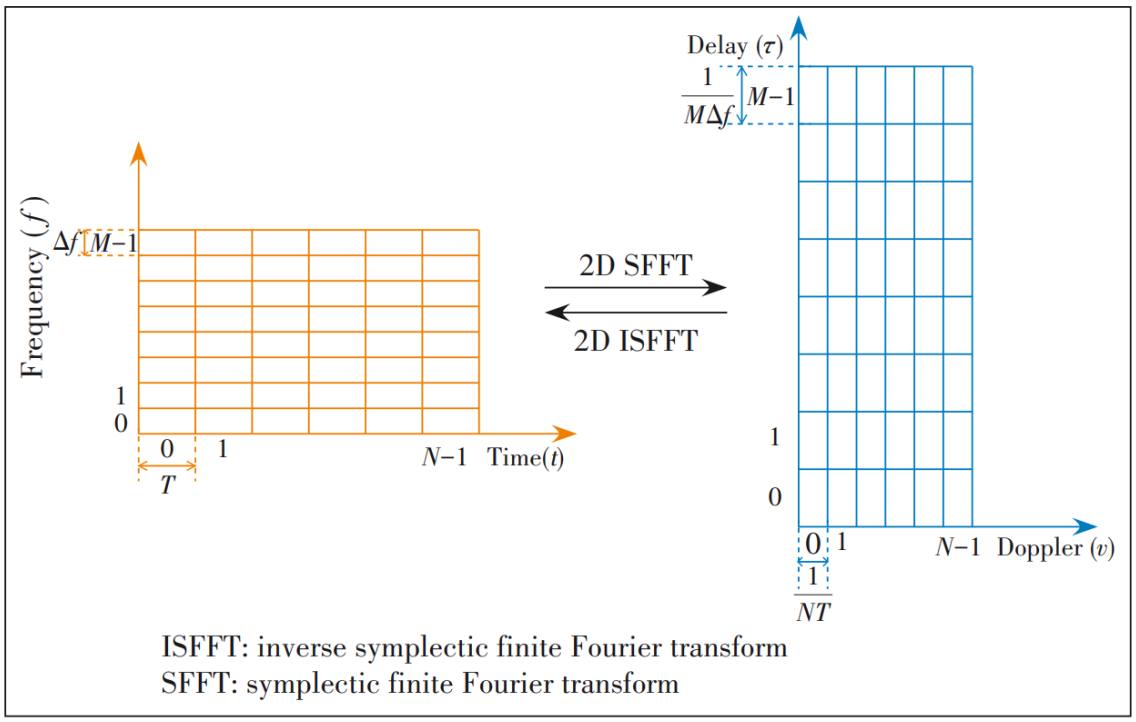

Fig. (2.7): Block transform between Delay-Doppler domain and Time-Frequency [91]

The 2D Discrete Symplectic Fourier Transform (DSFT) is able to realize OTFS modulation, and it is explained as follows [94]:

$$X[n,m] = \frac{1}{\sqrt{MN}} \sum_{k=0}^{M-1} \sum_{l=0}^{N-1} x(k,l) e^{j2\pi\left(\frac{nk}{N} - \frac{ml}{M}\right)} \quad (2.21)$$

$$x[k,l] = \frac{1}{\sqrt{MN}} \sum_{k=0}^{M-1} \sum_{l=0}^{N-1} X(n,m) e^{-j2\pi\left(\frac{nk}{N} - \frac{ml}{M}\right)} \quad (2.22)$$

The array is transformed into the other domain using DSFT, a sort of 2D sine wave complex extension. DFT generation followed by IDFT transposition is what's meant by DSFT. In fact, the result has nothing to do with whether FFT or IDFT is used in the first step. signals array size is fixed with $N \times M$, for two arrays X2[n,m] and X1[n,m], The property of cyclic convolution in DSFT can be achieved by the following formula (2.23) [95].

$$\mathrm{DSFT}(X_1[n,m] \otimes X_2[n,m]) = \mathrm{DSFT}(X_1[n,m]) \cdot \mathrm{DSFT}(X_2[n,m]) \qquad (2.23)$$

This is crucial for the design of receivers. Due to the cyclic characteristic, the only viable option for adopting the OFDM receiver structure and channel equalization approach is to expand to 2D. The following benefits of system structure in the delay-Doppler domain are [96]:

- Frequency diversity and Channel time feature can be produced.
- In the Delay-Doppler region, a fading time-varying channel can be converted into a practically fixed channel during the time interval.
- Any channel-based signal effect can be taken into account.

It is possible to characterize the output and input signals in the domain of Delay-Doppler using the 2D circular convolution described below [97].

$$y[k,l] = h[k,l] \circledast x[k,l] \qquad (2.24)$$

We may obtain the multiplication model in the frequency domain using the formula (2.25) [97]:

$$Y[n,m] = H[n,m]X[n,m] + V[n,m] \qquad (2.25)$$

Figure (2.8) illustrates the structure of the OTFS system [98].

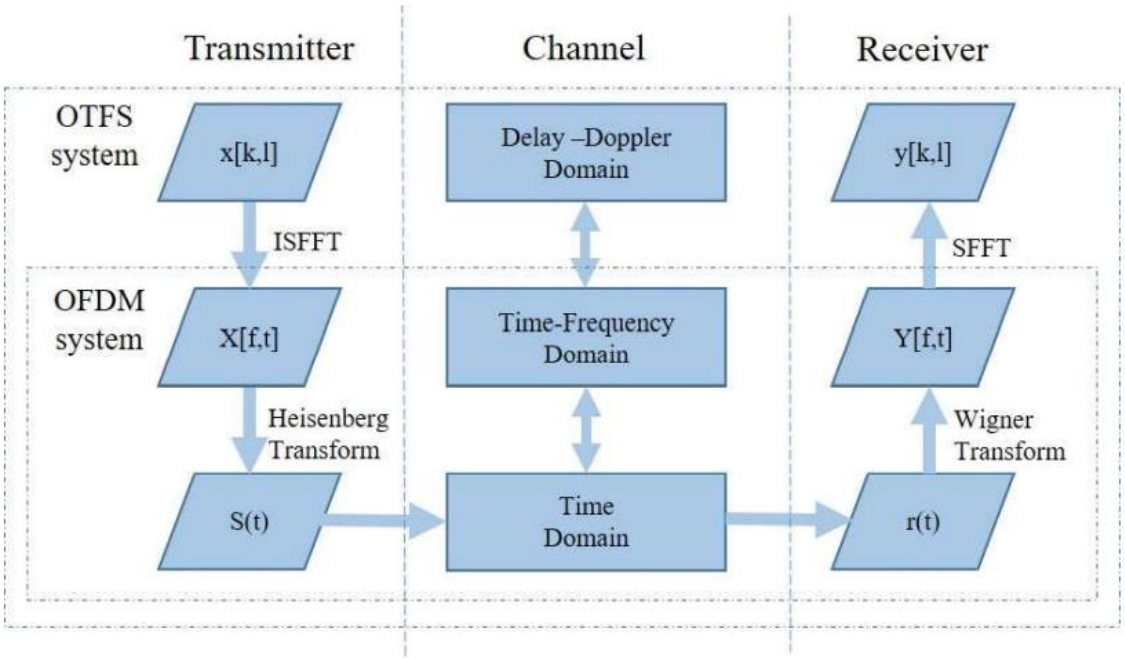

Fig. (2.8): System structure of OTFS modulation

Where $x(k,l)$ is the set of data symbol in the domain of delay-Doppler at the transmitter seen in Figure (2.8), and it will go through two phases to become time-frequency, the N-point IFFT comes first, then the M-point FFT, this might be viewed as the transmission of OFDM symbols [98].

Consequently, Heisenberg's transform can be realized by using M-point ISFFT, and the time domain point data symbol will be M×N. What fascinates is the fact that there is an inverse relationship between M-point IFFT and M-point FFT, therefore, we simply need to finish the entire processing using N-point IFFT and parallel to serial operation. With decoding and pre-coding blocks on N successive OFDM signals, OTFS is easily achievable. Furthermore, since OTFS is taken into account in the broadcasting scenario, CP must be inserted in advance of signals sent through the time channel in order to safeguard the overlay between neighboring resource blocks [98].

2.6 MIMO Systems

As illustrated in the figure 2.8, multiple antenna schemes consist of several transmissions and receive antenna configurations for improved system of system performance compared to systems of SISO [99]. These systems use various encoded algorithms for data processing and are detailed as the following [100].

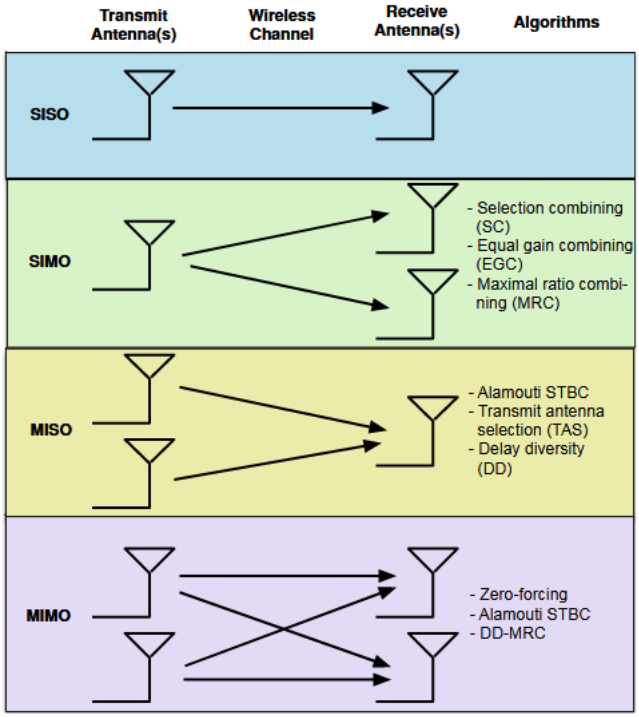

Fig 2.9: Multi-antenna configurations [100]

The MIMO systems were induced as technologies that offer high mobility data rates. High transfer rate, spatial diversity and a greater coverage are provided by MIMO systems [101]. They also offer better connection stability with no visible change in the strength and bandwidth of the transmission. MIMO decoding and data detection systems are subject to Channel State Information (CSI) [102]. The MIMO system grows in linear

terms with its performance when considering a flat fading channel and is known to the receiver. For a receiver, precise channel assessment is essential.

In comparison with SISO, SIMO and the MISO systems, the multiple input multiple output system is becoming very important in wireless communications [103]. A multiple antenna transmission and antenna will be employed, together with a MIMO communication system, to achieve enhanced antenna gain and to increase the noise ratio in this system. In recent times, numerous strategies were presented to use multiple antennas for the goal of producing diversity and multiplexing gain by utilising the result of non-constructive multipath ways [104].

A system with NT transmission antennas is studied and the NR receives antennas. Figure (2.10) is the MIMO architecture block diagram [105].

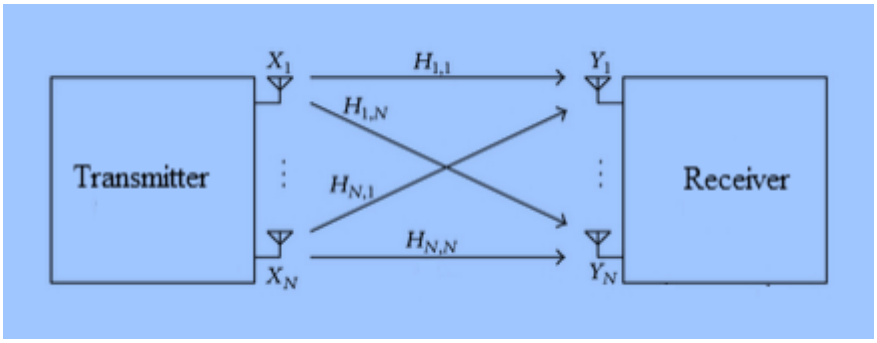

Fig. (2.10): Architecture of MIMO

The selective channel frequency can be converted into the narrow band or flat channel frequency by considering channel coherence higher than the bandwidth of the signal conveyed [105]. Furthermore, at the moment of the block communication, the channel was considered as stationary. Thus, the response of a channel will be fixed in one block, taking into account the model of Rayleigh block fading for the channels of flat MIMO. The channel reaction will randomly fluctuate from block to block. The signal received in

this system can be demonstrated in accordance with the equation stated in the following equation during training [106].

$$\boldsymbol{Y = H.S + N} \tag{2.26}$$

Where Y is the complicated and NR vector received NR signals, the S may be the complex NT vector of these transmitted signals in NT transmitters and N is an additive receptor noise complex NR -vector. With the same distribution in the Gaussian random variables with null mean variance, the noise matrix features are separate and N correlation matrix is given as follows [107]:

$$\boldsymbol{R_{nn} = E\{N^H.N\} = \sigma_n^2.N_R.I_{N_P}} \tag{2.27}$$

The Np is the number of such symbols per every antenna broadcast. Consider the same transmitting numbers and receiving antennas in the MIMO system. The (NR X NT), called Matrix H, indicates the complex fading coefficients. hm, n, the fading factor denotes the (m, N)-th element of the H matrix between the n-th and the receiving antenna. H and noise are separately of each other's primary parts. Estimation of the canal matrix requires a training symbol to be transmitted via the transmitting antenna. The main purpose of the estimate of this channel is the recovery of the matrix of channel H on the basis of the signal Y and S received. The results at the sites will be as follows [108]:

$$\boldsymbol{y_{n1} = h_{11}s_1 + h_{21}s_2 + n_1} \tag{2.28}$$

$$\boldsymbol{y_{n2} = h_{12}s_1 + h_{22}s_2 + n_2} \tag{2.29}$$

It will improve its performance by using numerous antennas for transmitters and recipients.

2.6.1 Precoding Algorithms of MIMO

A MIMO system employs several transmitter and recipient antennas to improve the reliability of the Wireless framework by spatial diversity and/or boosting spatial multiplexing data rates. A MIMO space multiplexing system broadcasts distinct information simultaneously to several receiving antennas on a number of antennas. The challenge for the recipient is to detect the individual information. The distinct data can be restored by simple linear detection methods. All transmitted signals are treated as interference with such algorithms, except for the desired signals of the target antennas. The linear detection technique of zero forcing (ZF) nullifies the signal that interferes with the following weight matrix [109]:

$$W_{ZF} = (H^H H)^{-1} H^H \qquad (2.30)$$

A study of several detector systems revealed that MIMO's most simple technique, the Zero Force Linear Detection Algorithm, can yield error rate performance equal to that utilised by MIMO Vertical-Bell Laboratories in many current standards Space-Time layered (V-BLAST). The fusion of MIMO and RoF-DAS techniques can considerably improve a wide range of RAUs.

In MIMO schemes the Alamouti STBC algorithm can also achieve spatial diversity advantages. The technology is known as spatial diversity transmission/receipt. The MIMO Alamouti STBC transmitter is equivalent to the MISO technique in signal processing and coding. The additional processing is due to the additional antenna on the recipient side, the diversity gain. The channel coefficients of MIMO Alamouti STBC decoder (h_{11}, h_{21}, h_{12}, h_{22}) are determined using the symbols containing the received

perambulations to decode the two periods of symbols. The following is depicted [108]:

$$x_1 = h_{11}y_1 + h_{12}y_2^* + h_{21}y_1 + h_{22}y_2^* \quad (2.31)$$

$$x_2 = -h_{11}y_2^* + h_{12}y_1^* - h_{22}y_2^* + h_{21}y_1^* \quad (2.32)$$

In MISO and SIMO systems, MRC algorithms and Delay Diversity have been discussed to obtain transmission and gains of diversity respectively. These methods can be gathered in a MIMO system, i.e. DD on the receiver side and MRC, to give spatial variation over standard SISO systems [108].

2.6.2 Massive MIMO

Multi-input (MIMO) technology is an issue from the last two decades since the dependability and capacity of wireless systems have been proven to be effective [109]. A huge number of antennas are employed in massive MIMOs, which means that the range is used in parallel with numerous antennas. This retains all the advantages and features of typical MIMO systems [109]. If the antennas number is higher, the degree of channel freedom will therefore improve performance [110].

For multi-antenna wireless communication Spatial modulation (SM) is an attraction [111]. If the Energy Efficiency (EE) is visible, and if the energy consumption is within a specific threshold, then the EE will enhance, as it is necessary to examine this parameter as in systems of MIMO, BS Density is increased. The design can be resilient to prevent the functioning of the system if one or several antenna units fail. The downlink is tedious. Figure (2.11) shows the uplink and downlink scenarios of Massive MIMO technique [112].

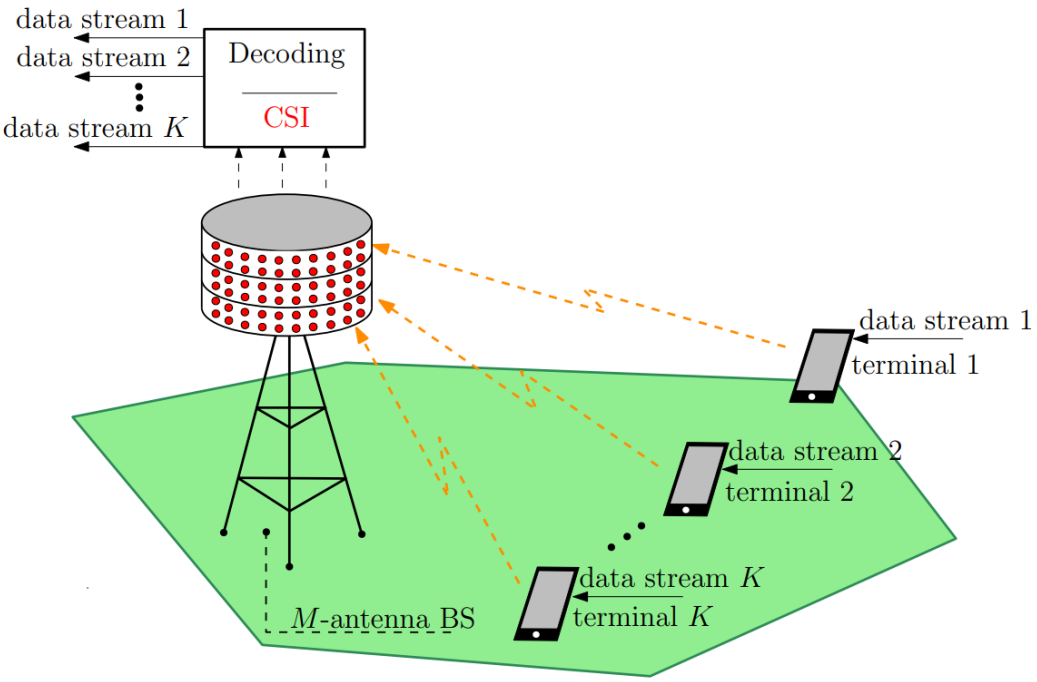

(a) Uplink.

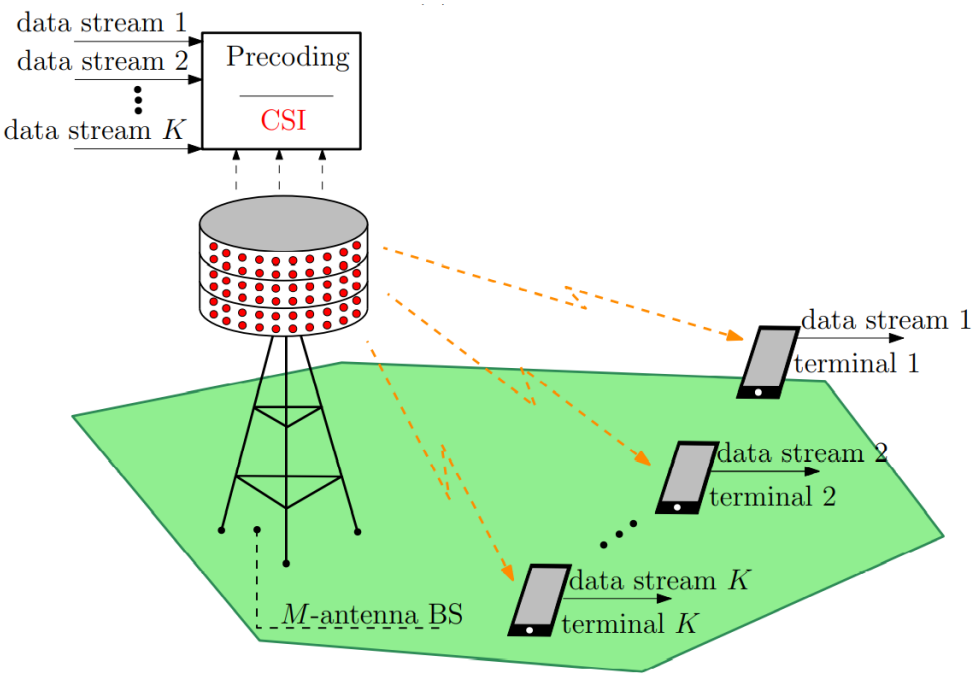

(b) Downlink.

Fig 2.11: Massive MIMO: (a) Uplink transmission, (b) Downlink transmission

2.6.2.1 Uplink massive MIMO based Field Propagation

It is predicted that 6G would boost spectrum efficiency by a factor of 10-fold over 5G as new applications are developed [43]. For 6G, the extreme large scale massive-MIMO (XL MIMO) is an effective strategy for performing this objective, when the BS employs a large antennas number to perform improved energy efficiency and higher spectral efficiency [43]. The highly dimension channel estimation of XL-MIMO, however, requires an unaffordable pilot overhead due to the fast increase of BS antennas.

For XL-MIMO, there are 2- common forms of low-overhead channel estimate algorithms, i.e., FF channel estimation and NF channel estimation [45]. The FF channel estimate in the first category takes channel sparsity in the angle domain into account [45]. According to the planar wave assumption, these methods modeled the channel of XL-MIMO in the FF. On the basis of this supposition, the angle is the only factor affecting the channel's array steering vector. The non sparse spatial channel can initially be depicted by the sparse angle-domain channel using the traditional DFT matrix. Some compressive- sensing (CS) techniques, including orthogonal matching pursuit (OMP), can therefore be utilized to predict this domain of sparse angle channel with minimal overhead of pilot [45].

The other classification is the NF channel estimation that takes into account the domain of polar of channel sparsity. Particularly, the channel of XL-MIMO can be better approximated because to the huge array aperture of XL-MIMO in the NF region with the spherical-wave consideration [46]. According to this supposition, the channel's array steering vector is related to more than just angle, but also associated with the distance between scatter and BS. A number NF channel estimating algorithms have recently been presented, all of which are based on the NF channel model [45-46].

More specifically, a novel representation was presented for sparse of the original XLMIMO channel in the domain of polar, where the traditional DFT matrix exclusively connected to the angle space was replaced by the transform matrix created from the distance space and joint angle. It has been hypothesized that the pilot overhead for NF channel estimation can be decreased by using the appropriate CS algorithms, which take into account the sparsity of channel in the domain of polar [46].

It is considered that each scatter is either in the FF or NF region in the current FF or NF channel model. It is more likely that the system of XL-MIMO will operate in a HF communication environment, whereas others might be found in the region of NF, other scatters may be in the region of FF. When using XL-MIMO, the channel is typically made up of both FF and NF contents of path. However, this hybrid-field channel capability is incompatible with the current FF or NF channel models, because of this, the HF XL-MIMO channel cannot be accurately estimated using the standard FF or NF channel estimating algorithms [45].

2.6.2.2 Signal Model of near field and far-Field uplink XL-MIMO

We assume that in order to connect with a single antenna user, the BS uses an N-element exceptionally large-scale antenna array. Let $\mathbf{b}^H \in \mathbb{C}^{1\times N}$ refers to the channel from the BS to the user. Consider the estimation of the uplink channel, corresponding signal model, which can be expressed by [45]:

$$\mathbf{u}^H = \mathbf{b}^H\mathbf{T}^H + \mathbf{n}^H \tag{2.33}$$

Where the received pilots are represented as $\mathbf{u}^H \in \mathbb{C}^{1\times M}$ of the user in M slots of time, transmitted pilot signals are represented as $\mathbf{T}^H \in \mathbb{C}^{N\times M}$ by the BS in M slots of time, and the $M \times 1$ received noise is represented by $\mathbf{n} \sim \mathcal{CN}(0, \sigma^2\mathbf{I}_M)$ in M slots of time with power of noise (σ^2).

During the conjugate transpose transformation, (2.34) can be further formulated as [46]:

$$\mathbf{u} = \mathbf{Tb} + \mathbf{n} \qquad (2.34)$$

The estimation of uplink channel is to determine b on by knowing that T & u are available. By using extremely large MIMO systems, the antennas number at the base station N is large. So as to decrease the overhead of pilot, it should investigate the channel estimation with low overhead, where the pilot's number M is much smaller than N. Two current models of channel for current channel estimation strategies will be presented.

2.6.2.3 Channel Model of near field and far-field uplink XL-MIMO

Particularly, as depicted in Figure (2.12), in wireless communication systems, the electromagnetic radiation field can be split into two categories, FF and NF, where differing fields will lead to distinct channel models.

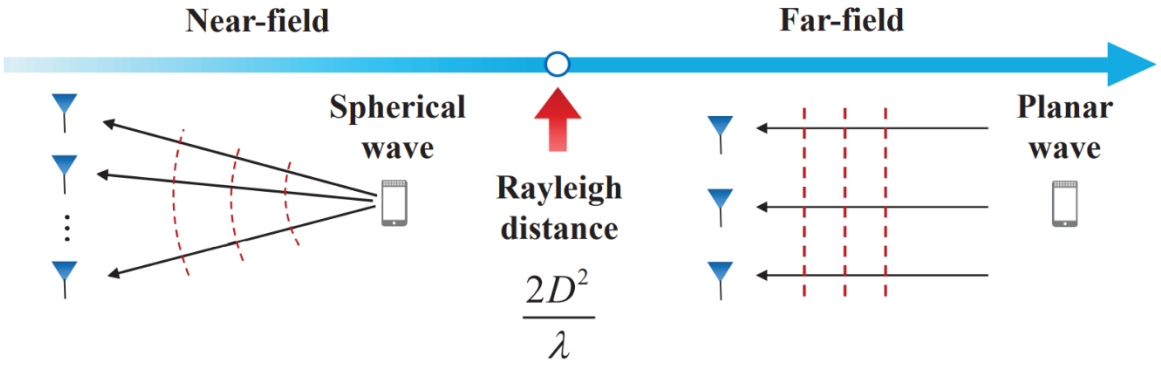

Fig.(2.12): The region of NF and the region of FF [43].

The bound between near and far fields is calculated by the- distance of Rayleigh- $= \frac{2D^2}{\lambda}$, where λ & D are the wavelength and aperture of the array, respectively. The full channel models for FF and NF uplink massive MIMO will be illustrated in Appendix B.

2.6.3 Downlink massive MIMO-OTFS transmission system

As shown in figure (2.13), an OTFS huge MIMO technique uses a BS with q antennas to support UEs, each of which only has one antenna. To make the massive MIMO-OTFS systems more resistant to channel order mis-match and zero location, downlink precoding is implemented [53]. QAM mapping is performed on the stream bits following precoding to create the digitally mapped sequence symbols and the binary data groups [53].

Through OTFS modulation, the 2D transmitted data block x is modulated in the delay-Doppler domain (transmitting windowing function and inverse symplectic finite Fourier transform (ISFFT)). Heisenberg is at the center of the frequency-time domain S. To do this, we must perform a transformation into the time domain [54].

To keep all symbols orthogonal, CP symbols are added to one-dimensional time-domain signals between transmitted and subcarriers for the UE. Upon arrival at the receiver, the time domain received signal r is decoded, removing the CP symbols, before undergoing parallel to serial conversion, also known as de-multiplexing [54]. After the one-dimensional signal has been de-multiplexed, it is changed to the time-frequency domain R using the Wigner transform. After that, OTFS postprocessing is performed on the 2D frequency-time domain R where it will be converted to 2D delay-Doppler from frequency-time domain and QAM demapping is performed, and the resulting binary information is stored that was sent [54]. Finally, equalization is done to delete impairments in the transmitted signal that would otherwise produce a 2D delay-Doppler signal [54]. Figure (2.13) shows block diagram of downlink OTFS-massive MIMO system [54].

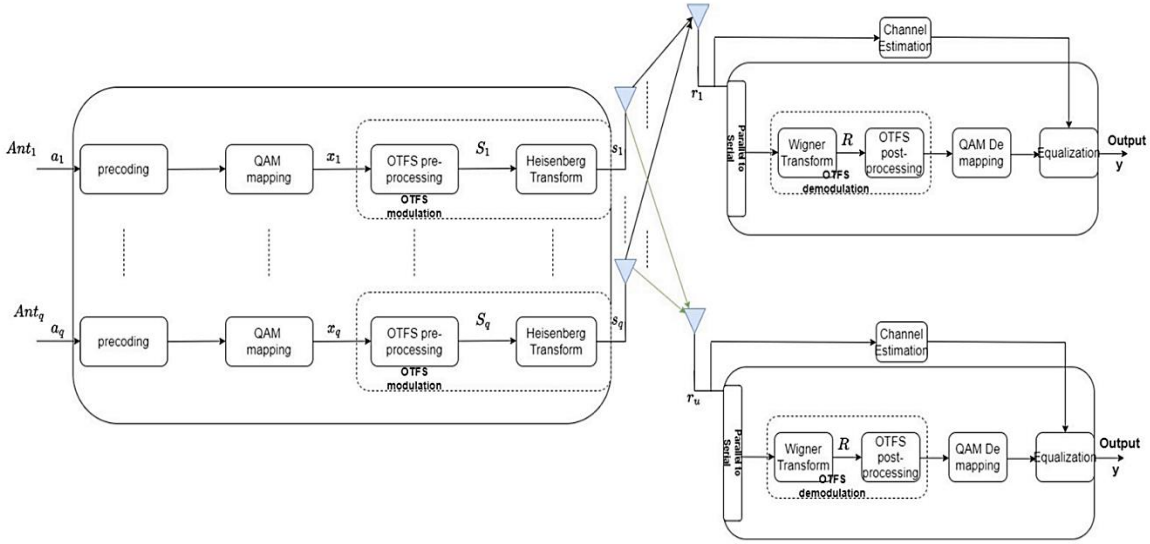

Fig. (2.13): Block diagram of downlink OTFS-massive MIMO [54]

In the massive MIMO-OTFS system model, y represents the signal at the receiver in the delay-Doppler domain. The signal that is received by the q th BS antenna is [54]:

$$y^q = H^q d^q + v^q \tag{2.35}$$

where H^q is the q th in the case of a BS antenna, the gain matrix for the delay-Doppler channel, v^q represent the qth antenna's additive white Gaussian noise (AWGN) appeared in the complete channel with covariance matrix and zero-mean of $\sigma^2 I_u$ because it that makes different noise obtained by each UE [55] and d^q depicts the vector of the transmission symbol of the q th BS antenna's transmitted information $\boldsymbol{a}$,

$$d^q = V^q a^q \tag{2.36}$$

Where pre-coding matrix is represented as V .

2.6.4 Channel Estimation for massive MIMO

Massive MIMO relies on channel state information (CSI) for signal decoding and detection. Information on the status of the communications link

between the transmitter and the receiver is known as CSI and depicts the joined effect of scattering, fading, and so on [113].

Massive MIMO's performance scales linearly with the number of transmitting and receiving antennas if the channel state information (CSI) is perfect, whichever is less. For a network using frequency division duplexing, CSI must be calculated during both the uplink and downlink transmission [114].

When in uplink, the user terminal sends orthogonal pilot signals that are used by the BS to estimate the channel. Additionally, the user acknowledges the base station's pilot signals during the download by providing the estimated channel information for the transmission [114].

The downlink channel estimation approach in FDD becomes extremely complicated and difficult to implement for a massive MIMO system with multiple antennas. The TDD and FDD modes of wireless communications are depicted in figure (2.14a), and the standard transmission of pilot and CSI feed-back mechanisms in TDD and FDD modes are depicted in figure (2.14.b) [115].

TDD offers a solution to the issue with FDD systems' downlink transmission. In TDD, the BS can predict the channel of downlink with the use of information in channel from the uplink by taking advantage of the channel reciprocity property [115]. The user will direct the pilot signals which is orthogonal toward the BS during uplink, and the CSI to the user terminal is estimated by the BS depend on these pilot signals. The BS will then beamform downlink data towards the user terminal according on the estimated CSI.

Pilot contamination occurs because there are a finite number of orthogonal pilots that can be transferred from one cell to another and is an important challenge through channel estimation of massive MIMO.

Additional hardware and processing complexity are also obstacles as a result of a higher antenna count. For massive MIMO systems, channel estimation of a little overhead and low complexity is highly desirable. Recently, various techniques have been developed for massive MIMO systems' channel estimation.

The Least Squares (LS) estimation has a low level of complexity, yet the technique's precision is not the best. For example, the linear MMSE technique is suggested to discuss a number of MMSE algorithm upgrades to be used for channel estimation.

The computational complexity of MMSE grows with the number of antennas, even if it gives ideal accuracy [116]. Since the procedure needs to invert a very big matrix, its complexity grows [116].

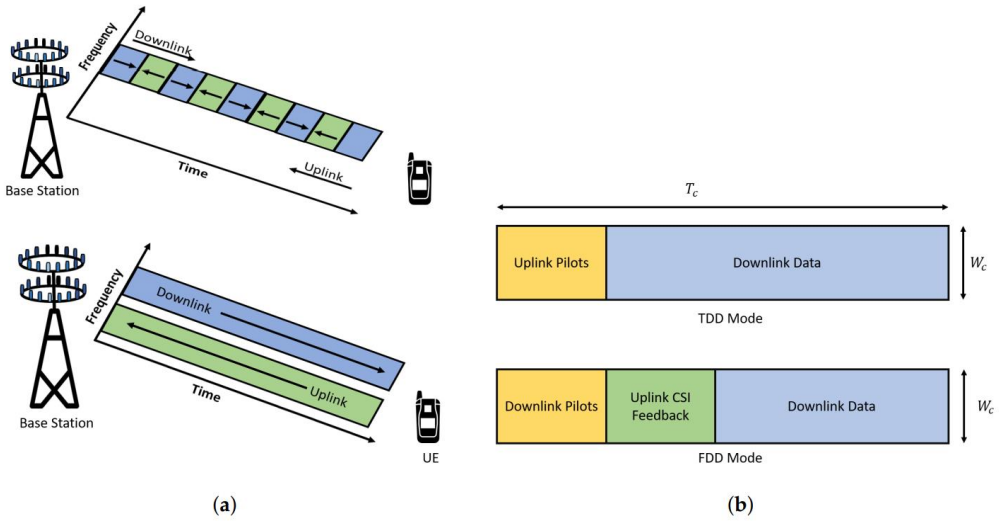

Fig. (2.14): (a) FDD and TDD mode: Massive works best in TDD mode. (b) Transmission of Typical pilot and CSI feedback mechanism in TDD and FDD mode [115]

2.6.5 Precoding of massive MIMO

Beamforming relies on the idea of pre-coding, which enables the simultaneous broadcast of several streams over a network of antennas. Pre-coding is crucial in mMIMO systems because it helps reduce the impact of path interference and loss, and increases the throughput [117]. Massive-MIMO system rely on the base station to estimate the CSI by analyzing uplink pilot signal or user terminals feedback.

Due to a number of external conditions on the wireless channel, the received CSI at the BS is controlled and is not perfect. Downlink performance at the BS is highly dependent on the estimated CSI even when the base station does not get perfect CSI [118].

As a result, the base station uses the pre-coding approach and approximated CSI to reduce interference and increase SE. The effectiveness of massive MIMO in downlink depends on the pre-coding method used and an exact estimation of CSI [119].

While the pre-coding technology has enormous benefits for mMIMO system, it also adds computational-complexity to the system as a whole [120]. With more antenna, the computational complexity is increased. Therefore, it is more practical to use low-complexity, high-efficiency pre-coders in massive MIMO systems. The Figure (2.15) explains the pre-coding in M-antenna BS and N-user with massive MIMO systems.

By using massive MIMO techniques, many nonlinear and linear pre-coders have been suggested. Despite that the Tomlinson Harashima precoding, nonlinear pre-coders like Dirty Paper Precoding (DPP), and Vector Perturbation (VP) achieve better results, when we have large antenna system, these techniques have very high complexity in computational [121].

The linear pre-coders like as Zero-Forcing (ZF), Maximal Ratio Combining (MRC), MMSE and so on have smaller computational-complexity and can provide near-ideal assessment. Figure (2.15) shows precoding principle [122].

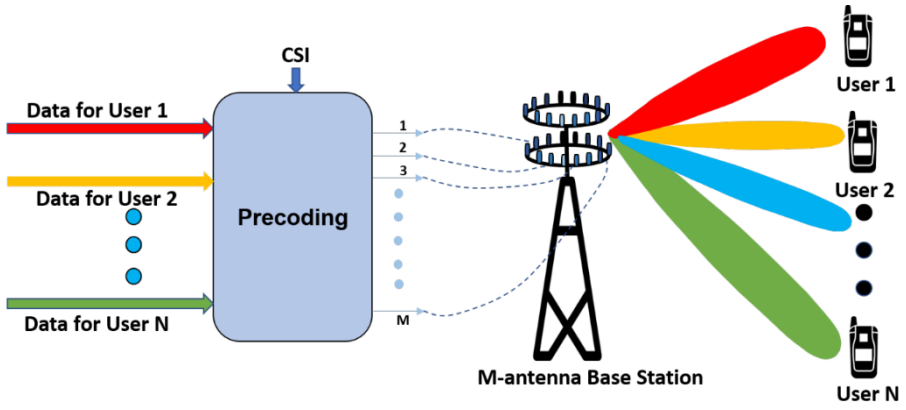

Fig. (2.15): Multiple (M) antennas at BS communicating with N users for Precoding in a massive MIMO system [122]

2.7 RoF Link configurations

As shown in Figure (2.16) [48], the RoF link can be viewed as a subsystem in a wider RF system. Radio signals from radio antennas are transmitted through fibre optics to boost the signal's transmited from the station [48].

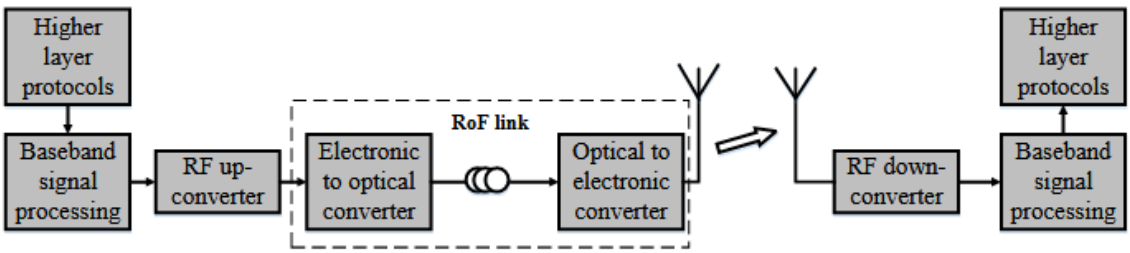

Fig. (2.16): RoF link [48]

Data from the higher-level protocols are transmitted for basic signal processing where modulation and coding processes occur. This transmits the fundamental band signal for an optical to optical transducer and transmits the optical signal to the optical transducer (typically a photodiode) at the receiving end via the fibre cable to collect the signal before the wire is linked. The signal will be translated to RF and applied to a RoF connection. The receiving device (mobile telephone, laptop etc.) is transformed by the RF signal to the baseband before it is transmitted to high-level protocols.

The easiest is a fibre-over-FF connection, in which the RF signal can be utilised to modulate the laser transmission and the resulting optical signal transmits to a PD receiver via a fibre optic cord as shown in Figure (2.17) [48]. The PD recalls and amplifies the RF signal for wireless transmission

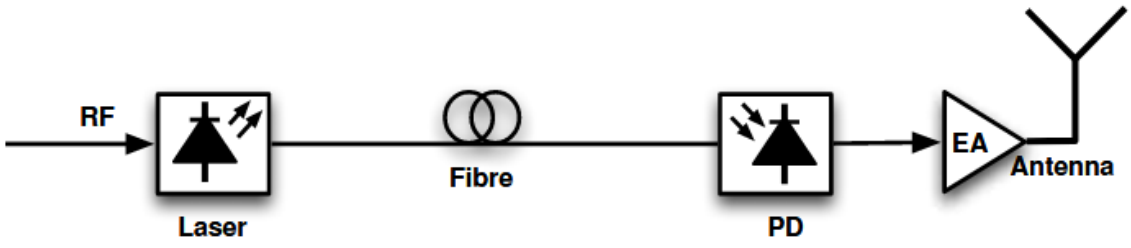

Fig. (2.17): RF-over-fibre link

With the benefit of the RF-over-fiber connection, all other functions are carried out in the RAU in addition to signal amplifying and optoelectronic conversion, making it easy to operate and update operations. The fundamental problem of the RF-over- fibre links is that RF-optical components with minimal noise and distortions are difficult to accomplish at such frequencies, as analogue transmission, especially at high frequencies, cannot be distorted particularly (beyond 3 GHz).

A choice for RF-Over-Fiber is the IF-Over-Fiber Link, which is normally utilised in a high-frequency domain where the RF signal is translated into a lower frequency (IF) and used for laser transmission modulation. As demonstrated in Figure (2.18) [48], optical fibre will revert back to the frequency of its RF signal before the wireless transfer to the PD sensor.

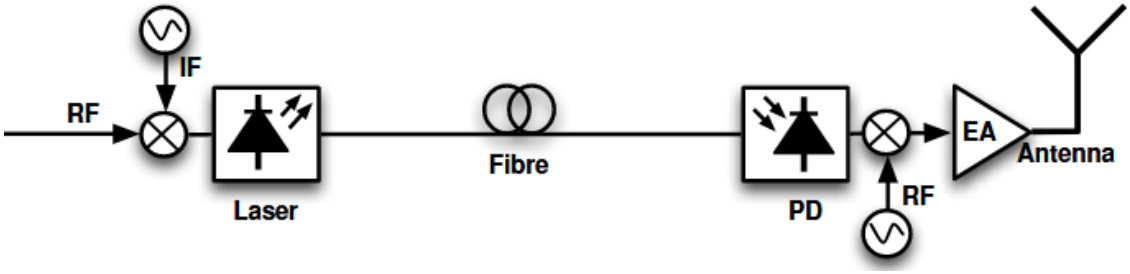

Fig. (2.18): IF-over-fibre link

The advantage is that it enables the employment of a simple direct detection (IM-DD) intensity modulation and a low frequency semiconductor laser diode transmitter, while local oscillators and mixers are additional expenses in connection with the converting of IF/RF. In general, the RF signal generated as an analogue RoF transmission waveform is usually supplied and employed in the recipients to modulate an optical source. However, an optical source can be modified and supplied via an optical fibre before using this RF signal. The PD retrieves a digital RF signal from the receiver and transforms it in the analogue signal, as seen in Figure (2.19) [48].

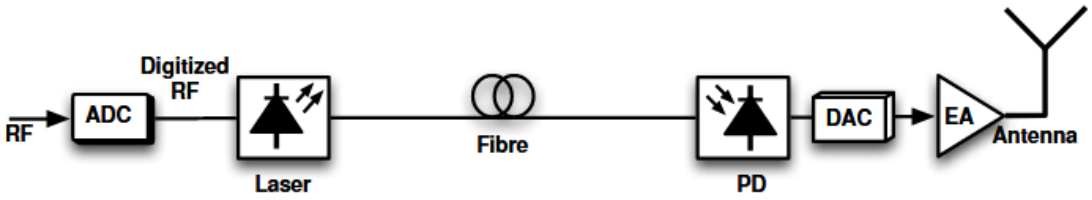

Fig. (2.19): Digitized-RF-over-fibre link [48]

This RoF link is referred to as a digital RF connection over a fibre. Digital RF signal digitisation is carried out before the laser transmitter with an analog-to-digital converter (ADC) and after the PD receptor the digital RF signal is converted back to its analogue form with a digital DAC converter.

The benefit of the fiber-on-fiber Digitized RF link is to prevent nonlinearity of analogue transmission, since it can retain its dynamic range regardless of the transmission distance until the received signal is below the connection sensitivity [49]. The component sites are however scattered. The link is increasingly complex compared to other arrangements between the CU and RAU.

2.8 Hybrid OFDM RoF-Based WDM-PON/MMW Downlink System Design

Data are separated into many parallel low-rate sub-carriers in an OFDM transmitter from the single source data [51]. These subcutaneously are modulated in distinct modulation techniques such as QAM, QPSK on different subcontractors and must be mutually orthogonal. IFFT is used to convert complex QAM symbols to OFDM subcontractors (OFDM symbols). Figure (2.20) shows architecture of hybrid OFDM RoF-depend WDM-PON/MMW downlink [52]. There are four main subsystems in the downlink, containing CS, MBS-located remote antenna unit (RAU), WDM-PON based ODN, and SBSs-located remote radio heads (RRHs). Considering the bandwidth requirements for a backhaul link, we look into the four-wavelength WDM-PON. Based on the selected modulation method at the CS, e.g., M-QAM, each subcarrier is assigned a complex symbol by the OFDM modulator, which is used to transmit the data. The intensity modulation foundation of the optical modulator [52].

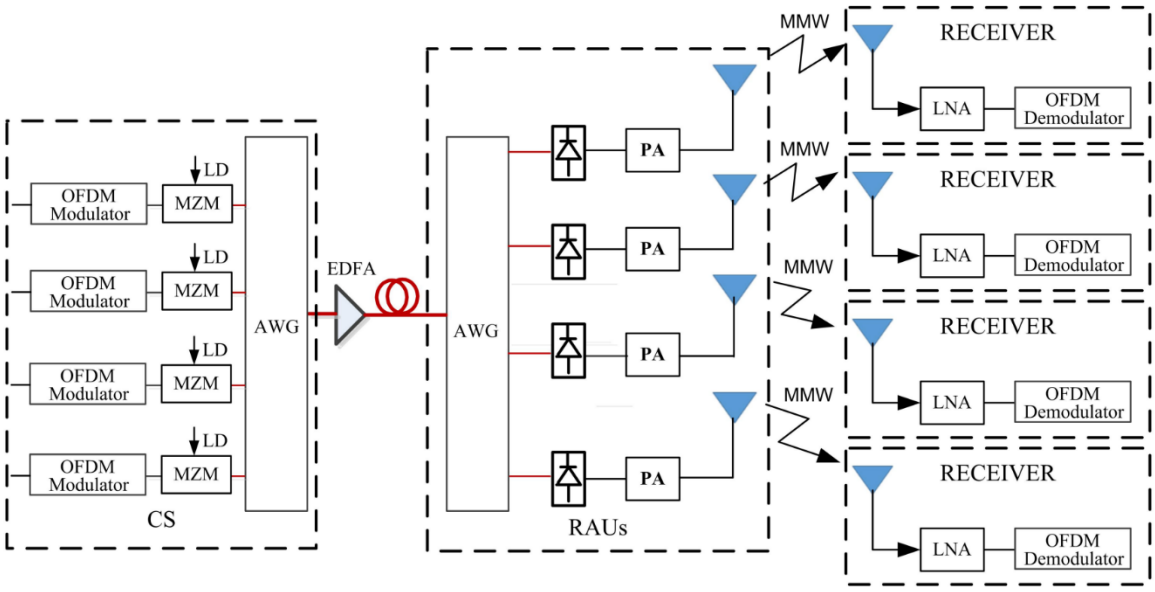

Fig. (2.20): Schematic of Hybrid OFDM RoF-Based WDM-PON/MMW backhaul Transmission system [52]

In combinations, the signals of two OFDM transmitters are applied to the MZM module. A light signal from the CW laser source is imposed on this OFDM signal. The mathematical modelling of RoF-MMW bachhaul transmission will be illustrated at Appendix C.

Thus, the signal is transformed by a modulator MZM from an electric domain into an optical fibre. Both 'I' and 'Q' in-phase components for IMDD are sent individually by QAM modulation. The modelling details of Dual output Mach-Zehnder Modulator is shown in appendix D.

The optical to RF converter of the optical-OFDM signal in the receptors section is used to convert its electrical equivalent, that is, the RF-OFDM signal [52]. The picture detector is used to do this. Following this, OFDM process of demodulation begins. Where the OFDM RF modulated signal is separated into the many streams for each sub-individual carrier's detection. The resulting QAM signal is sent to a QAM demodulator where the components 'I' and 'Q' are demodulated and supplied to the visualizers.

2.8.1 Mathematical Modeling of MMW-RoF Super high speed transmission System

With this scheme, a flexible-frequency MMW signal could be generated, presenting a simple and flexible method for MMW signal generation. In our framework, a signal with a frequency separation of six times the input electrical signal frequency is selected. An optical amplifier (EDFA) is used to boost the optical power, and an optical bandpass filter (OBPF) is used to reduce the amplified spontaneous emission noise. The optical signal at the output of the optical MMW signal generator can be expressed by [47]:

$$E(t) = A_{+}\cos[(\omega_0 + 3\omega_{\mathrm{LO}})(t+\tau_d) + \varphi_{+}(t+\tau_d)] + A_{-}\cos[(\omega_0 - 3\omega_{\mathrm{LO}})t + \varphi_{-}(t)] \quad (2.37)$$

where $\varphi_{+}(t) = \varphi_0(t) + 3\varphi_1(t), \varphi_{-}(t) = \varphi_0(t) - 3\varphi_1(t), A_{+}$and A_{-}denote the amplitudes of the third-order upper and lower sideband, respectively, and ω_0 and $\varphi_0(t)$ are the angular frequency and phase of optical signal from the laser, respectively, ω_{LO} and $\varphi_1(t)$ are the angular frequency and phase of the electrical signal from the local oscillator (LO), respectively, and τ_d is the time delay corresponding to the optical path differences between the two optical sidebands.

The polarization of the generated signal is then adjusted by a polarization controller (PC). The generated two-tone optical signal is then inputted into a second MZM, which is connected to a RF input from a vector signal generator (Agilent PSG). Both generated optical sidebands are modulated by the wireless signals, and a RoRoF signal consisting of the wireless signals superposed on the MMW carrier is generated. The signal after being modulated by the wireless signals at the optical modulator biased at a quadrature point could be written as [47]:

$$\begin{aligned} E_1(t) = \quad & IL \cdot E(t) \cdot \cos\left(\frac{\pi}{2V_\pi}S(t) - \frac{\pi}{4}\right) \\ = \quad & IL \cdot A_+ \cos\left(\frac{\pi}{2V_\pi}S(t) - \frac{\pi}{4}\right) \\ & \times \cos\left[(\omega_0 + 3\omega_{\mathrm{LO}})(t+\tau_d) + \varphi_+(t+\tau_d)\right] \\ & + IL \cdot A_- \cos\left(\frac{\pi}{2V_\pi}S(t) - \frac{\pi}{4}\right) \\ & \times \cos\left[(\omega_0 - 3\omega_{\mathrm{LO}})t + \varphi_-(t)\right] \end{aligned} \tag{2.38}$$

where IL is the insertion loss, V_π is the switching voltage of the optical modulator, and $S(t)$ is the wireless signal applied to the modulator. The generated signal is amplified by the second EDFA and filtered out by another OBPF. The signal is then input into an SMF and transmitted to a RAU. When distributing along the fiber with a propagation constant of $\beta(\omega)$ and an amplitude attenuation of γ, the optical sidebands are transmitted at different velocities because of fiber chromatic dispersion. After transmission over a z-length fiber, the signal becomes [49]:

$$\begin{aligned} E_2(z,t) = \quad & IL \cdot A_+ \cdot \cos\left(\frac{\pi}{2V_\pi}S\left(t - (\omega_0 + 3\omega_{\mathrm{LO}})^{-1}\beta\left(\omega_0 + 3\omega_{\mathrm{LO}})z\right) - \frac{\pi}{4}\right)e^{-\gamma z} \\ & \cdot \cos\left[(\omega_0 + 3\omega_{\mathrm{LO}})(t+\tau_d) - \beta(\omega_0 + 3\omega_{\mathrm{LO}})z + \varphi_+(t+\tau_d)\right] \\ & + IL \cdot A_- \cos\left(\frac{\pi}{2V_\pi}S(t - (\omega_0 - 3\omega_{\mathrm{LO}})^{-1}\beta(\omega_0 - 3\omega_{\mathrm{LO}})z) - \frac{\pi}{4}\right)e^{-\gamma z}. \\ & \cos\left[(\omega_0 - 3\omega_{\mathrm{LO}})t - \beta(\omega_0 - 3\omega_{\mathrm{LO}})z + \varphi_-(t)\right] \end{aligned} \tag{2.39}$$

We can rewrite (2.39) as [47]:

$$\begin{aligned} E_2(z,t) = \quad & B_+ \cos\left[(\omega_0 + 3\omega_{\mathrm{LO}})(t+\tau_d) - \beta(\omega_0 + 3\omega_{\mathrm{LO}})z\right. \\ & \left. + \varphi_+(t+\tau_d)\right] + B_- \cos\left[(\omega_0 - 3\omega_{\mathrm{LO}})t\right. \\ & \left. - \beta(\omega_0 - 3\omega_{\mathrm{LO}})z + \varphi_-(t)\right] \end{aligned} \tag{2.40}$$

Where:

$$B_{\pm} = IL \cdot A_{\pm.} \cdot \cos\left(\frac{\pi}{2V_{\pi}} S\left(l - (\omega_0 \pm 3\omega_{\mathrm{LO}})^{-1}\beta\left(\omega_0 \pm 3\omega_{\mathrm{LO}}\right)z\right) - \frac{\pi}{4}\right) e^{-\gamma z} \quad (2.41)$$

The signal then is up-converted to a radio-on-radio (RoR) signal at 90GHz by a high-bandwidth photodiode (u2t − PD). The emitted signal is represented by [51]:

$$I(t) = \mu \cdot |E_2(z,t)|^2 = \mu \cdot B_+ \cdot B_- \cdot \cos \times \begin{bmatrix} 6\omega_{\mathrm{LO}}t + 3\omega_{\mathrm{LO}}\tau_d - \beta(\omega_0 + 3\omega_{\mathrm{LO}})z \\ +\beta(\omega_0 - 3\omega_{\mathrm{LO}})z + \varphi_+(t+\tau_d) - \varphi_-(t) \end{bmatrix} \quad (2.42)$$

By using the relations:

$$\beta(\omega_0 \pm 3\omega_{\mathrm{LO}}) = \beta(\omega_0) \pm 3\omega_{LO}\beta'(\omega_0) + \frac{1}{2}(3\omega_{\mathrm{LO}})^2\beta''(\omega_0) \quad (2.43)$$

We can rewrite (2.43) as

$$I(t) = \mu B_+ B_- \cos \begin{bmatrix} 6\omega_{\mathrm{T}.O}t + 3\omega_{\mathrm{I}.O}\tau_d + \varphi_+(t+\tau_d) \\ -\varphi_-(t) - 6\omega_{\mathrm{LO}}\beta'(\omega_0)z \end{bmatrix} \quad (2.44)$$

where μ is the photodiode efficiency. It should be noted that the terms of optical carrier ω_0 and the dc component are not detected by the photodiode. Based on the signal formula shown in (2.44), it is observed that there is no fading in the RF signal at the frequency of $6\omega_{\mathrm{LO}}$ when using only the sideband components to carry the data signals. The signal in the form of (2.44) is then directly emitted into free space by a horn antenna and is collected by another antenna at a receiver site. The received signal at the output of the antenna could be written by [48] :

$$I_r(t) = \frac{I(t) \times G_t \times G_r}{\mathrm{Loss}} \times r \times e^{-j\theta} \quad (2.45)$$

where G_t and G_r are the gain of the antennas at the transmitter (RAU) and the receiver (RRH), r and θ are random amplitude and phase because of Rician fading, and Loss is the free-space loss calculated by Friss equation [52].

The signal is then down-converted to the original wireless signals by a W-band double-balanced mixer (DBM) and an LO and amplified by a low-noise amplifier. The frequency of the output signal from the LO is same as the frequency of the MMW signal generated at the transmitter site, i.e. $6\omega_{\mathrm{LO}}$. We suppose that the electrical field of the signal from the LO is expressed as [49]:

$$E_2(t) = E_2 \cos\left(6\omega_{\mathrm{LO}} t + 6\varphi_2(t)\right) \tag{2.46}$$

where E_2 is amplitude of the generated signal and $\varphi_2(t)$ is phase jitter of the input electrical signal to the frequency multiplier (multiplication factor of 6). Finally the transmitted IF is recovered by mixing the received MMW signal with the signal generated from the LO, and can be written by

$$r(t) = \frac{\mu \times \beta_+ \times \beta_- \times G_t \times G_r \times E_{\mathrm{LO}}}{\mathrm{Loss}} \times r \times e^{-j\theta} \times \kappa \times \cos\left[\varphi_0(t+\tau_d) - \varphi_0(t) + 6\left(\varphi_1(t) - \varphi_2(t)\right) + \left(3\varphi_{LO}\tau_d - 6\omega_{LO}\beta'(\omega_0 z)\right)\right] \tag{2.47}$$

2.9 Modern Modulation formats

A digital modulation format is a set of discernible symbols. Each symbol is defined from a finite set of states. These states can be frequencies and the associated modulation format is known as frequency shift keying (FSK), or amplitudes for amplitude shift keying (ASK), or phases leading to phase shift keying (PSK), or both phases and amplitudes for quadrature amplitude modulation (QAM). In case of amplitude/phase modulation, the combination of states can be represented by a constellation [80].

A modulation scheme is also characterized by the average energy of its constellation denoted as E_s and its bitrate. If each symbol is transmitted during time Ts, the symbol rate can be defined as $R_s = 1/T_s$ symbols/s (or baud). The corresponding bit rate Rb is related to the symbol rate R_s by [80]:

$$R_b = log_2(q)\ R_s = k_N R_s \quad (2.48)$$

The symbol k_N is represented by the below vector:

$$c_k = c_{k,1}, c_{k,2}, \dots, c_{k,N} \quad (2.49)$$

so that *N* is dimensions number.

2.9.1 Quadrature phase shift keying

To overcome the limitation in the spectral efficiency of a single bit per information symbol, multi-level modulation formats are needed. The first to be investigated in optical communication was QPSK which is a multi-phase modulation scheme with four distinct symbols exp(*i*Φ*s*) having the same amplitude and four equally separated phases as shown in Figure 2.21. Hence, QPSK can encode two bits in each symbol, one in-phase and the other in-quadrature. The bits are mapped to the symbols using natural coding or a binary gray coding where the bit sequences assigned to two neighboring constellation points differ in only one bit.

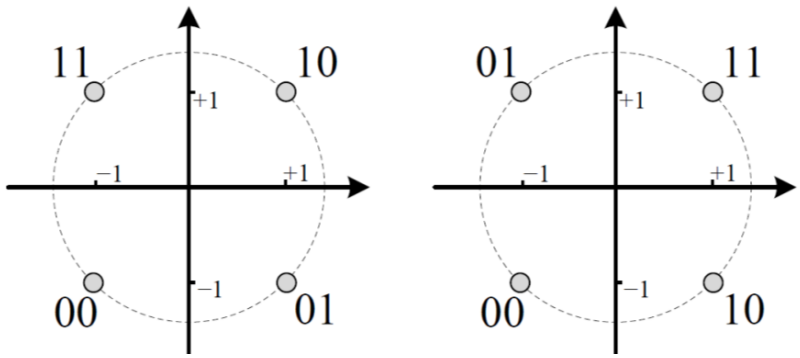

Fig. (2.21): Mapping of bit to symbol using (left) natural-mapping and (right) Gray-coded mapping of bit to symbol for QPSK [80]

The extremely investigated modulation technique in coherent transmission systems is (PM-QPSK) because of many reasons. The complexity of transmitter is little as it is performed with binary active signs, essentially tracking of phase by DSP algorithms, can be implemented at acceptable complexity and the susceptibility of QPSK is appropriated for very high distances like long reach links.

The constellation of QPSK will be presented as below:

$$C_{QPSK} = (\pm 1, \pm 1) \quad (2.50)$$

While PM/QPSK expressed as:

$$C_{PM-QPSK} = (\pm 1, \pm 1, \pm 1, \pm 1) \quad (2.51)$$

The x polarization and y polarization constellations for PM/QPSK are presented in figure (2.22). It was noticed that the constellation for both states of polarization is independent.

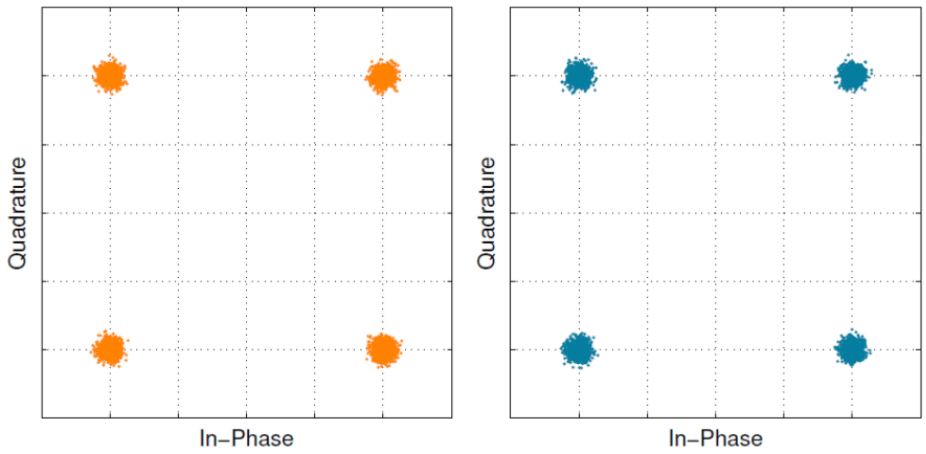

(a) x-polarization (b) y-polarization

Fig. (2.22): Constellation for PM-QPSK signal (a) x axis (b) y axis [80]

A perfect system of PM/QPSK is presented in the below figure. Both signals are composed with perpendicular polarized states by performing a polarization-beam-combiner (PBC). There is another way for QPSK format

implementation by performing a Mach-Zehnder modulator (MZM) put up with the phase-modulator. Additionally, it is enjoyable to see QPSK is originally coded with gray code when performed by I/Q active signs.

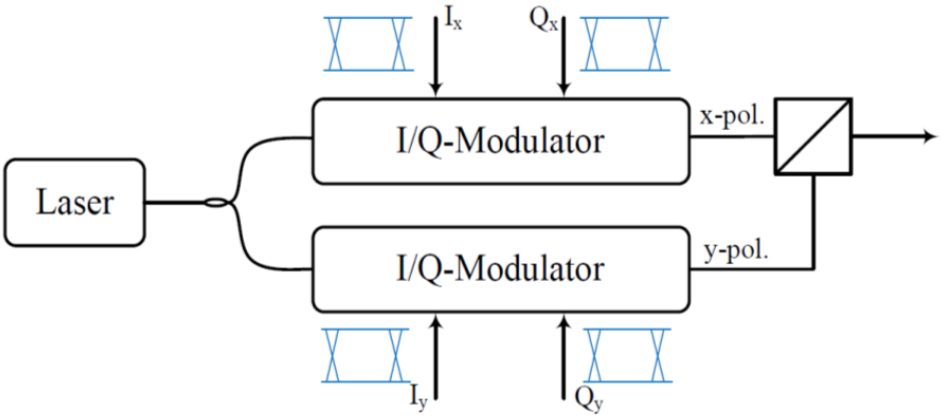

Fig. (2.23): A typical PM-QPSK transmitter [80]

2.9.2 16 QAM (Quadrature amplitude modulation)

Quadrature amplitude modulation (or q-QAM) consists in modulating both phase and amplitude of the signal. The q symbols can be represented by a complex number in polar coordinates: $A_s exp(i\Phi_s)$. Different flavors of QAM exist such as rectangular QAMs that can be easily implemented with two amplitude modulations on quadrature carriers.

The spectral efficiency of a q-QAM constellation is given by $k_c = \log_2 q$. The main advantage of multilevel modulation formats is the increased bitrate over a limited spectral bandwidth. For future optical communication systems, 16-QAM is being considered to achieve a 2-capacity increase factor or higher compared to QPSK. This capacity increase comes at the cost of complex transmitters and receivers as well as an augmented sensitivity to both linear and non-linear effects. Rectangular type of 16QAM has the advantage that it can be performed by equi-spaced four-level signs that can be obtained in by joining two binary channels by an RF-coupler. PM/16QAM constellation will be illustrated as below:

$$C_{PM-16QAM} = \{(\{\pm 1, \pm 3\}, \{\pm 1, \pm 3\}, \{\pm 1, \pm 3\}, \{\pm 1, \pm 3\})\} \quad (2.52)$$

PM-16QAM contains spectral efficiency of 4 bits/symb/pol in the x- and y-polarization states as presented below. The ideal PM/16QAM diagram is presented in Fig. (2.24).

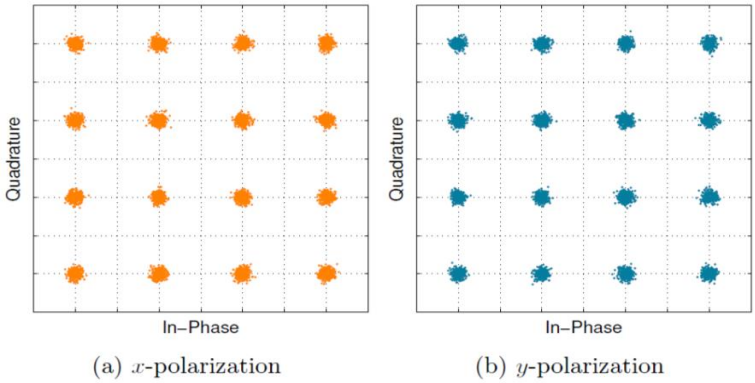

Fig. (2.24): Constellation of PM-16QAM channel (a) x axis and (b) y-axis [80]

I/Q-signs are activated by 4PAM channels generated from binary signals. Many transmitter designs performed, like performing both I/Q-modulators in series or performing modulators with 4 MZMs. As compared with QPSK, the PM/16QAM is not naturally Gray-coded and a pre-coding step is required. As a result of PM-16QAM sensitivity to noise of laser-phase, differential-coding for bits required. A typical PM-16QAM transmitter is presented below:

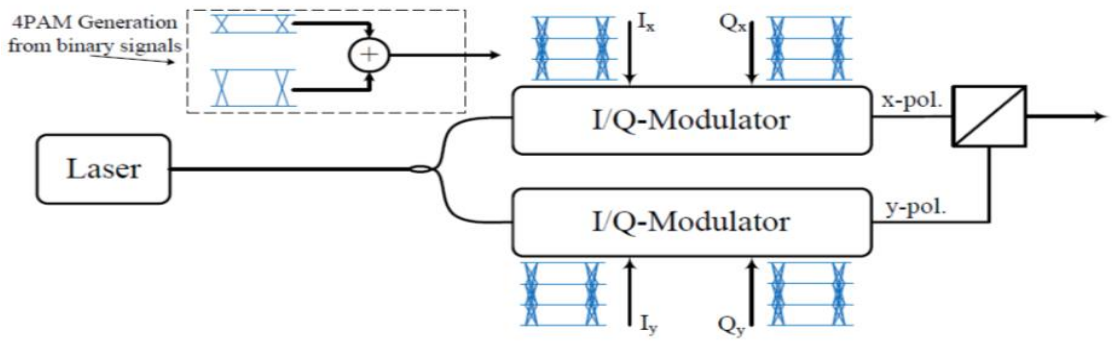

Fig. (2.25): A typical PM-16QAM transmitter [80]

2.9.3 Mach-Zehnder modulator

A MZM is an interferometer composed of two 3 dB couplers and two arms of Lithium Niobate crystal as shown in figure (2.26). The modulation occurs by applying a driving voltage to the arms that modifies their refractive index, controlling hence the phase of the light propagating through the arms and creating constructive and destructive interference at the output of the MZM. This interference translates into amplitude fluctuations of the optical signal. The input-output characteristic of an MZM is given by [123]:

$$E_{out} \alpha E_{in} \cos\left(\pi \frac{V_1 - V_2}{2V_\pi}\right) \qquad (2.53)$$

where E_{in} and E_{out} are the fields at the input and output of the modulator respectively, V1 and V2 are the voltages applied to the arms, and Vp is the drive voltage corresponding to a phase shift from a constructive (maximum) to a destructive (minimum) interference (transmittance). With adequate electrical voltages, MZMs can be used for digital modulations (on-off keying, binary phase shift keying, QAM...) or analog modulations such as OFDM.

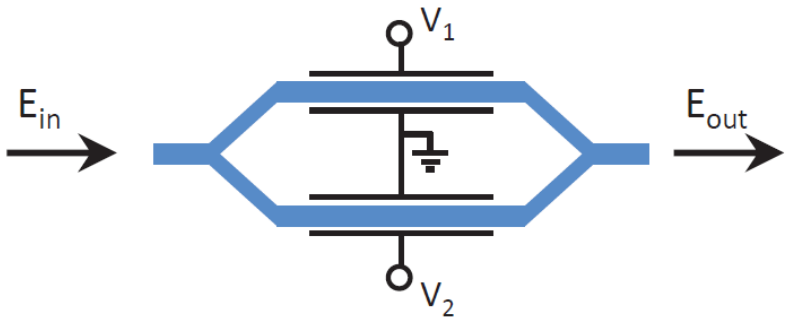

Figure (2.26): schematic figure of an MZM [123]

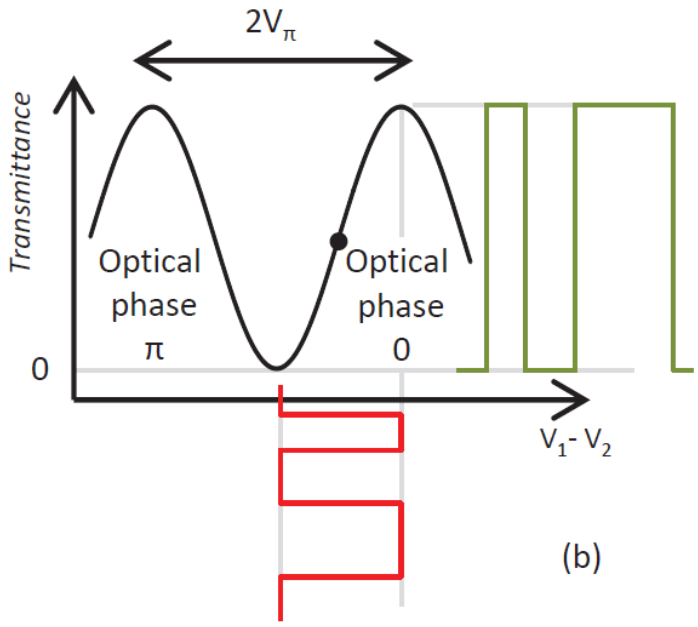

Figure (2.27): Power transmittance with MZM biased at the quadrature point [123]

Chapter Three

Proposed OFDM-RoF-MMW based massive MIMO Systems

3.1 Introduction

This chapter explains the system's description for the massive MIMO techniques and OFDM-RoF-MMW systems which are the proposed works for our thesis. There are two main proposed systems will be illustrated. The first proposed system is an efficient wireless transmission between user and base station based on orthogonal Time Frequency Space (OTFS) Modulation.

A proposed system including Massive MIMO-OTFS techniques can be modified for downlink scenario. Many precoding techniques will be presented to obtain best NMSE for different values of SNR. Both wireless systems implemented by using MATLAB2020a software. Many techniques will be added to improve the performance of the system and to increase the overall bit rate.

Our suggested system will be investigated under different metrices such as SNR, NMSE, number of users, and number of base station's antennas. From other side, to obtain ultra-high capacity between central base station (CBS) and remote antenna unit (RAU) a backhaul hybrid RoF-MMW-OFDM system will be proposed. The designed RoF-MMW-OFDM system will be implemented using VPI Photonics version 9.8

All optical OFDM system will be implemented as complementary solution to increase the capacity of backhaul transmission system to achieve ultra-high-capacity system with long transmission distances. The main diagram for the general proposed systems B5G is shown in figure (3.1).

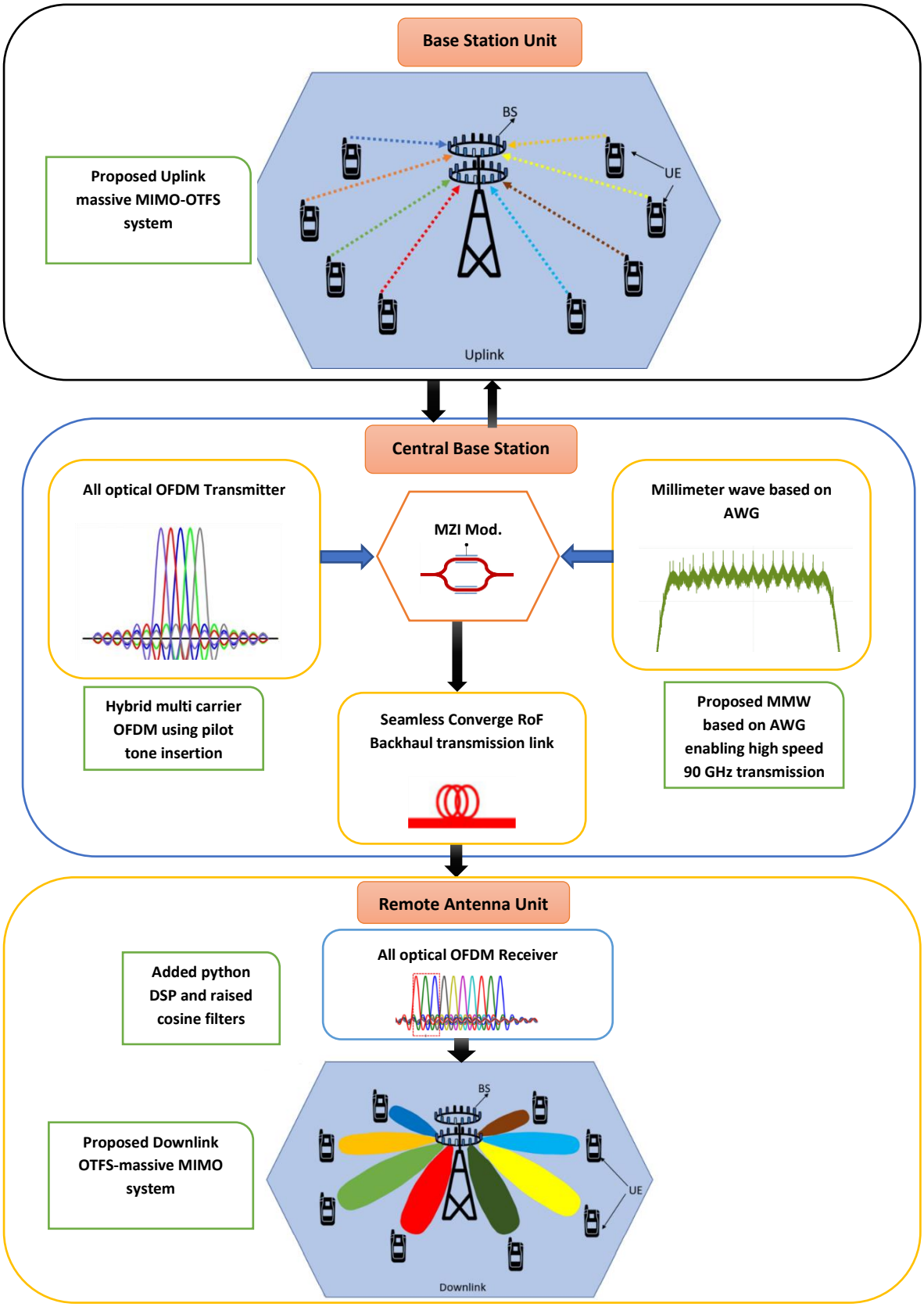

Fig. (3.1): General Block diagram of Proposed System for B5G

3.2 System Description of Wireless Transmission systems

System Description for MIMIO uplink wireless transmission systems will be presented in the following sections. At first, a wireless transmission system based on 2×2 MIMO system will be proposed. Then, a proposed mMIMO system based on OTFS will be implemented. Both systems will be tested under different metrices to obtain best technology with higher overall uplink and downlink transmission performance.

3.2.1 MIMO 2×2 System Design

This section presents proposed Multiple Input Multiple Output (MIMO) system, that use more antennas than one at the transmitter and receiver sides of a regular wireless communication system. To decrease the effects of losses and fading over communication transmission link, an efficient diversity reception technique had been used in the proposed system. Figure below shows block diagram of proposed MIMO transmission system.

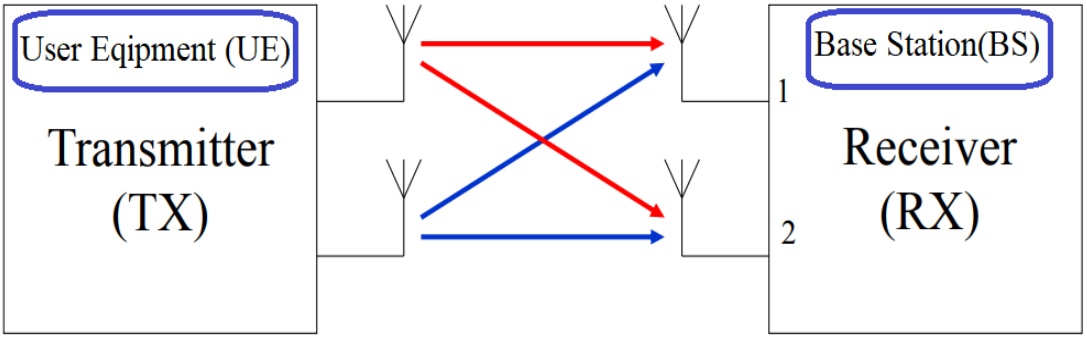

Fig. (3.2): Proposed diagram of 2×2 MIMO uplink wireless transmission link

The simulated 2×2 MIMO system archives an end-to-end wireless system containing the transmitted user signal, channel modelling, and received signal at base station with de-modulation of the required signal. The main parameters of the proposed system will be presented in table (3.1).

Table (3.1): Parameters of proposed 2×2 MIMO uplink system

Parameter	Value
Frame length	100
Number of packets	100-1000
Eb/No	0-20 dB
Tx Number of antennas(N)	2
Rx Number of antennas(M)	2
Type of Modulation	BPSK, QPSK

The channel here will be assumed to be perfect for all systems at the receiver side. The simulation will be run over a different value of Eb/No to obtain BER different results that allow the comparison between different systems.

The computation complexity of the transmitter diversity system is similar to receiver diversity system. There is a comparison between the diversity of transmitter and receiver by making a simulation of BPSK or QPSK transmitter over flat fading Rayleigh channel by adding additive White Gaussian Noise (AWGN). For diversity of transmitter, two transmitted antennas used with one receiver's antenna. From diversity of receiver side, we use one transmitted antenna and two receiver's antennas.

3.2.2 Description of proposed massive MIMO-OTFS system

In this section, we use multiuser MIMO to demonstrate how OTFS is employed in large MIMO networks to further energy efficiency and improve spectrum. Figure (3.16) explains the architecture of massive MIMO-OTFS. BS is provided with N_t antennas to support users with a single antenna in a continuously.

Inter-user interference can be reduced with the use of pre-coding in the downlink. In FDD systems, uplink channel feedback is used to produce downlink faulty CSI, which is then used for downlink pre-coding. The transfer block-data $\mathbf{X}^{DD}$ in the domain of Delay Doppler will be pre-coded, followed by modulation of OTFS and transmission by N_t antennas. The demodulation of OTFS is achieved on the user's end to get the data block $\mathbf{Y}^{DD}$ from receiver signals in the domain of Doppler-delay. On the basis of the downlink CSI, equalization is carried out to remove inter-symbol interference.

Figure (3.3) shows the diagram of massive MIMO architecture based on OTFS for downlink transmission.

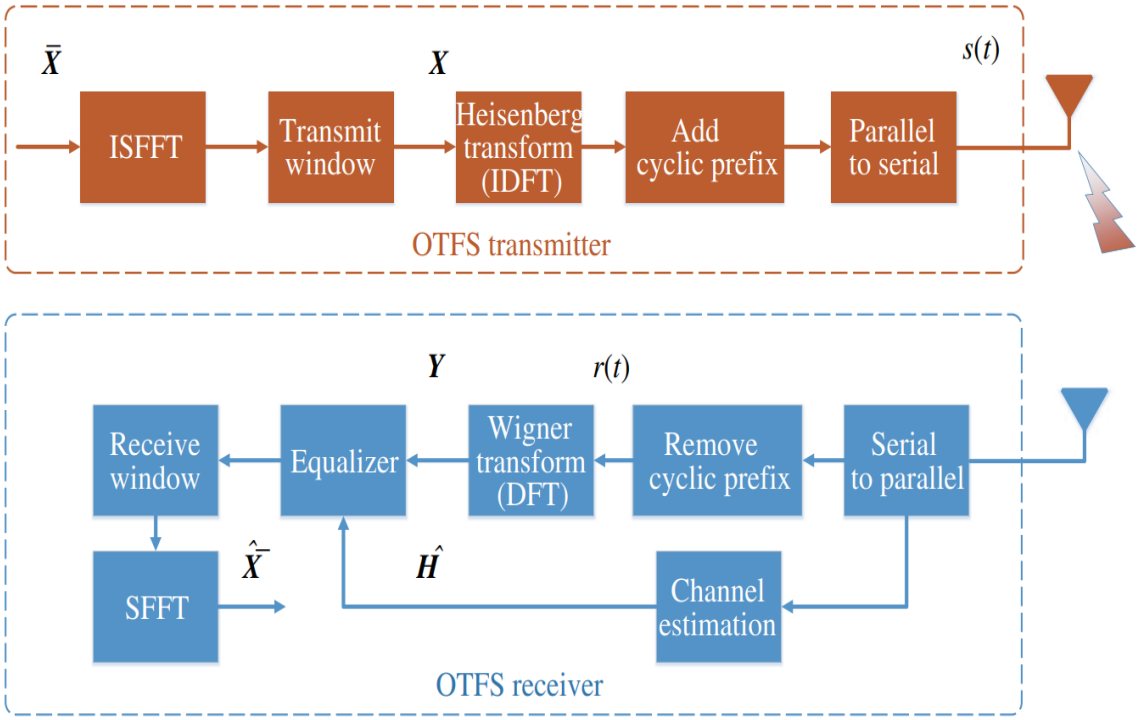

Fig. (3.3): Massive MIMO architecture based on OTFS for downlink transmission

Figure below shows the Simulink of orthogonal time frequency transmitter.

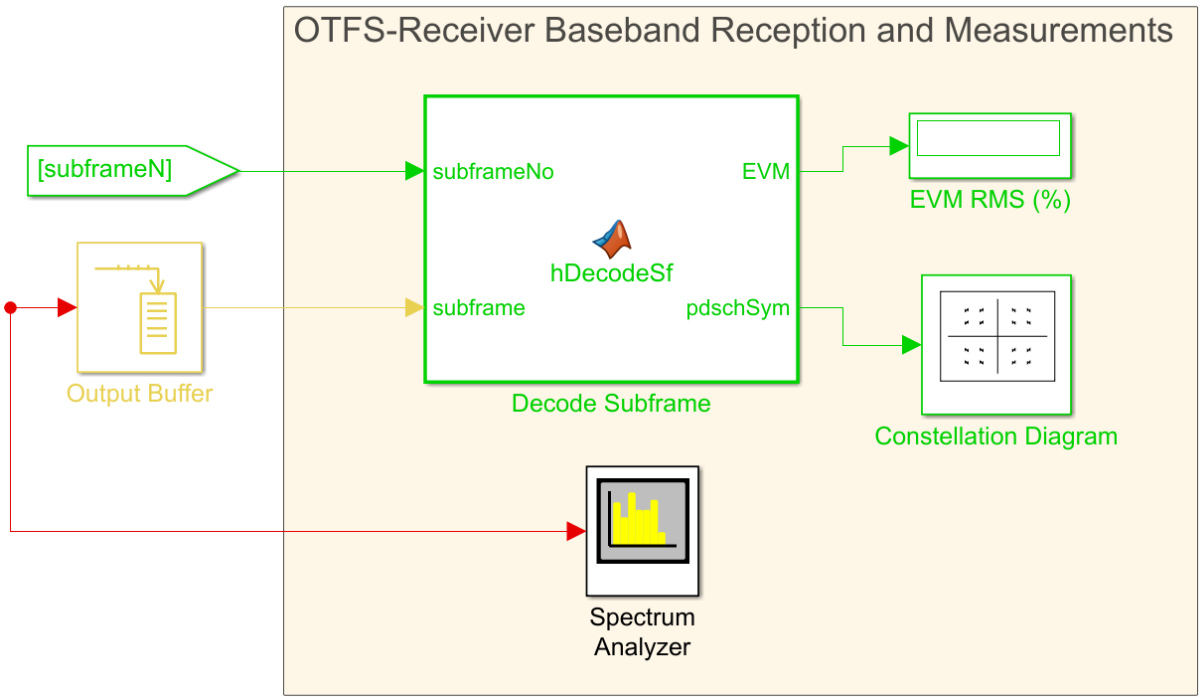

Fig. (3.4): Proposed Transmitter of massive MIMO-OTFS system

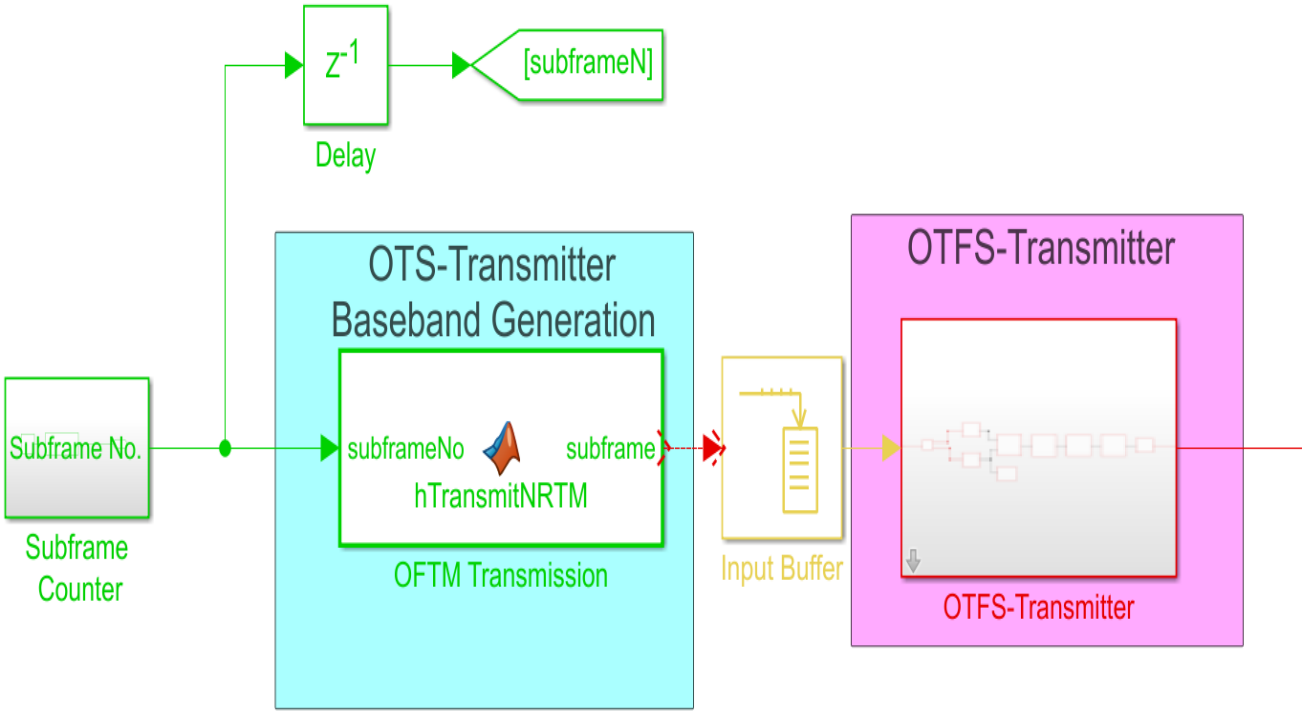

Fig. (3.5): Proposed Receiver of massive MIMO-OTFS system

Figure (3.5) shows the proposed Receiver of massive MIMO-OTFS system. There are many analyzers that can be added to test the system performance under different conditions. Figure (3.6) illustrated the hole proposed receiver of massive MIMO-OTFS system.

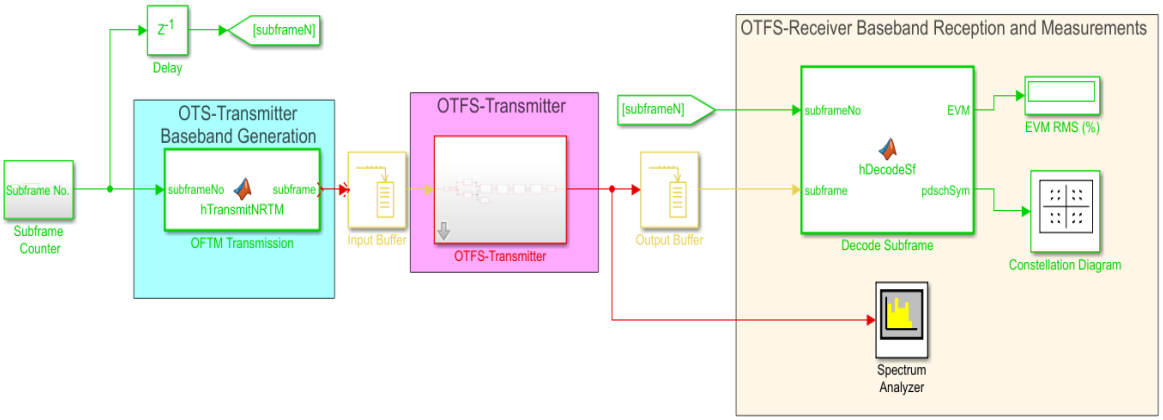

Fig. (3.6): Proposed Simulink system of massive MIMO-OTFS system

The process of transmission and reception of massive MIMO-OTFS system will be summarized in figure (3.7) that contain a flow chart for the implementation steps of massive MIMO-OTFS system.

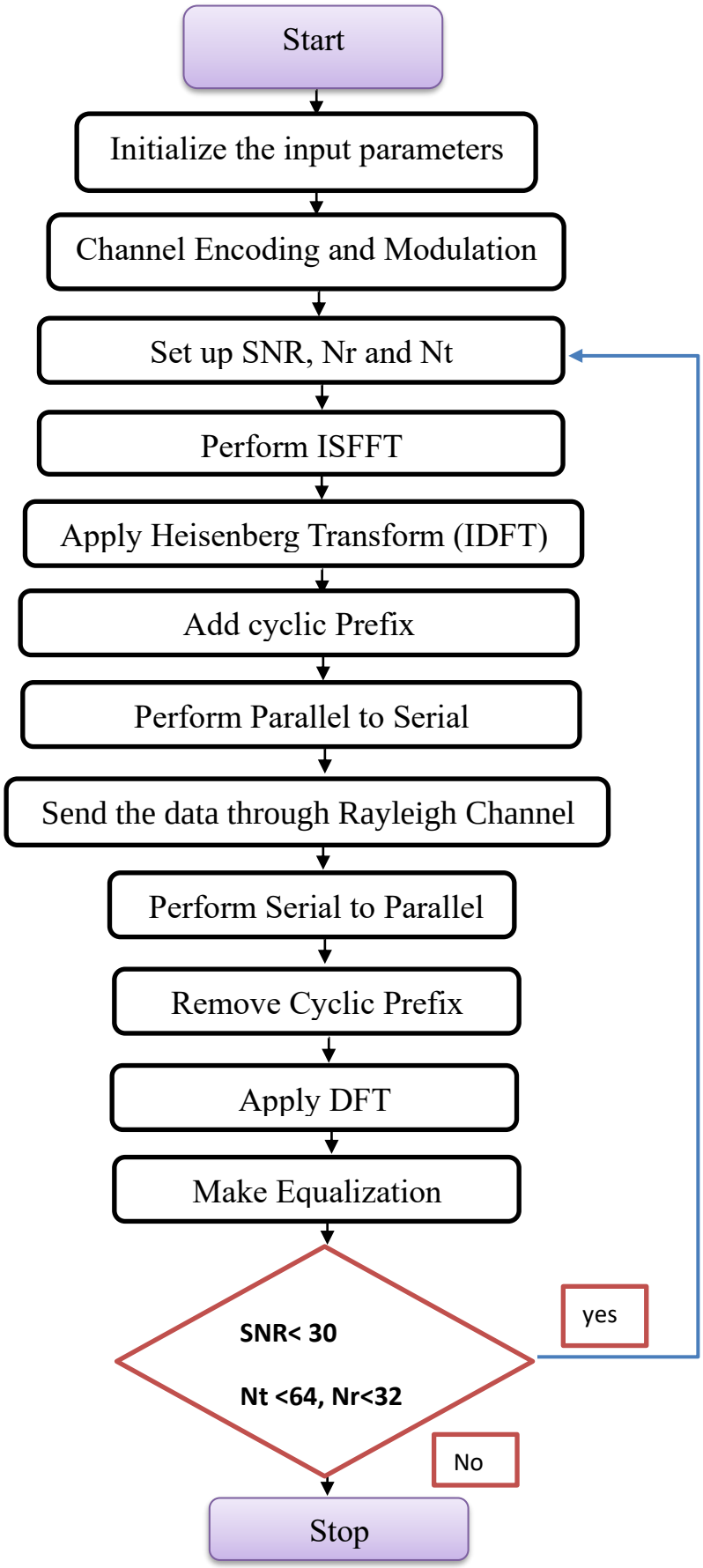

Fig. (3.7): Steps of design the uplink massive MIMO-OTFS system

Table (3.2) shows the main parameters that used in the simulated system by using MATLAB 2020a.

Table (3.2): Designed OTFS system Parameter

Name of parameter	Unit	Value
Carrier frequency	GHz	2.15
duration of Cyclic prefix	μs	16.6
Subcarrier spacing	kHz	15
FFT size		512,1024
User velocity	m/s	10 ~ 160
Number of BS antennas		1 ~ 64
OTFS frame size	(M,N)	(600, 12)
Number of user antennas		1
Number of users	Ue	1~ 30
Transmission bandwidth (Number of blocks)		50

3.3 System Description for proposed OFDM over RoF-MMW systems

In this section, the design of OFDM over RoF-MMW systems will be presented. At first, a presentation for VPI software and main parameters of the simulation framework will be illustrated. Then the proposed multi carrier OFDM transmitter will be presented. After that, the MMW generation based on AWG will be proposed. The description of seamless converge RoF channel will be presented in the next section. The last part of the proposed system will be explained in OFDM receiver section to integrate the overall backhaul hybrid OFDM-RoF-MMW system.

3.3.1 Global parameters of the proposed systems using VPI photonics

It is possible to accurately and efficiently model any system of transmission, containing mesh networks, ring networks, and bidirectional links, using a complex and durable simulation scheduler, realistic simulation models,

and combination of a powerful graphical interface. It is possible to simulate the time domain optical field in details, enabling for example, estimate of eye diagram analysis, and bit error rate. The ability to follow, visualize, and analyze signal attributes along a link is made possible by time-averaged signal representation, which eliminates the need for lengthy simulations when modeling complicated systems.Systems like VPItransmission Maker Optical Systems let us model equipment behavior in a computer simulation environment. Components based on (internal) material and structural properties are represented by detailed physical models. It is possible to obtain parameters for black-box and datasheet models from external measurements as well as datasheets. Component producers and system integrators benefit from a variety of abstraction levels in equipment modeling. Table (3.3) lists the global parameters included in each system.

Table (3.3): Main Factors of OFDM-RoF-MMW System

Factor	Value	Units
Software for Simulation	VPI photonics V.9.8	
Bit rate	20-50	Gb/s
Window of Time	$0.506*10^{-7}$	S
bandwidth of Simulation	18*bit rate	Bit
Length of Fiber	10-120	Km
Type of Fiber	Single Mode Fiber	
Bits / symbol	4,6 and 7 for QAM formats	bit
Frequency Center of host	$193.1*10^{12}$	Hz
Type of Data	PRS	
Spacing of Channel for DEMUX and MUX	$50 * 10^{9}$	Hz
Type of Laser	CW laser	

In actuality, each system is constructed with unique parameters based on the system's desired performance and the overall bit rate obtained. In these suggested systems, the global parameters are regarded as constant parameters that can be used in every situation. In the appendix (E), all the details and variables utilized in these simulation systems are described and demonstrated. The performance of every transmission network can be impacted by each component of a system that has been constructed. In this thesis, the most effective tool for designing all types of optical networks and systems was VPI Transmission Maker.

3.3.2 Proposed OFDM-RoF-MMW system

In our proposed system, an OFDM signals will be modulated using Mack Zehnder Modulator with the millimeter wave carrier in the main central station and transferred into an optical signal and then send to the unit of remote antenna by PON-WDM utilizing RoF technology.

The designed systems implemented using VPI photonics software tool. In order to analyze the ability of the designed backhaul hybrid system, the availability of an OFDM over RoF based on MMW-WDM-PON transmission link will be designed and implemented under the exists of many impairments from both electrical and optical domain including nonlinearity of fiber, fading of wireless networks, and other noise effects such as photodetector (PD) noise, amplifier noise, and clipping noise. The following figure shows the design of hybrid OFDM transmission along MMW-WDM-RoF -PON link.

Signal-Error-Rate (SER) of the designed system will be analyzed with many parameters in system like modulation index to give design information for system performance.' For higher data rates, this work explores the WDM-PON with various wavelengths, taking into account the backhaul link requirements in terms of capacity.

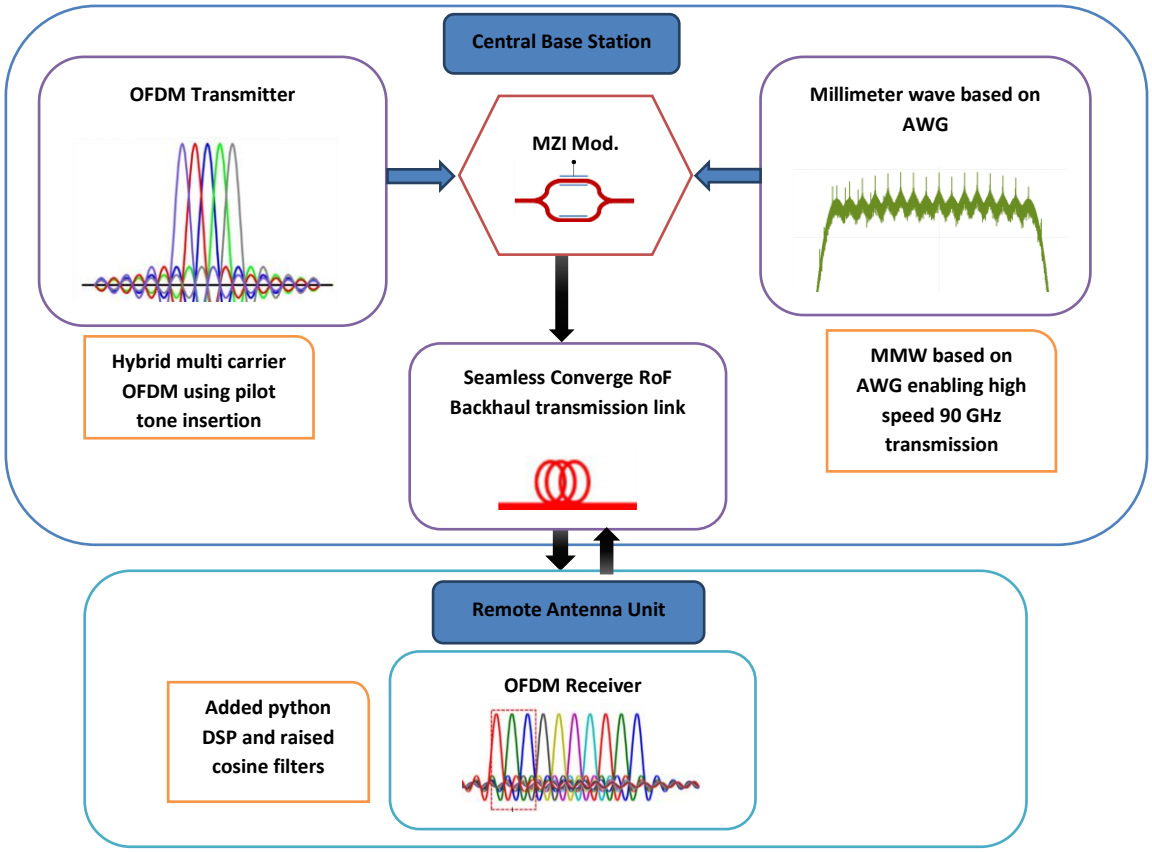

Fig. (3.8): OFDM-RoF-MMW-WDM/PON proposed system

Also, the wavelength's number is sufficient for the system to test all the wavelength combination cases caused by the FWM effect, including nondegenerate and degenerate parameters. In the central station, based on the given modulation format, for example using M-QAM, orthogonal frequency division modulator maps the input information onto symbols which is complex and transferred by each sub-carrier.

The positive and real time domain signal is required because the optical modulator is depending on the intensity modulation technique. By using orthogonal frequency division modulator, every signal of OFDM is modulated on MMW-RF sub-carrier. By using Subcarrier Intensity Modulation (SIM) technique, in Mach-Zehnder Modulator (MZM), a modulated MMW-RF carrier is obtained to drive the intensity of optical carrier's (for each wavelength) .

In our proposed system, the Mack Zender modulator is used to modulate the optical carriers with OFDM signals for better performance and simplifying the transmitter. Optical carriers are demonstrated at wavelength demultiplexer named as AWG to get the required number of carriers. Then multiplexed using WDM before being modulated with MZM then transmitted through a fiber.

3.3.2.1 OFDM transmitter

The block diagram of transmitter for OFDM is shown in Figure (3.9). Pasedo random data sequences (PRDS) are used to be transmitted using OFDM coder. The Coder_OFDM module generates electrical signals corresponding to the parts of real and imaginary of an OFDM signal. Power loading schemes are used to represent the OFDM subcarriers. Then a FuncSineEl module used to generate a constant bias and an electrical sine wave are superimposed. We used Fork_2 module to divide sine wave into two identical paths to be multiplied each by raised cosine filter using multiplier module to form the in components of phase and quadrature of OFDM signals.

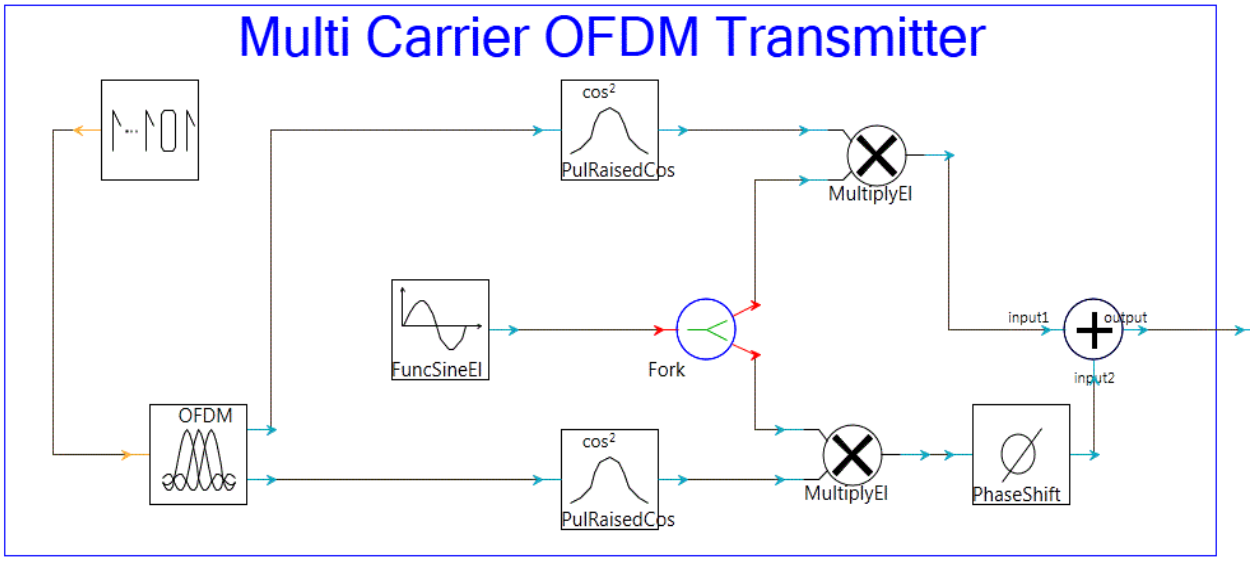

Fig (3.9): Block diagram of multi carrier OFDM Transmitter

3.3.2.2 MMW generation

MMW carriers' generation includes many parameters to be set to create carriers at milli meter band. At first, the Laser CW_DSM module used to produce the continuous wave (CW) laser signal. We used FuncSineEl module produces an electrical sine waveform superimposed on a constant bias. By using MZM, we modulated the laser carrier and generated sine wave to create modulating wave. AWG used to specify the number of required carriers to be output to an ideal WDM multiplexer. Fig (3.10) shows block diagram of MMW generation.

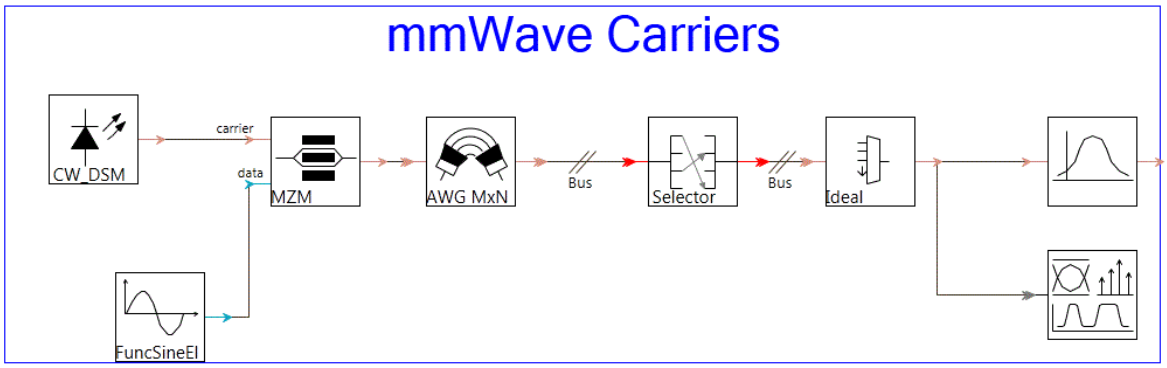

Fig (3.10): Block diagram of proposed MMW generation

The selector used to set the required carriers to be used in the simulation. The output signal filtered and modulated with OFDM signals by using MZM. The table (3-4) illustrates the parameters of AWG.

Table (3-4): Factors of AWG

AWG Mux/Demux		
Factor	**Value**	**Units**
Spacing of Frequency	50	GHz
Number of output/inputs ports	16/1 or 32/1 for Demux and 1/16 or 1/32 for Mux FOR 16 and 32 OFDM	
first channel Frequency	192.725	THz
last channel Frequency	193.475	THz
Frequency of Reference channel	193.1	THz
Type of Passband	Gaussian	

3.3.2.3 Design of RoF system

According to figure (3.11), a ROF system is composed of single mode fiber with a full consideration for all the fiber losses due to linear and non-linear effects.

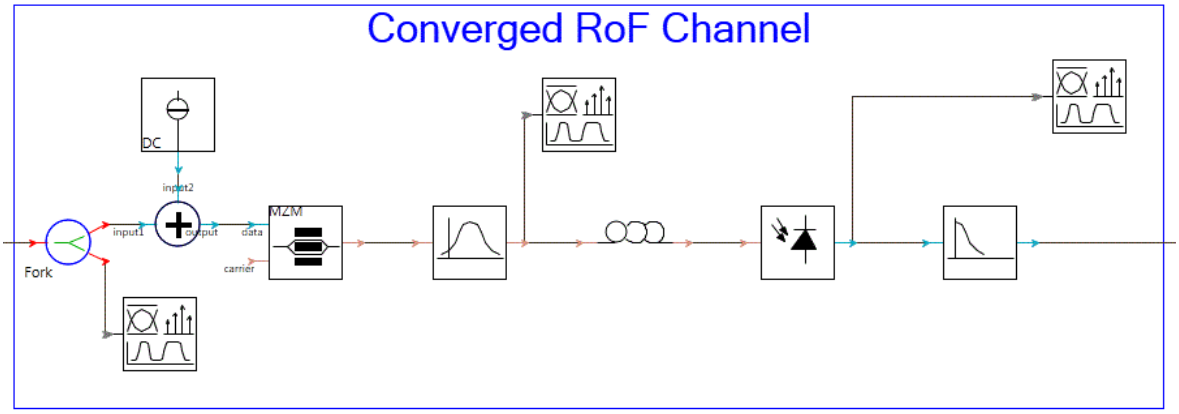

Fig (3.11): Block diagram of proposed converge RoF

The RoF channel receive the modulated OFDM-MMW signal from MZM modulator through optical filter and after a specified transmission distance the received signal detected by photo diode (PD) detector.

3.3.2.4 System Description for Receiver of OFDM-RoF-MMW System

Figure (3.12) presents the block diagram of receiver part for RoF-OFDM system. The received signal from PD separated by Fork module through two identical parts. By using MultiplyEL module each signal multiplied by sine wave to demodulate the in-phase and quadrature parts of signal to remove the MMW carrier. Then, OFDM de-coder module used to extract the required data and show the resulted SER and constellation diagrams using OFDM_SC_Analyzer module.

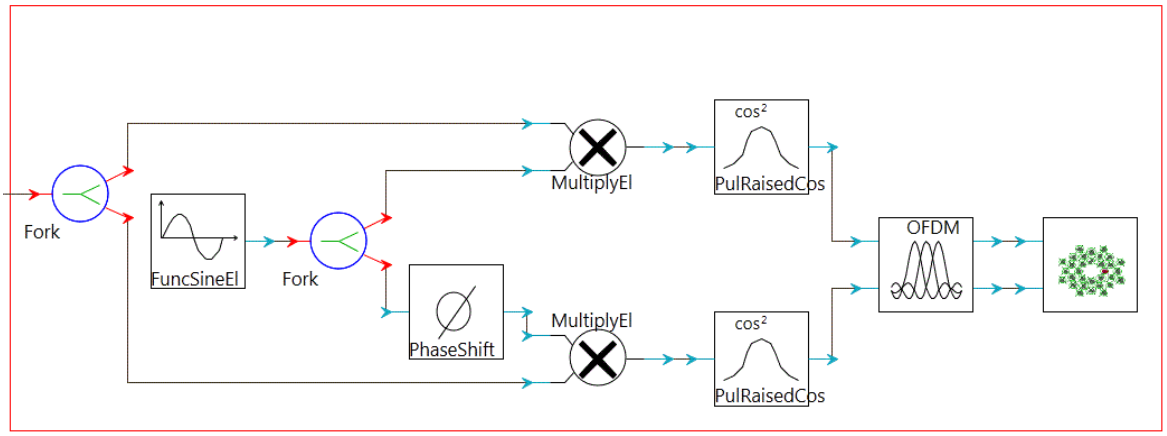

Fig (3.12): Block diagram of receiver part for RoF-OFDM system

The proposed system supports bit data signals up to 50 Gbit/s created by the Pseudo Random Bit Sequence Generator (PRBSG) coupled to the QAM sequence generator with m bits per symbol. By Using multiple narrowband subcarriers to transmit many low-rate data streams from a single high-rate data stream, an ultra high capacity system should be obtained. There are fewer distortions in narrowband subcarrier data streams than in high-speed ones, therefore they don't need to be equalized. Figure (3.13) illustrates the full proposed wireless backhaul RoF-MMW for MC-OFDM transmission system at mQAM Format. Python DSP used to compensate PAPR losses and drift losses in the receiver section and it is presented in appendix (F).

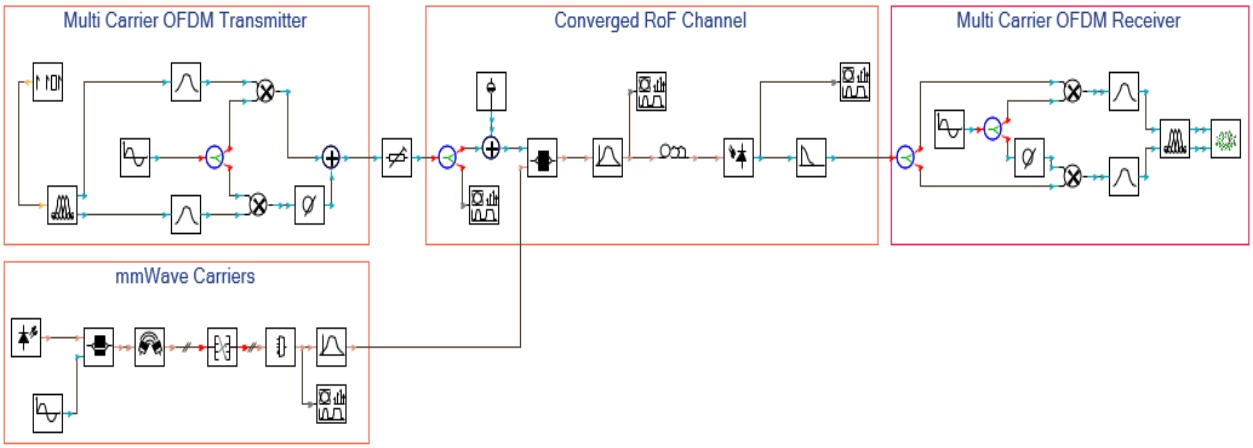

Fig. (3.13): Wireless Back Haul Millimeter Wave Radio over Fiber (RoF) for MC-OFDM Transmission System at mQAM Format

3.3.3 Proposed all optical OFDM System

The concept of all optical OFDM systems is illustrated in this section. The efficiency of the scheme depends on the modulation of the subcarrier, optical gate stability and the accuracy of the passive system performing the optical FFT. The simulation parameter of the proposed system is given in Table (3.5). The system is consisting of three parts:

Table (3.5): AO-OFDM main parameters

Parameters	Values	Units
Default Data rate	240	Gb/s
The operating system for central frequency	193.1	THz
Link range	100-1000	Km
Channel spacing	20	GHz
Modulation Technique	QPSK	
Laser type	Cw laser	
Bits per symbol	2	
AWG channels	16 for 16-subcarrier 32 for 32-subcarrier	Channels

3.3.3.1 Transmission demonstration of all optical OFDM(AO-OFDM):

The transmitter subsystem consists of an optical comb, AWG, optical modulator, and an optical multiplexer. Comb generation is necessary for AO-OFDM systems, due to different subcarriers must be produced from the same laser source to maintain the orthogonal between the OFDM subcarriers. The signal passed through the AWG performing the IFFT is modulated by quadrature modulator to OFDM signals. An IQ modulator consists of two Mach Zehnder modulator (MZM) with two orthogonal components produces an optical QPSK modulation signal. In the upper arm, the intricate envelope's in-phase component modulates the optical carrier, while in the lower arm; the quadrature-phase component modulates an optical carrier shifted by 90. Figure (3.14) shows the proposed transmitter of all optical OFDM for 16-subcarrier.

Following the modulation of the optical OFDM subcarriers, it will be aggregated to form the optical OFDM signal by an optical multiplexer. To keep the OFDM signals orthogonal, OFDM symbol duration is set to $Ts = 1/\Delta fs$, where Δfs is the frequency spacing of the comb. After that, all signals are multiplexed by DWDM with 20 GHz channel spacing. Figure (3.15) illustrates the proposed transmitter for polarization-multiplexed optical signals with quadrature modulation.

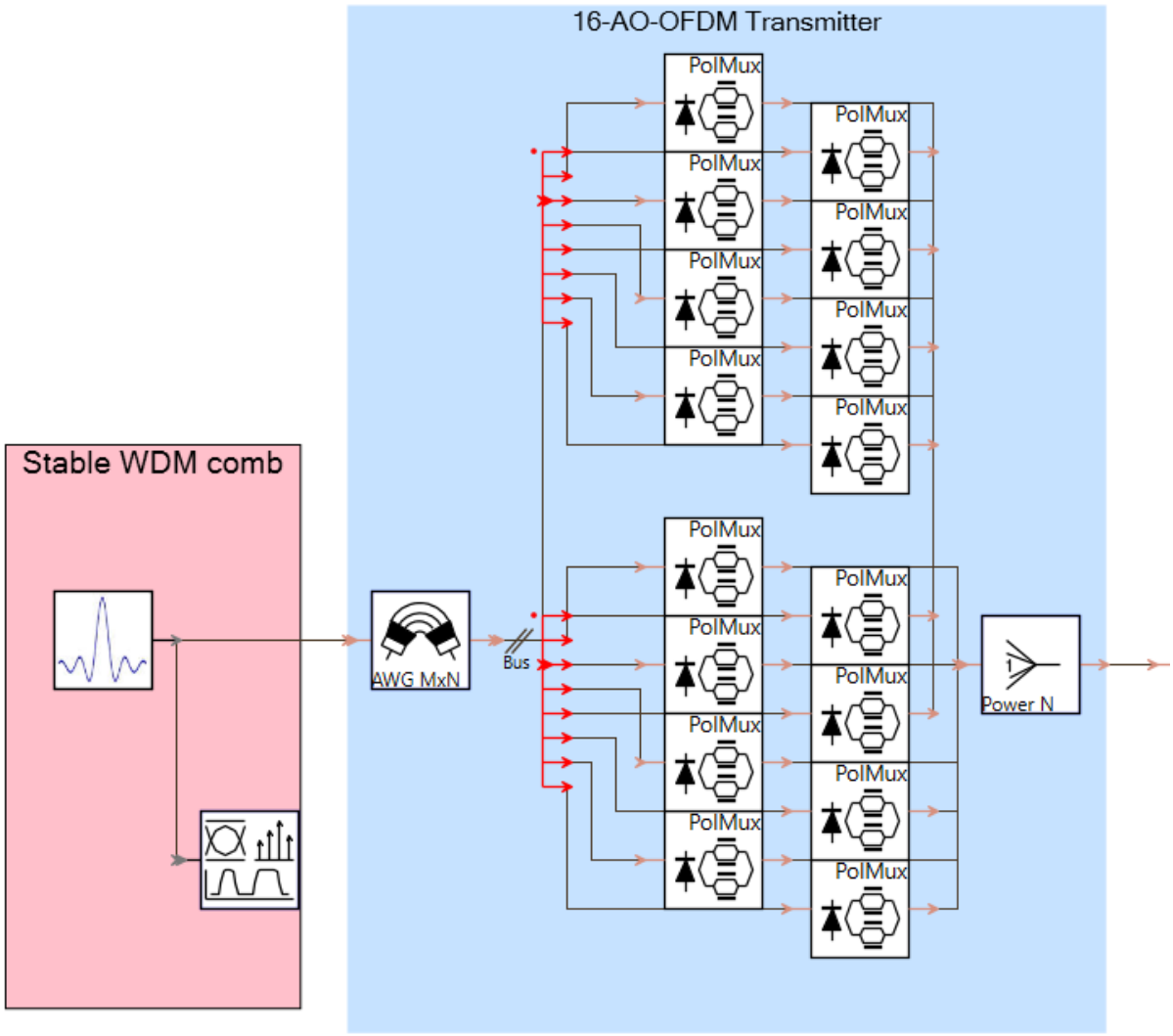

Fig. (3.14): Proposed Transmitter section of 16- Subcarrier All Optical OFDM transmission system

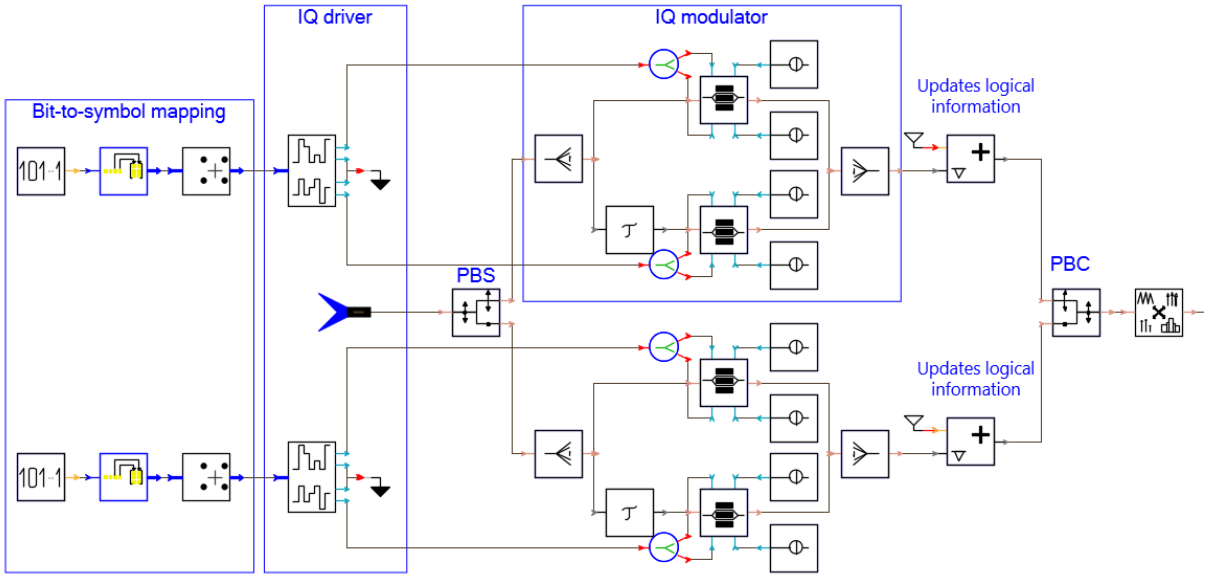

Fig. (3.15): Proposed transmitter for polarization-multiplexed optical signals with quadrature modulation

A bit to symbol mapping process is the first step in performing each transmitter of all optical OFDM system by mapping the bits in a required constellation. By using dual polarization property, two polarized signals performed by using polarized beam splitter. In phase Quadrature (IQ) driver used for generates driving signals for optical transmitters. IQ modulator used for modulating the signals to be transmitted. Polarized beam combiner (PBC) used to couple the x and y signal to achieve polarized signal.

3.3.3.2 Proposed Channel of AO OFDM system

In this section the proposed channel of AO OFDM system will be explained. A fork module used to split the signal into two identical signals. The first signal directed to DWDM and second signal power controlled and AWGN added to it then amplified by using gain controlled optical amplifier. Setting the specified OSNR that expressed in dB and defined for one channel and a specific noise bandwidth by adding noise to the input signal. The OSNR can be expressed as:

$$\text{OSNR [dB]} = 10 * \text{Log10}(^{Pch}/_{Pase})$$

Where:Pch is channel power and $Pase$ is the power of optical noise measured in both polarizations over a bandwidth specified by parameters OSNR bandwidth.

Figure (3.16) shows the channel part of AO OFDM system and setting OSNR value.

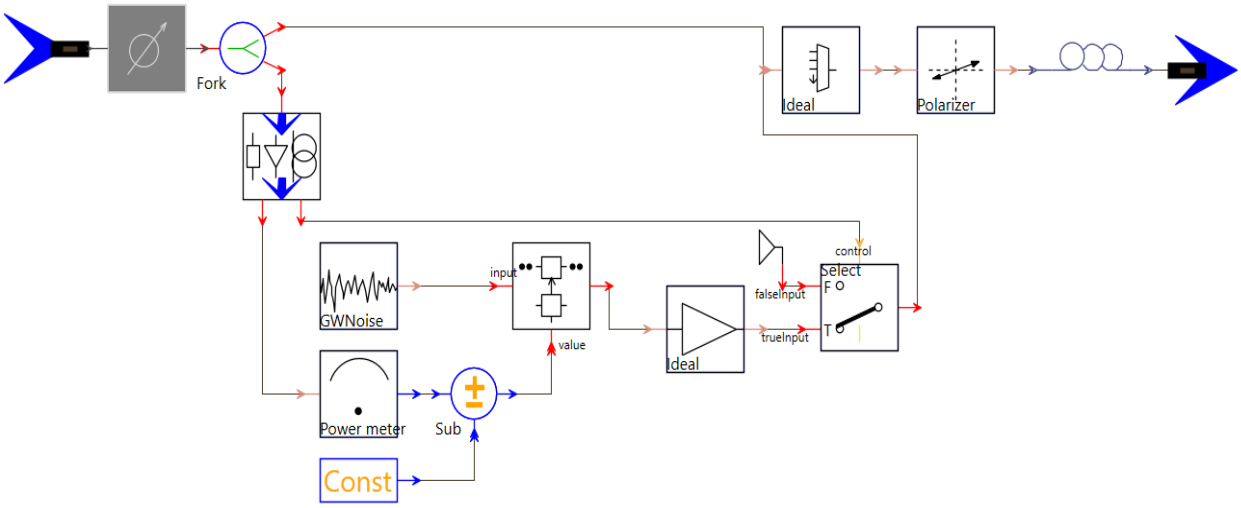

Fig. (3.16): Channel parameters of AO OFDM system

3.3.3.3 Proposed receiver of AO OFDM system:

In this section, the design of optical FFT required for all optical OFDM will be presented. The receiver side consists of optical FFT, DWDM demultiplexer, and optical demodulator. All the transmitted operation should be reversed in the receiver side to recover the data from the source. The OFFT circuit is composed of a cascaded multi-mode interferometer (MMI). Each MMI's lower arm includes a phase shifter and optical time delayer. The first-time delay for the MMI is changed to $Ts/2$, while the time delay for two more parallel MMI is set to $Ts/4$, later the parallel four is set to $T2/8$. The phase shift is set to $\pi/2$ rad. The output of 8 MMI is selected by a selector collected all IQ signals. To achieve 16-subcarrier all optical OFDM we make other identical 8-subcarriers and add all 16 subcarriers by using two bus creator. DWDM demultiplexer is used directly to spill the subcarriers. The output from each De DWDM is subsequently filtered by the optical band-pass filter and then detected using an optical demodulator of QPSK.

To achieve optical FFT, we used multi-mode interference (MMI) device module that distributes optical power from one or several input ports among several output ports and is based on destructive/constructive interferences occurring in the MMI area with a large number of guided modes. The description of MMI coupler principle will be explained in figure(3.17).

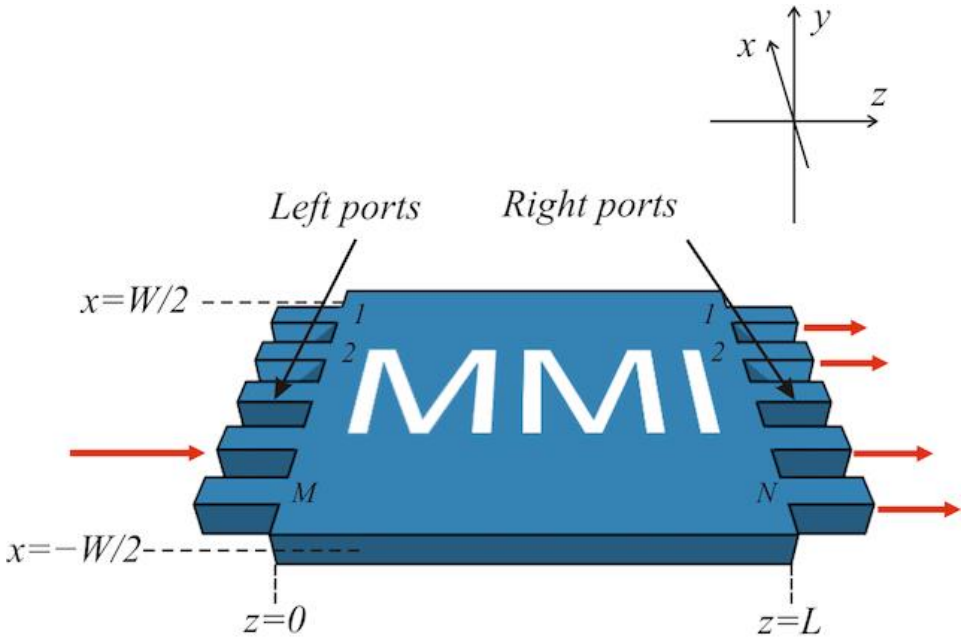

Fig.(3.17): MMI coupler principle

The central structure of an MMI device is a planar waveguide of width W (specified by the Width parameter) designed to support a large number of guided modes (typically many more than three). To provide a waveguide with a large number of modes, its width W is typically in the tens of micrometers range. In order to launch light into and extract light from that multimode waveguide, a number of access single-mode channel waveguides are placed at its beginning z = 0 and at its end z = *L*.

The MMI guide sidewalls are at x = −*W/2* and x = *W/2*. The number of left and right access waveguides is defined by the parameters:

M = Number of ports left and N = Number of ports right, respectively.

To achieve optical FFT for 16 AO OFDM we used Integrated DFT filter to Demultiplex 16x20GSamples/s OFDM super-channel using MMI couplers, phase shifters and optical time delay modules as shown in figure (3.18).

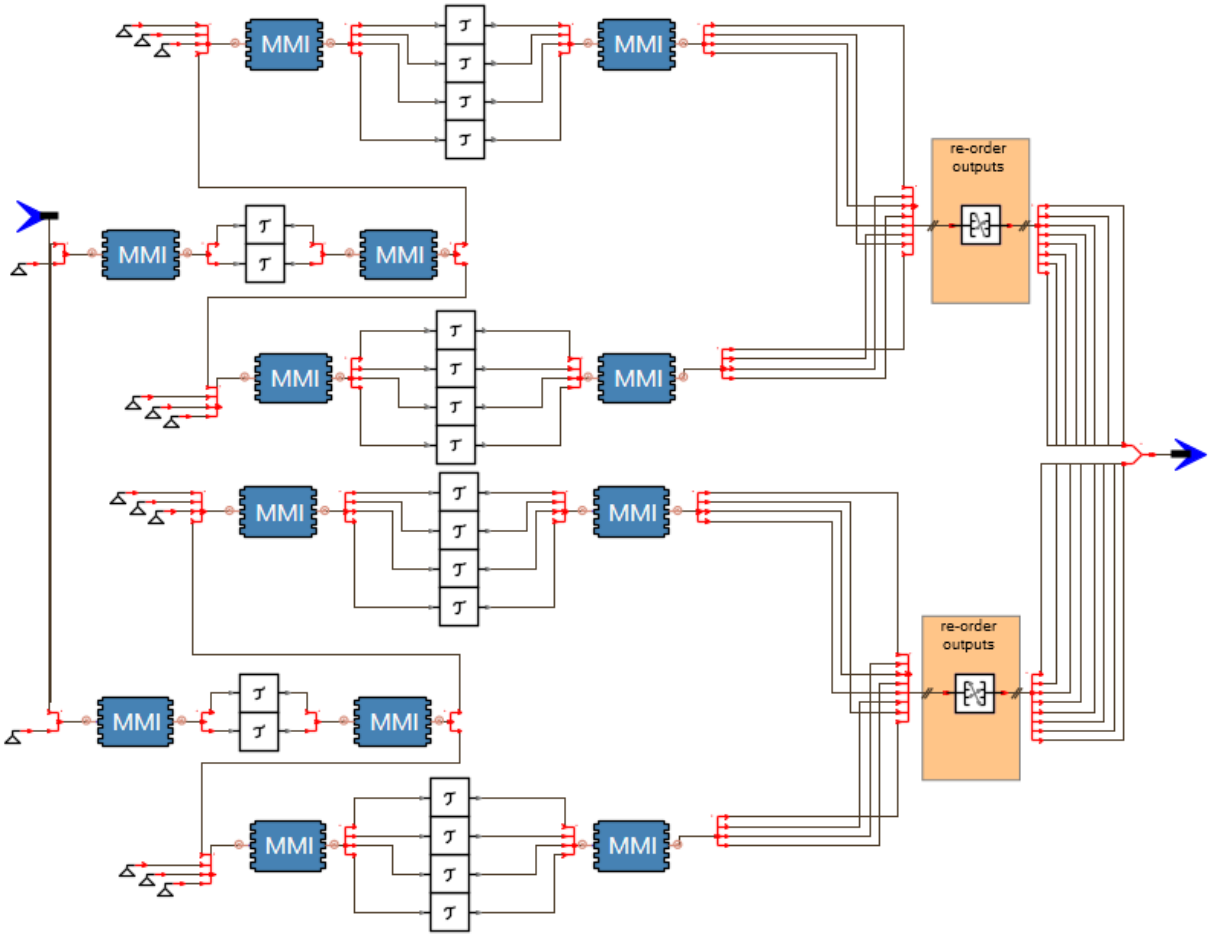

Fig. (3.18): Integrated DFT filter to Demultiplex 16-AO OFDM super-channel using MMI couplers

From other side after achieving the optical FFT, an amplitude modulator acts as optical gate for the received signals. Then, the dual polarization section applied to the signals to extract the polarized signals. Then analogue to digital convertor (ADC) and clock performed for the received signals to extract the required data. The achieved information then analyzed and appeared by using the BER 4D analyzer. Figure (3.19) shows the polarization receiver for AO OFDM system.

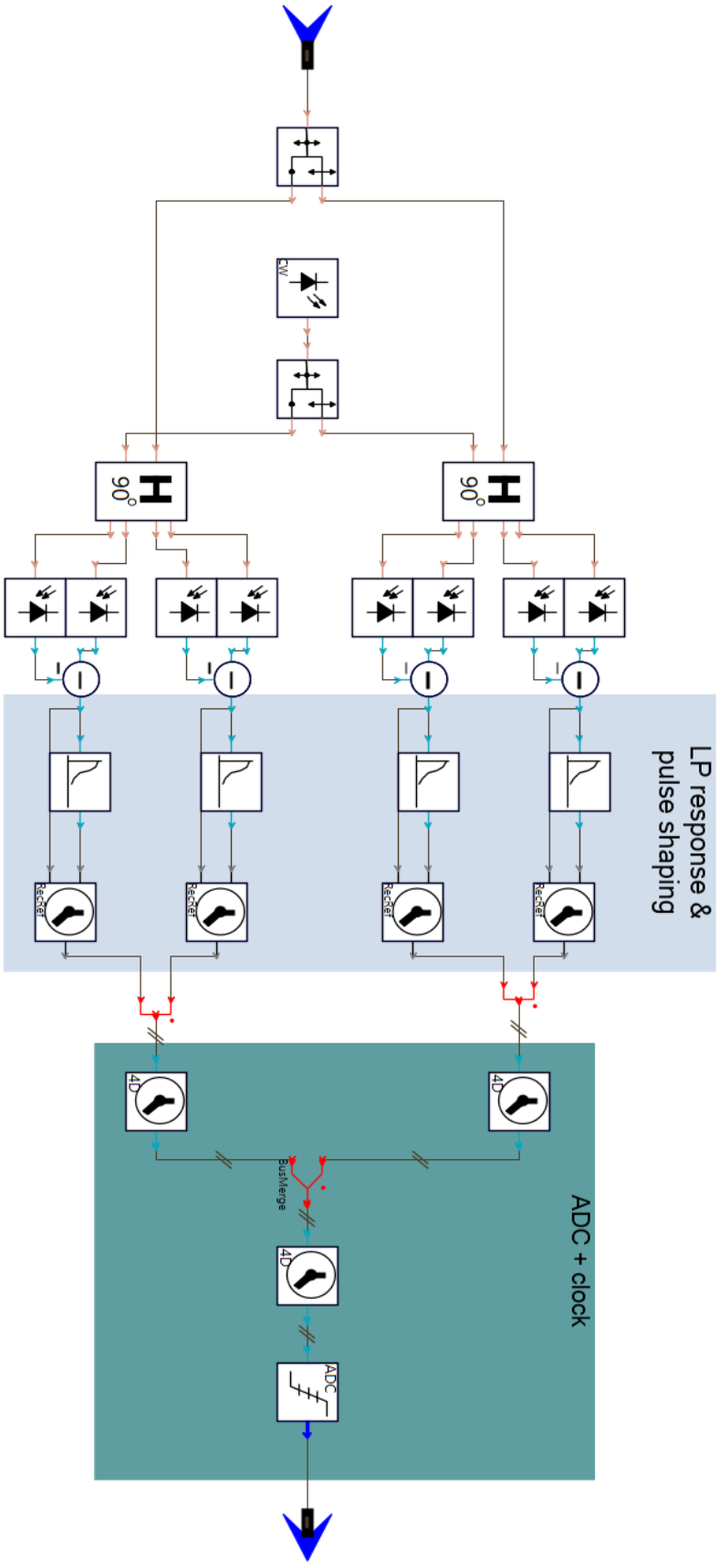

Fig. (3.19): Proposed dual polarization receiver of AO OFDM system

The complete receiver of all optical OFDM system is illustrated in figure below:

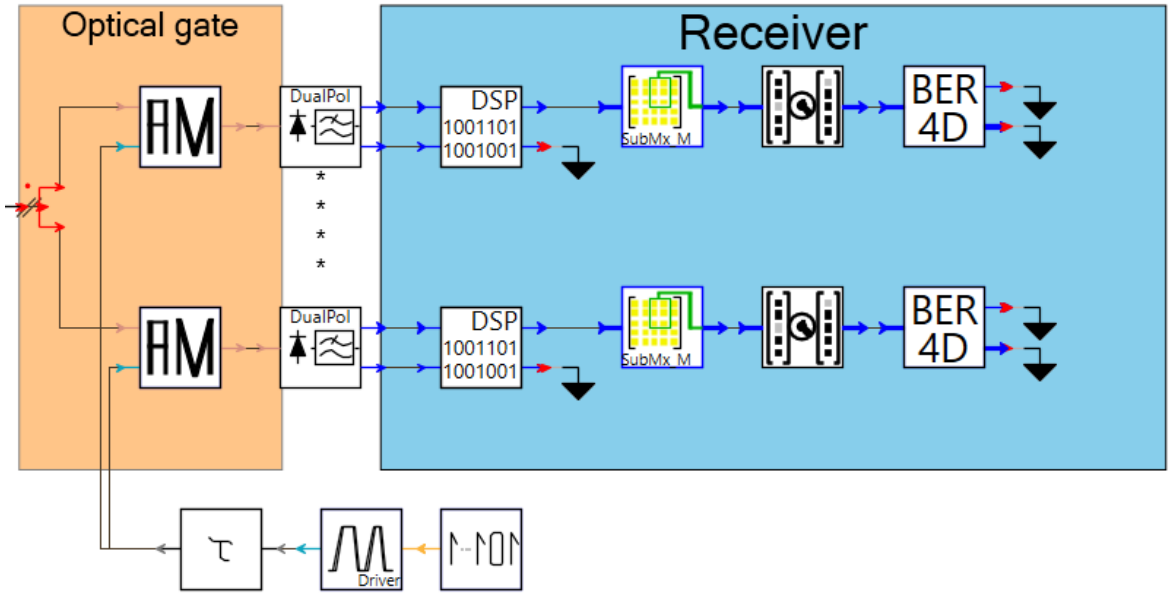

Fig. (3.20): Proposed receiver section of 16- Subcarrier All Optical OFDM transmission system

The complete proposed 16-AO OFDM system is shown in figure (3.21).

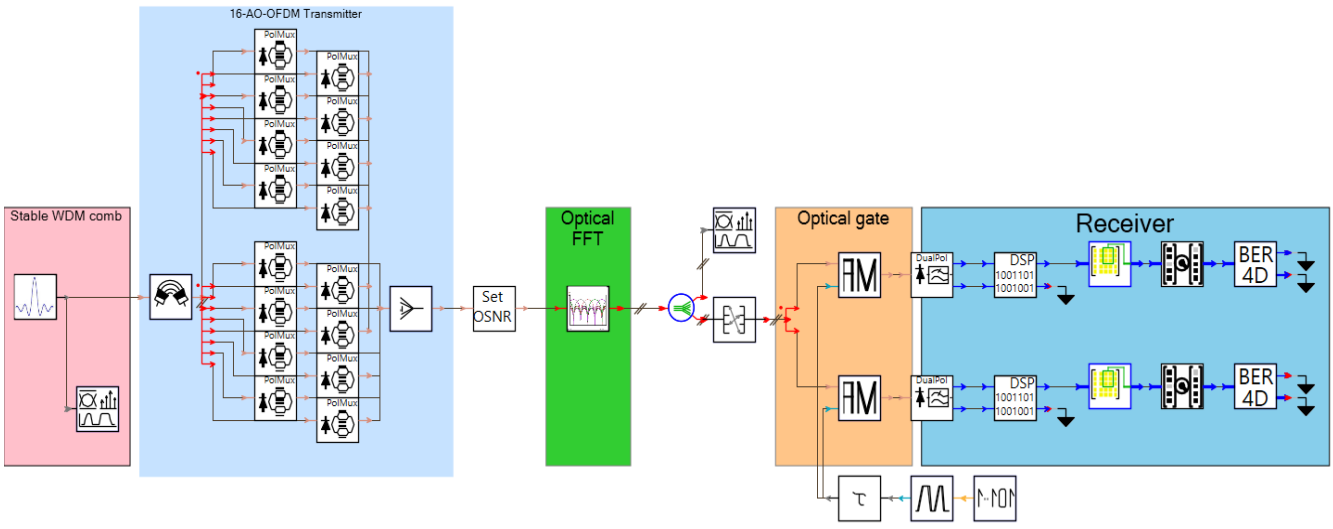

Fig. (3.21): 16- Subcarrier All Optical OFDM transmission system

To achieve higher bit rates and get best transmission capacity in backhaul systems we will increase the order of AO OFDM subcarriers, so that a 32 AO OFDM performed. The same procedure used in 16-AO OFDM used by doubling the transmitters to be 32 transmitters combined by beam combiner and transmitted. Figure (3.22) shows the transmitter of 32 AO-OFDM.

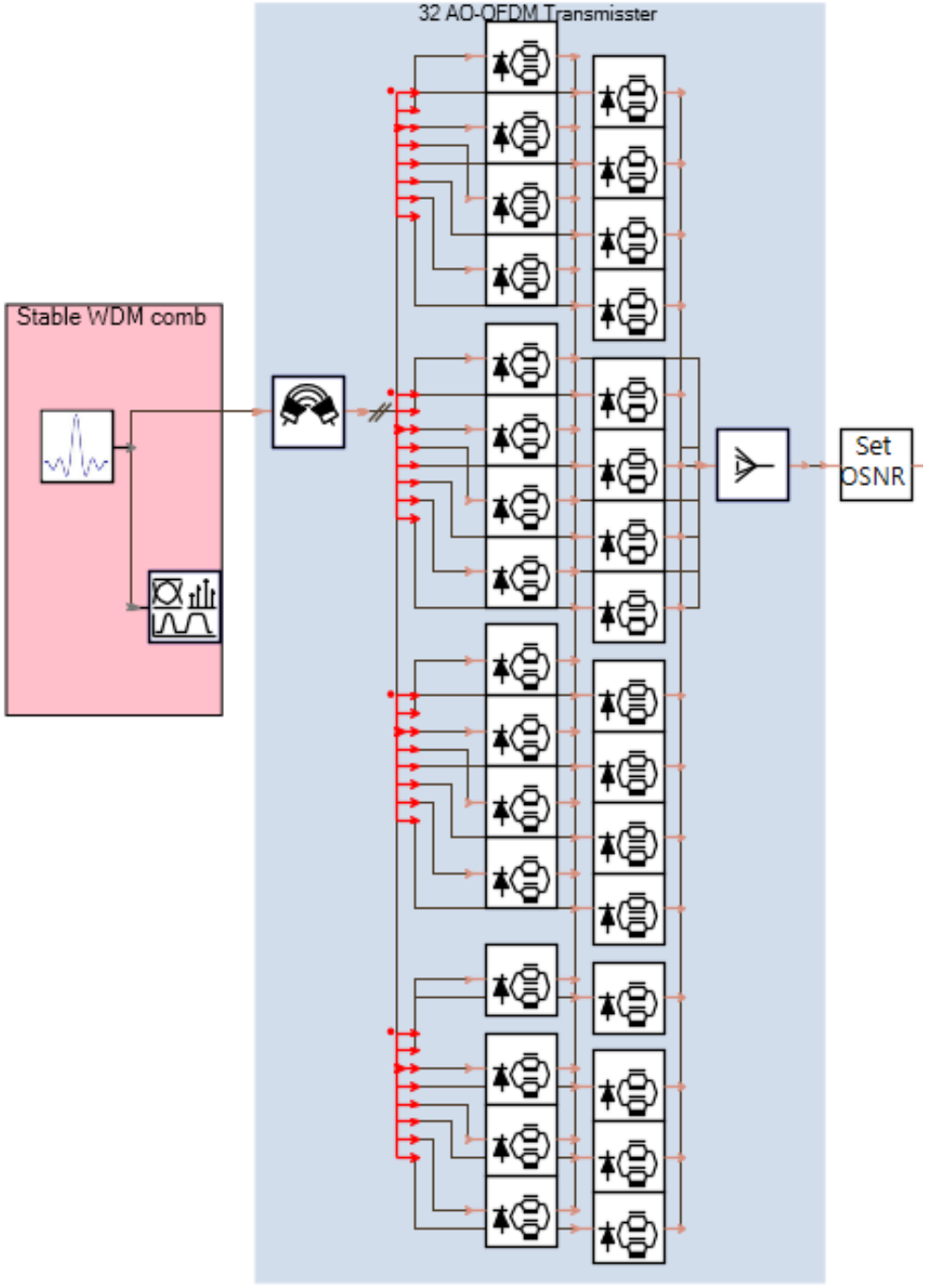

Fig. (3.22): Proposed Transmitter section of 32- Subcarrier All Optical OFDM transmission system

From other side, using the optical FFT in 32 AO OFDM system will be performed by doubling the MMI couplers of 16 OFDM and add them by using bus merging. Figure (3.23) shows the optical FFT of 32 AO OFDM system.

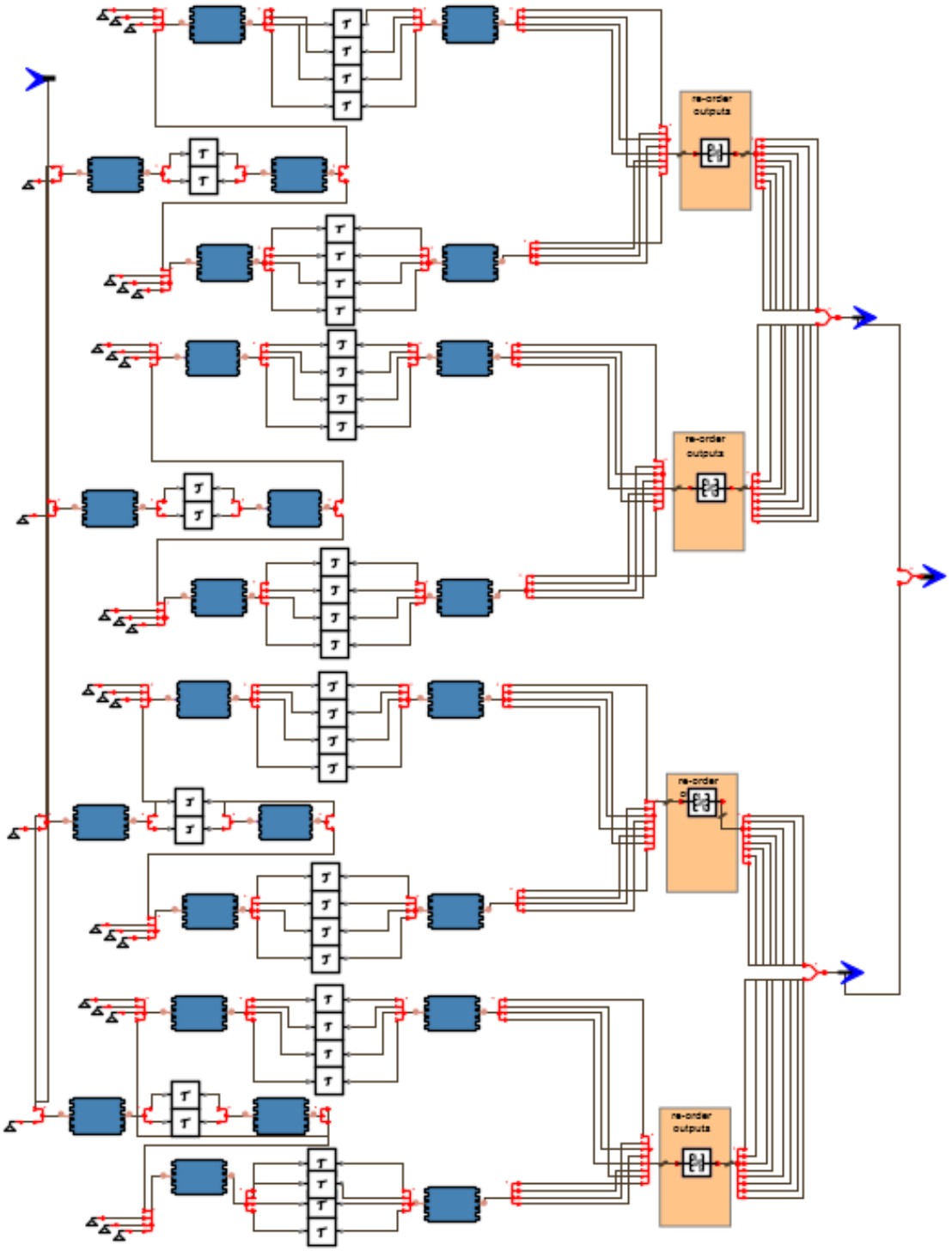

Fig. (3.23): Integrated DFT filter to Demultiplex 32-AO OFDM super-channel using MMI couplers

The proposed system with 32 subcarriers offers the highest data rates among all the recent systems. The complete proposed 32-AO OFDM system is presented in figure below:

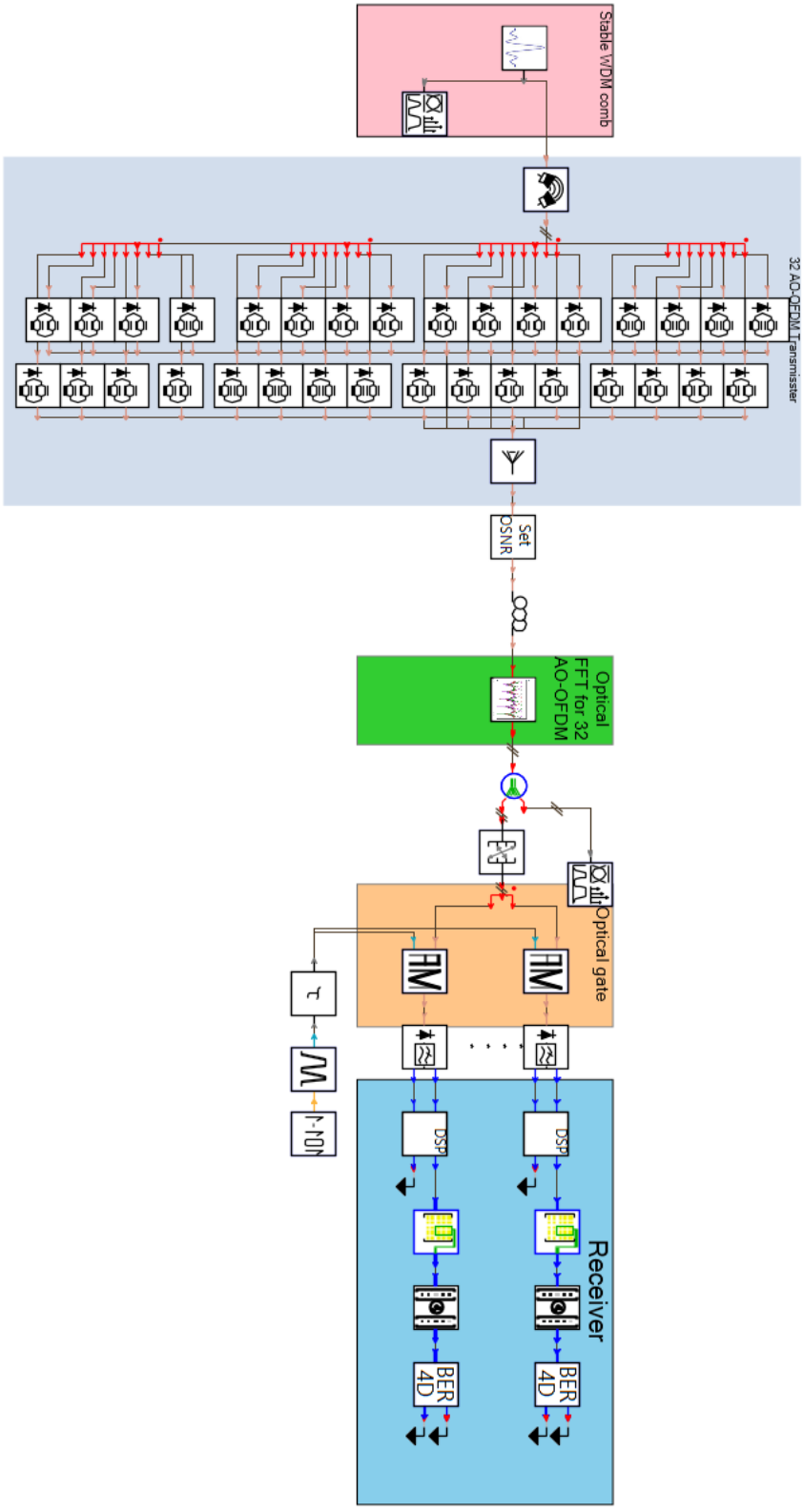

Fig. (3.24): Proposed 32 - Subcarrier All Optical OFDM transmission system

Chapter Four

Simulation Results and Discussion

4.1 Introduction

In this chapter the performance of massive MIMO techniques and OFDM-RoF-MMW systems had been presented. At first the performance of proposed uplink XL massive MIMO system based on hybrid field propagation will be presented. Also, the performance of precoding techniques of XL mMIMO system will be illustrated. Then, the capability and error performance of OFDM-RoF-MMW systems will be illustrated. Finally, a performance of massive MIMO-OTFS system performance will be discussed. The offered transmission systems will be investigated using different data rates, distances and modulation techniques to show system performance under different conditions.

4.2 Uplink Massive MIMO system results:

The results and discussion of uplink MIMO systems will be discussed in this section. The systems will be discussed under two scenarios, the first using 2×2 MIMO transmission system and the second scenario by using XL mMIMO transmission system.

4.2.1 Uplink 2×2 MIMO System results:

End-to-end MIMO system has been covered in the simulation that offering the transmitted and/or encoded signal, reception signal, demodulation of the received signal, and channel model. The no-link diversity is also provided (receive antenna case- single transmit) and theoretical assessment of 2^{nd} order link diversity for comparison. Here, it is assumed that all systems have perfect channel knowledge at the receiving end. To get required BER results,

we will compare between various systems, by running the simulation over a variety of Eb/No points.

As for computational complexity, the system of transmit diversity is not dissimilar from the system of receive diversity. The simulation results demonstrate that the same diversity order is provided by using 2 antennas of transmission and 1 reception antenna as the system of maximal-ratio combined (MRC) of two receive antennas and one transmit antenna. An acceptable value of BER (10^{-3}) achieved with SNR value above 12 dB using MCR diversity method. Figure (4.1) shows the performance of uplink 2×2 MIMO system by using MRC method. To obtain fit values, curve fitting process applied to MCR curve.

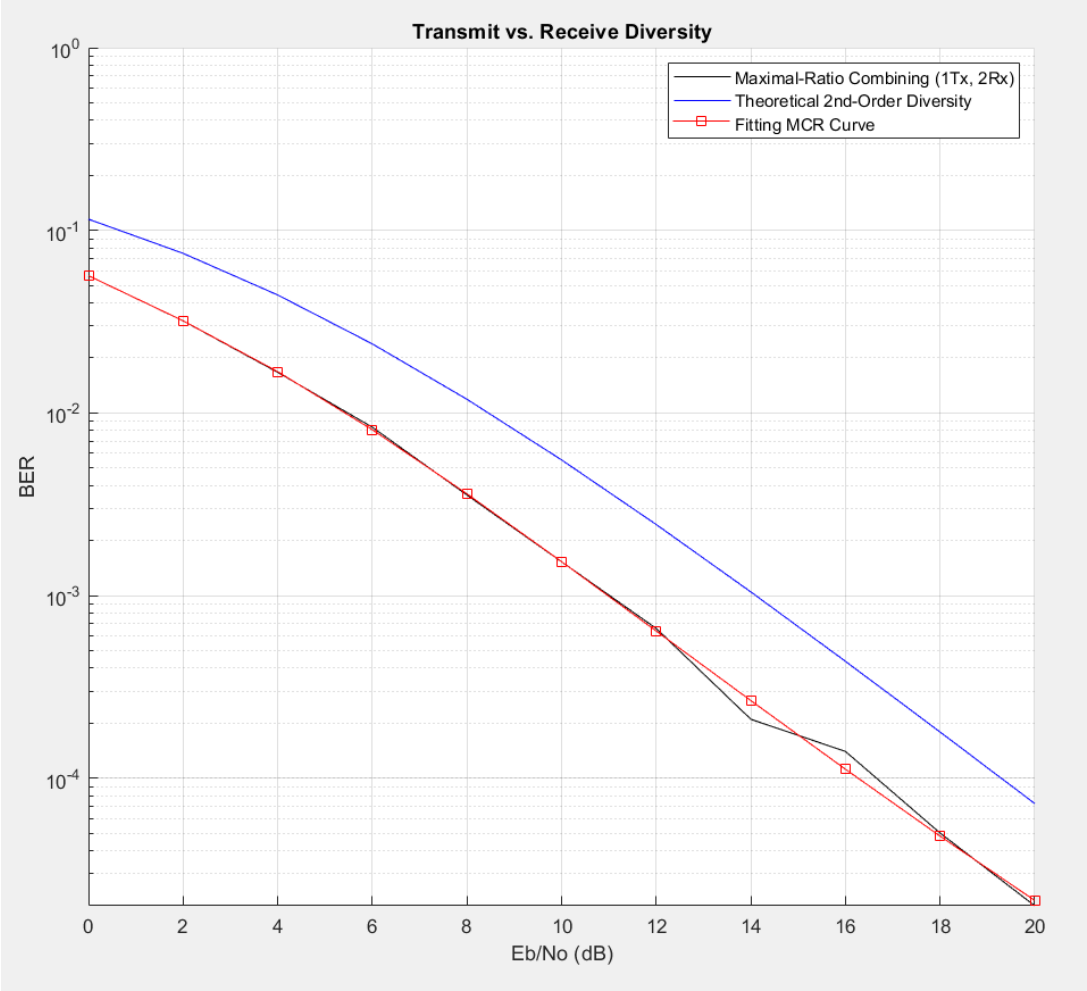

Fig. (4.1): Performance of uplink 2×2 MIMO system by using MRC method

Also note that compared to MRC receive diversity, diversity of transmission has a disadvantage of three dB. This is due to assuming that our simulations have that the total power of transmission would be the same in both scenarios.

The performance would be the same if we calibrated the sent power such that the power of receiving for these two scenarios is the same. Since it normalises the overall power across all the diversity branches, the assessment of theoretical of the 2nd link of diversity matches that of the system of diversity transmission. Also, the archived results show the advantage of using MRC method above Alamouti method by achieving better BER under the same conditions. Figure (4.2) presents a BER vs SNR comparison between different diversity methods.

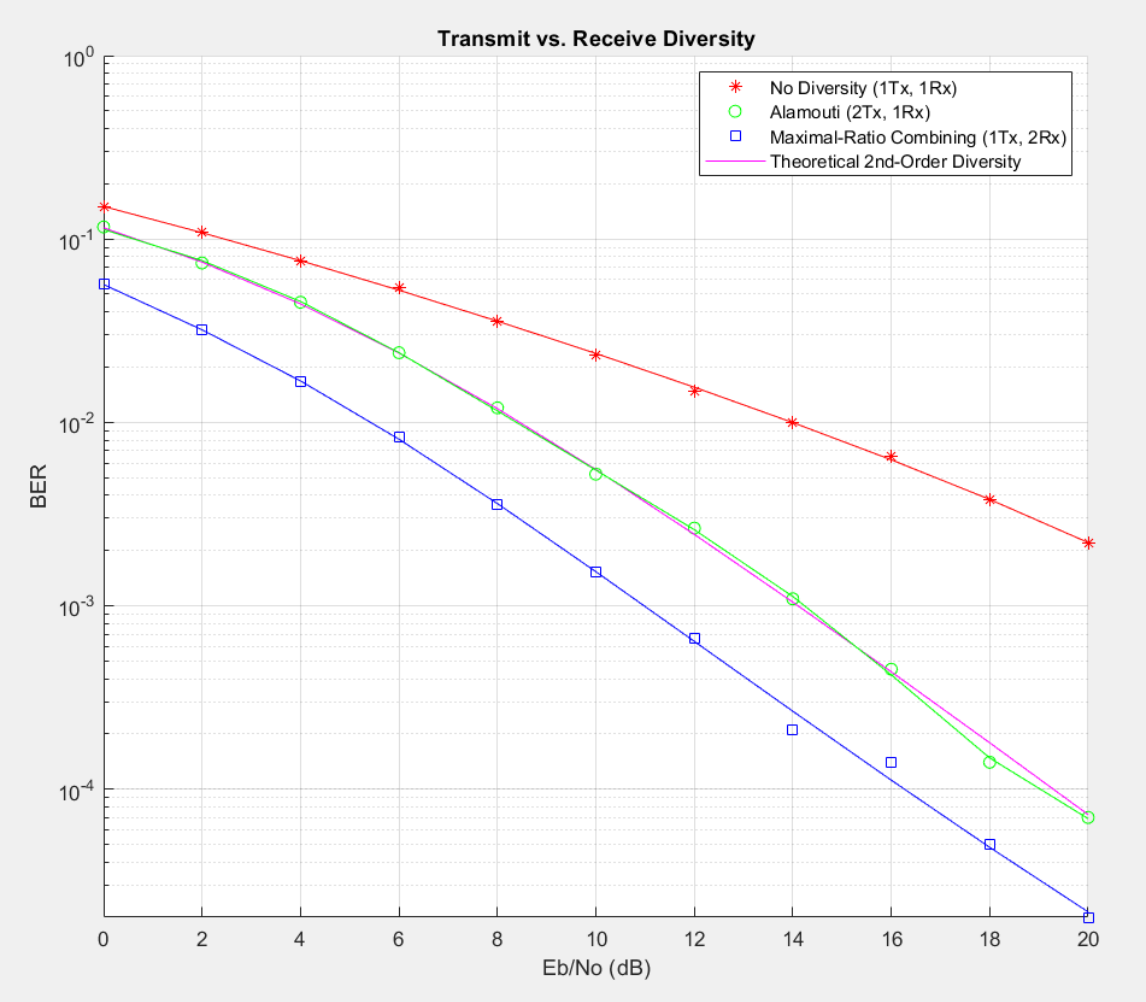

Fig.(4.2): Performance results of 2×2 MIMO under different diversity conditions

4.2.2 Results of Massive MIMO -OTFS system:

In this section, the results of designed massive MIMO-OTFS downlink system will be presented as the best choice for B5G wireless downlink transmission systems. We put the developed system under many conditions to test the designed massive MIMO -OTFS system by applying the NMSE and BER. The usual estimation of channel depend on technology of impulse is offered as a benchmark, for which we employ NMSE of the classic impulse-depend estimation of channel method which is calculated.

The received spectrum analyzer shows the shape of the received signal as shown in figure (4.3). The signal had been successfully received and can extract the OTFS signal by several steps to get the required information. The received instantaneous constellation of designed massive MIMO -OTFS system for selected user 2 D channel will be shown in figure below.

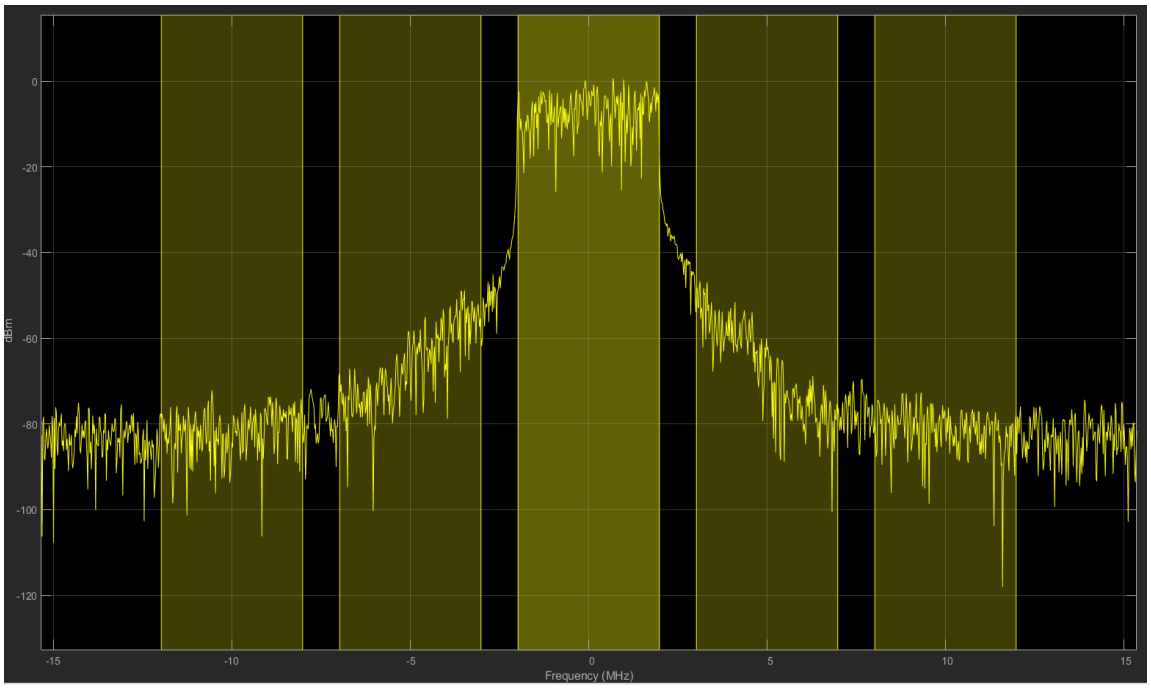

Fig.(4.3): Received spectral analyzer of massive MIMO-OTFS signal

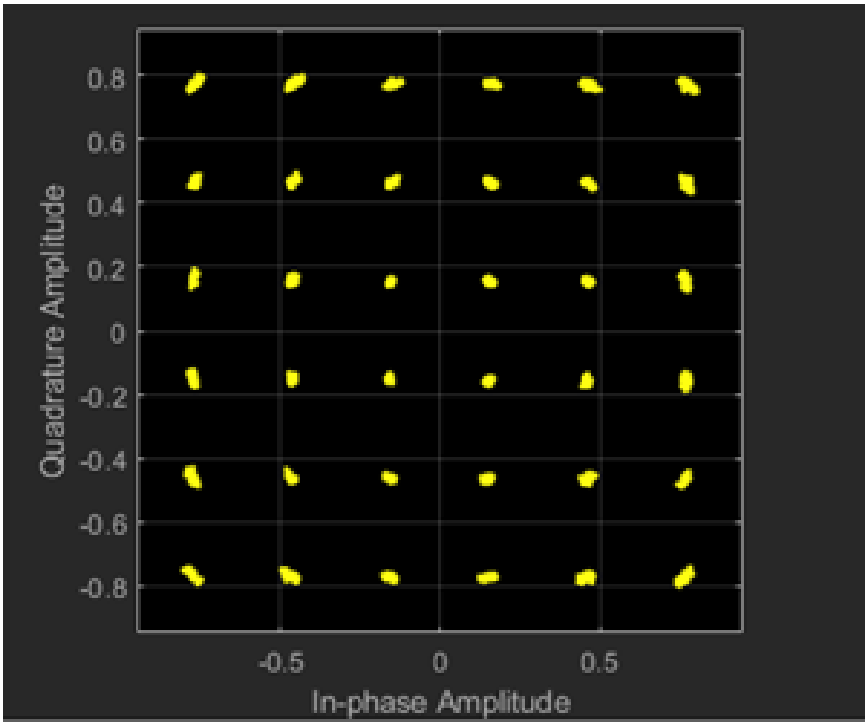

Fig.(4.4): Received instantaneous constellation of massive MIMO-OTFS signal

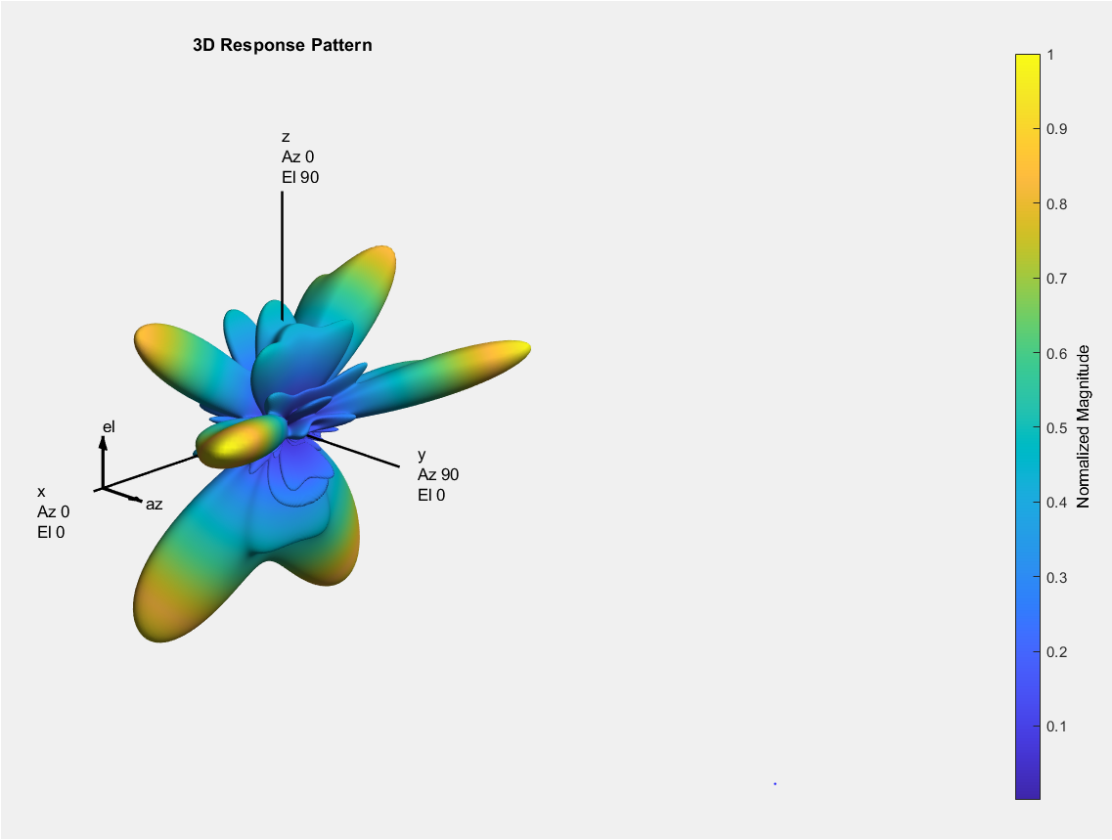

Fig.(4.5): Received instantaneous constellation of massive MIMO-OTFS signal

Figure (4.5) shows the 3-Dimensional pattern response for the received massive MIMO-OTFS signal. The array response pattern shows distinct data streams represented by the stronger lobes. These lobes indicate the spread or separability achieved by beamforming. The figure (4.5) of the 3-Dimenssion Pattern response compares the patterns realized by the optimal, fully digital approach, with those realized from the selected hybrid approach, for a single-user system. The status of received real time signal Error Vector magnitude (RMS EVM) and the BER each user with obtained number of bits the will be shown in the table below:

Table (4.1): The received RMS EVM and BER for each user in mMIMO-OTFS

No of users	RMS EVM	BER	No. of Bits
1	0.38361	10^{-8}	9354
2	1.0311	10^{-9}	6234
3	2.1462	10^{-10}	3114
4	1.0024	10^{-12}	6234

The receiver modeled per user compensates for the path loss by amplification and adds thermal noise. Like the transmitter, the receiver used in a MIMO-OTFS system contains many stages including OTFS demodulation by perform serial to parallel, removing cyclic prefix, perform DFT, MIMO equalization, QAM demapping, and channel decoding.

For the massive MIMO system modeled, the displayed receive constellation of the equalized symbols offers a qualitative assessment of the reception. The actual bit error rate offers the quantitative figure by comparing the actual transmitted bits with the received decoded bits per user. Figure (4.6) illustrates the Received constellation diagrams for each user with different decoded streams of massive MIMO-OTFS signal.

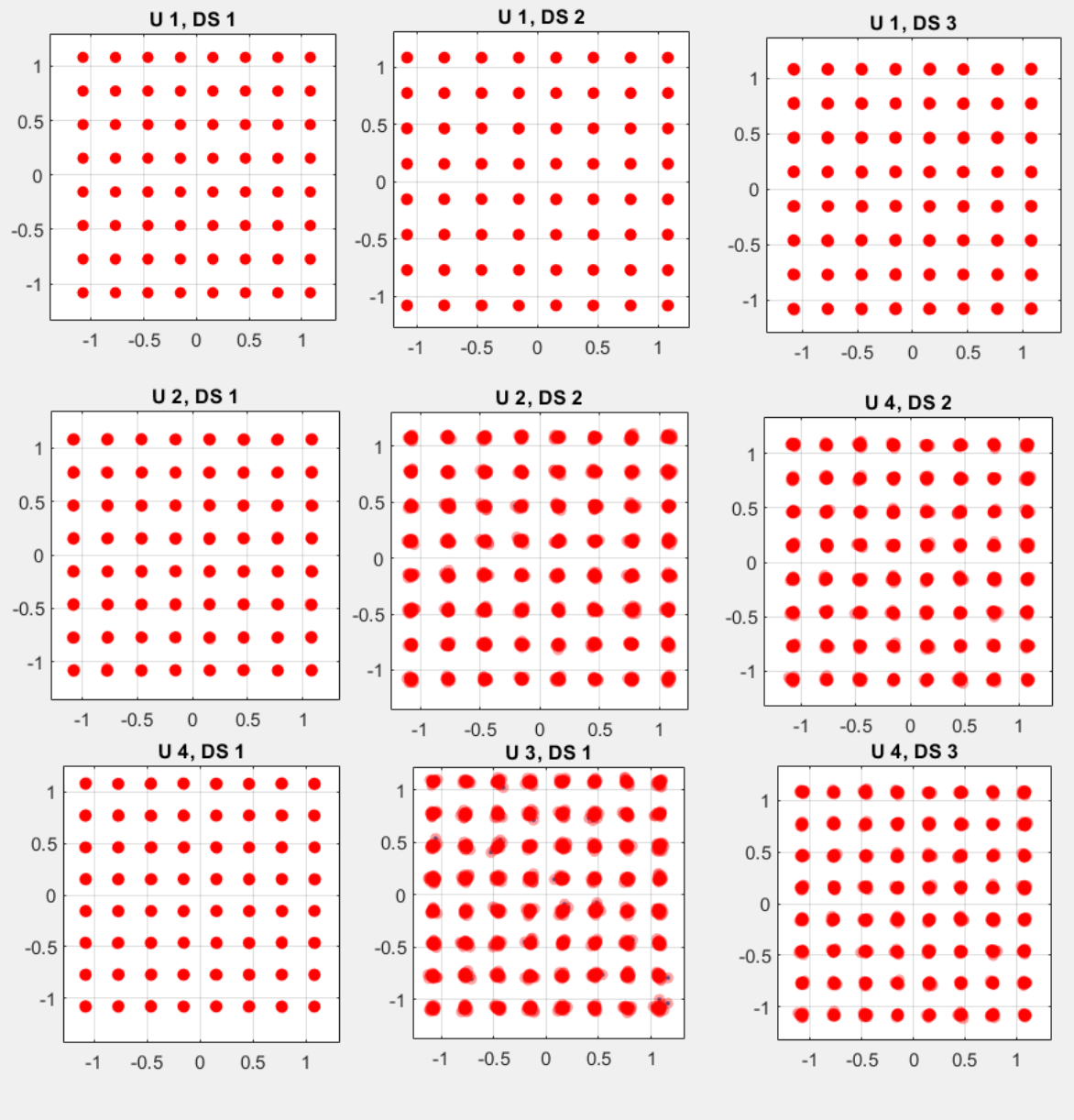

Fig.(4.6): Received constellation diagrams for each user with different decoded streams of massive MIMO-OTFS signal

For comparison, the NMSE will be provided for the conventional depend estimation of channel method when the classic algorithm is applied to recover h. We create the 3GPP standard for space channel modelling while taking into account urban-macro cell conditions. Because of the limited capacity of computational resources, it is important to highlight that N for simulations cannot be set with high values. When N surpasses 10, there are formulation problems for channel estimate since the limited N is unclear. The ration of pilot overhead η is defined as the resource units number needed for transmission of pilot divided by the overall number of unit's resources at the domain of delay-Doppler. We will make a comparison between the assessment of NMSE, the conventional impulse, and the conventional depend technique of estimation of channel againstη, SNR, BS antennas number, and velocity of the user.

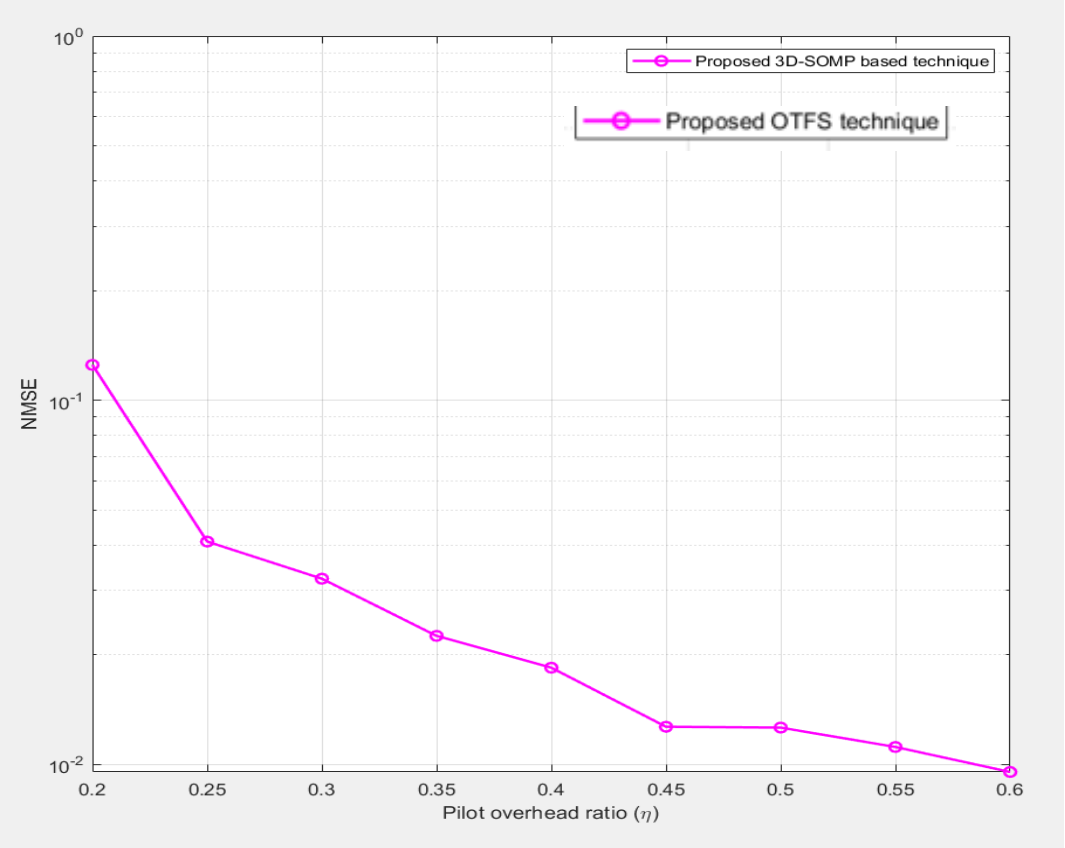

Fig. (4.7): Assessment of comparison for NMSE against η for designed Massive MIMO-OTFS system

In figure (4.7), we explain the performance of NMSE compared with the η for our designed system, where SNR is 10 dB, the velocity of user is 150 m/s, and the number of BS antennas is 32. We obtain that the designed orthogonal time frequency space technique get better performance than the systems based on traditional impulse method, when the ratio of overhead for the same pilot is considered.

In cases where 2 adjecant impulses are less than $M_{\max}$ alongside the delay dimension and less than $N_{\max}$ alongside the dimension of Doppler, the standard impulse-based technology does not function properly since there is not enough pilot overhead. As a result, the assessment of NMSE of the conventional impulse-depend estimation of channel method will degrade due to interference from neighboring impulses. In contrast, the suggested OTFS depend channel method makes use of non-orthogonal pilots. The needed pilot overhead is substantially lower than that of the conventional impulse-depend estimation of channel.

For instance, the suggested OTFS depend method of channel only needs (32%) η to reach the NMSE of (0.03). Conventional impulse-based channel methods require (60%) pilot overhead ratio for an NMSE of (0.3). Figure (4.8) shows the performance of NMSE compared with the base station number of antennas for our OTFS designed system. Additionally, the suggested OTFS method of channel overcome the conventional depend method of channel implementation in terms of performance with a large η, This is a direct effect of utilizing the deployments of OTFS massive MIMO. In Figure (4.9), we offer the comparison assessment of NMSE versus N_{t} for our designed system, where the SNR is set as (10 dB), the η is set as (50%), and the velocity of user set as (150 $\frac{m}{s}$).

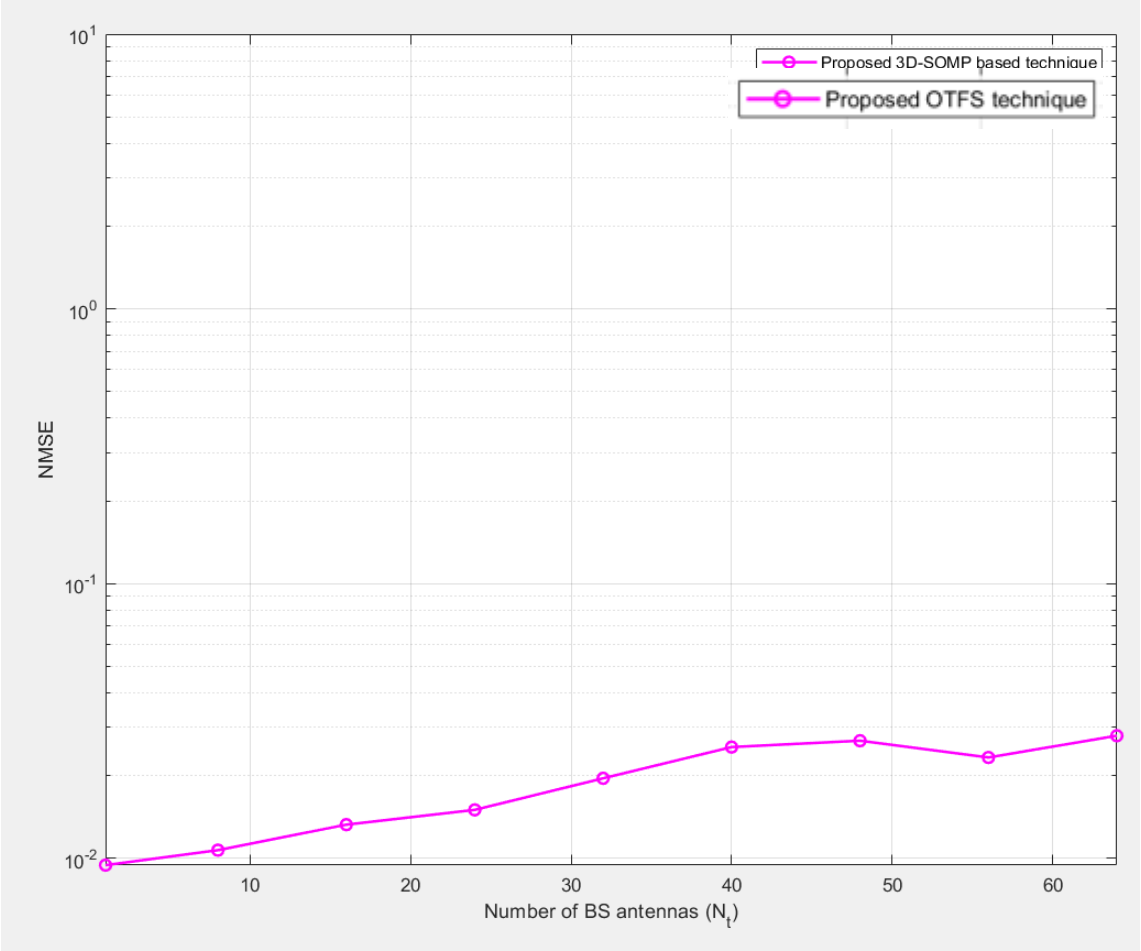

.Fig. (4.8): The performance of NMSE compared with the base station number of antennas for designed downlink Massive MIMO-OTFS system

We can see that the assessment of NMSE for the conventional impulse depend on the estimation method of channel severely degrades (NMSE > 10^{-1}) when there are more than 8 BS antenna. This is occurring because when the η is constant the number of N_t is large. In contrast, the suggested OTFS depend technique doing completely with a high value of N_t. The different assessment between the conventional algorithms of OFDM and the suggested algorithm of OTFS is decreased as N_t increases. This issue could be addressed by improving the η or SNR. Figure 4.9 displays assessment comparison between the NMSE and SNR for designed work. The N_t is set as (32), the η is set as (50%), and velocity of user is (100 m/s).

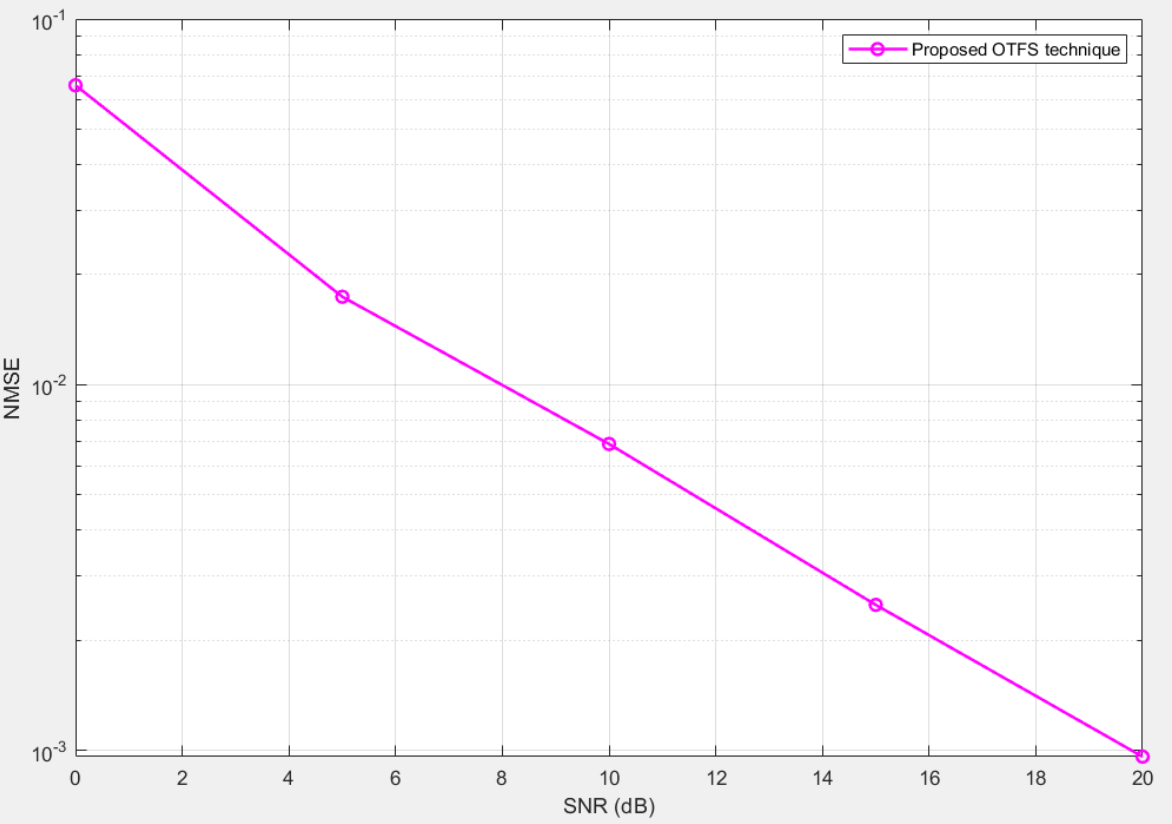

Fig.(4.9): Assessment comparison between the NMSE and SNR for massive MIMO-OTFS system

The findings show that the suggested OTFS method works better than the conventional impulse methods. Because of the interference among several antennas produced from the imperfect η, the conventional impulse depend estimation of channel method has NMSE floor. For the suggested OTFS approach, the assessment of NMSE is increased with the higher SNR. In Figure 4.10, we offer the comparison of the velocity of user v and the performance of NMSE. The$\eta = 50\%$, and the SNR = 5 dB. We find that as the user's velocity increases, the performance of NMSE of the channel estimation decreases. This is due to that when the velocity of user v increases then the Doppler spread $\nu_{\max} = \frac{v}{\lambda}$ will increases and the channel supports $\left[-\frac{N_{\max}}{2} : \frac{N_{\max}}{2} - 1\right]$ along the Doppler dimension is developed.

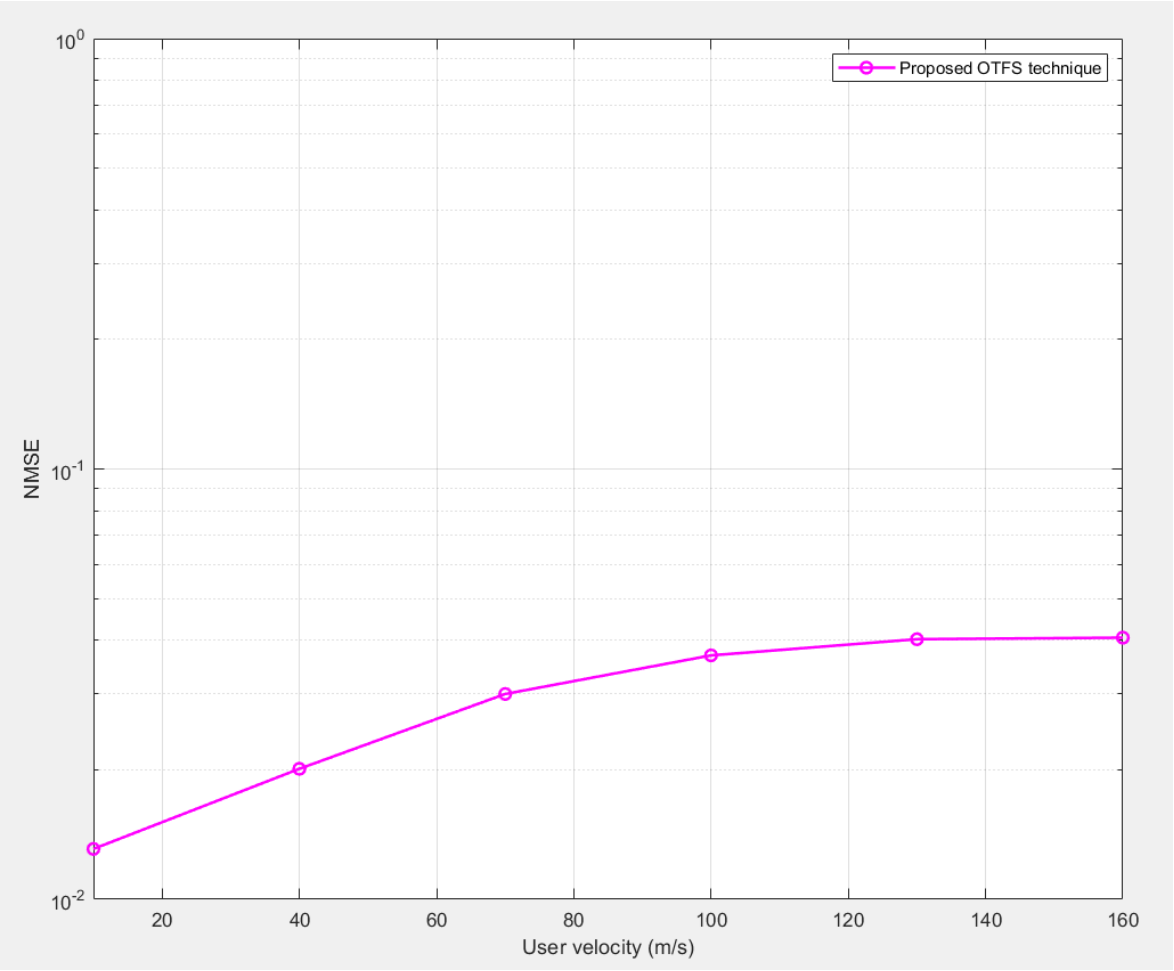

Fig. (4.10): Performance of NMSE compared with the velocity of user for designed downlink Massive MIMO-OTFS system

Thus, to ensure a constant NMSE, the required η is increased. As the velocity of user increases the performance of NMSE of channel estimation degrades with a constant $\eta = 50\%$ in this simulation.

Finally, we compare the SNR against the BER for the designed system OTFS in Figure (4.11). Velocity of the user =100 m/s. Then, we compare the SNR against the BER for both the systems (OTFS and OFDM) as shown in figure (4.12)

The ICI introduced by the significant Doppler dispersion in this highly mobile scenario reduces the assessment of BER of OFDM system, and this is illustrated by the 'OFDM beneath ICI' curve.

With perfect knowledge of CSI, we can employ discovering of MMSE to defeat the ICI represented by the 'perfect CSI with OFDM' curve, which performs better than the scenario 'OFDM beneath ICI' curve. In system of OTFS, perfect and estimated CSI applying the conventional impulse-depend technique, and estimated CSI using suggested are individually applied for detect of for signal of OTFS during the delay-Doppler 2D deconvolution.

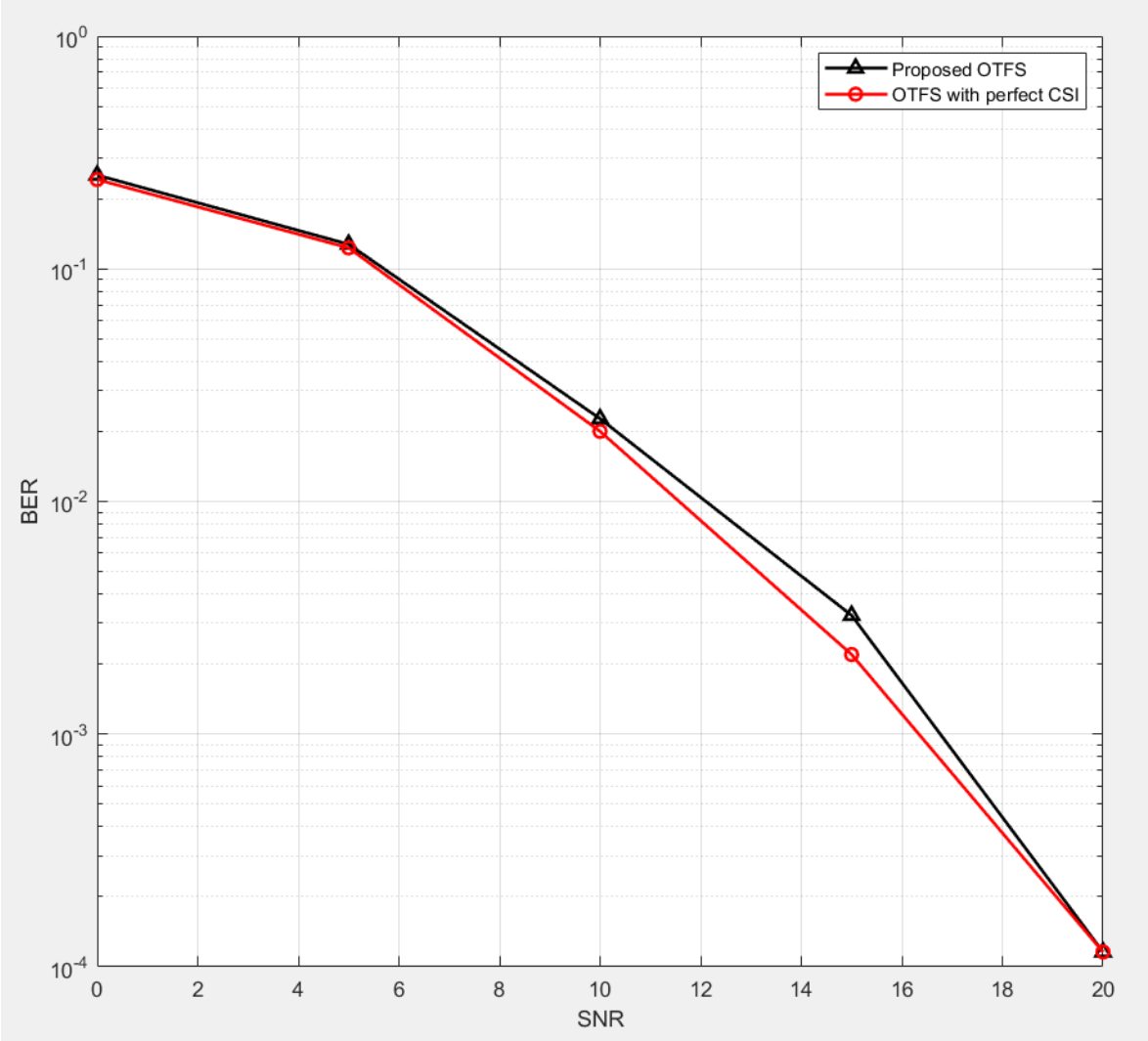

Fig.(4.11): Performance comparison between SNR and BER for downlink Massive MIMO system under OTFS modulation scheme

With perfect CSI in the high SNR domain, we see that the system of OTFS performs better than the system of OFDM. This is due to the fact that systems of OTFS are able to exploit the benefits of frequency-time channel

diversity in their transmissions. In addition, we see that the suggested 3D-SOMP method can provide acceptable performance of BER equivalent to nearly perfect CSI in systems of OTFS. The conventional impulse depend technique of estimation channel gets inaccurate CSI, which negatively impacts performance of BER.

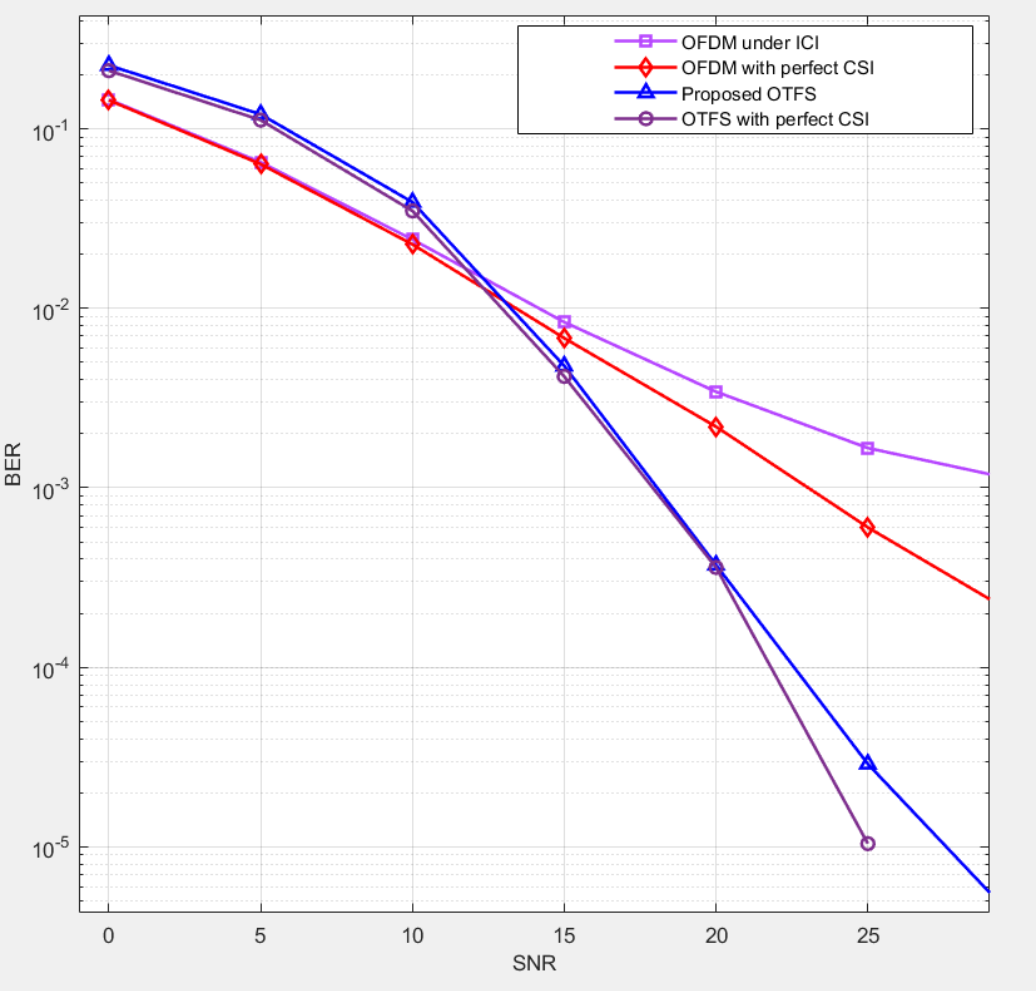

Fig.(4.12): Performance comparison between SNR and BER for downlink Massive MIMO system under different modulation schemes

As compared with ordinary MIMO system, a very high performance of massive MIMO-OTFS system can be achieved by using our designed system for both downlink and uplink scenarios. Due to the high number of antenna arrays used, the best spectral and energy efficiencies achieved among all recent MIMO systems under the same conditions. The use of massive MIMO-OTFS system

enables the transmission of OTFS signals in very high transmission data rates by using (256) OTFS subcarriers.

Figure (4.13) will be illustrated for uplink scenario to explain the difference between the use of ordinary MIMO systems and designed massive MIMO-OTFS system by comparing the achieved BER for each system with respect to range of SNR values.

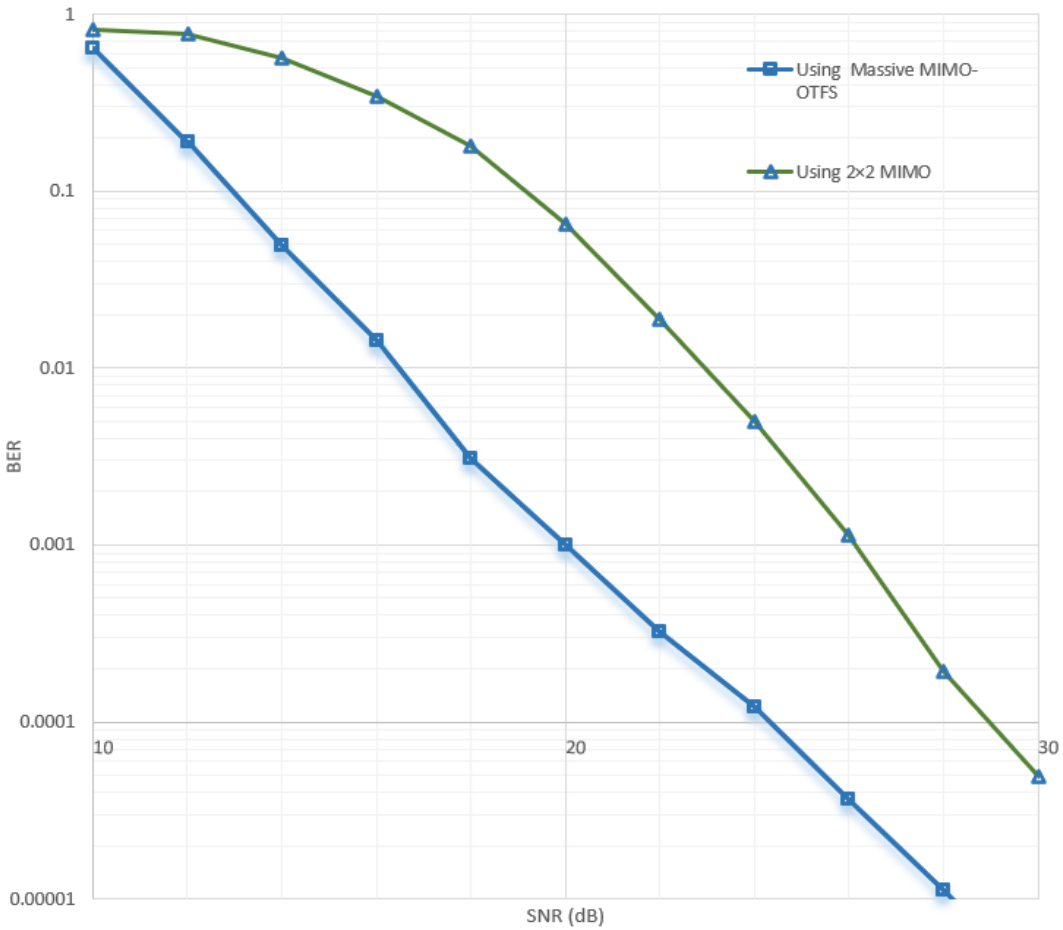

Fig.(4.13): SNR(dB) vs BER for Uplink MIMO and massive MIMO-OTFS systems

The same systems tested under the same conditions for downlink scenario. The results also show the preference of massive MIMO-OTFS among ordinary MIMO system

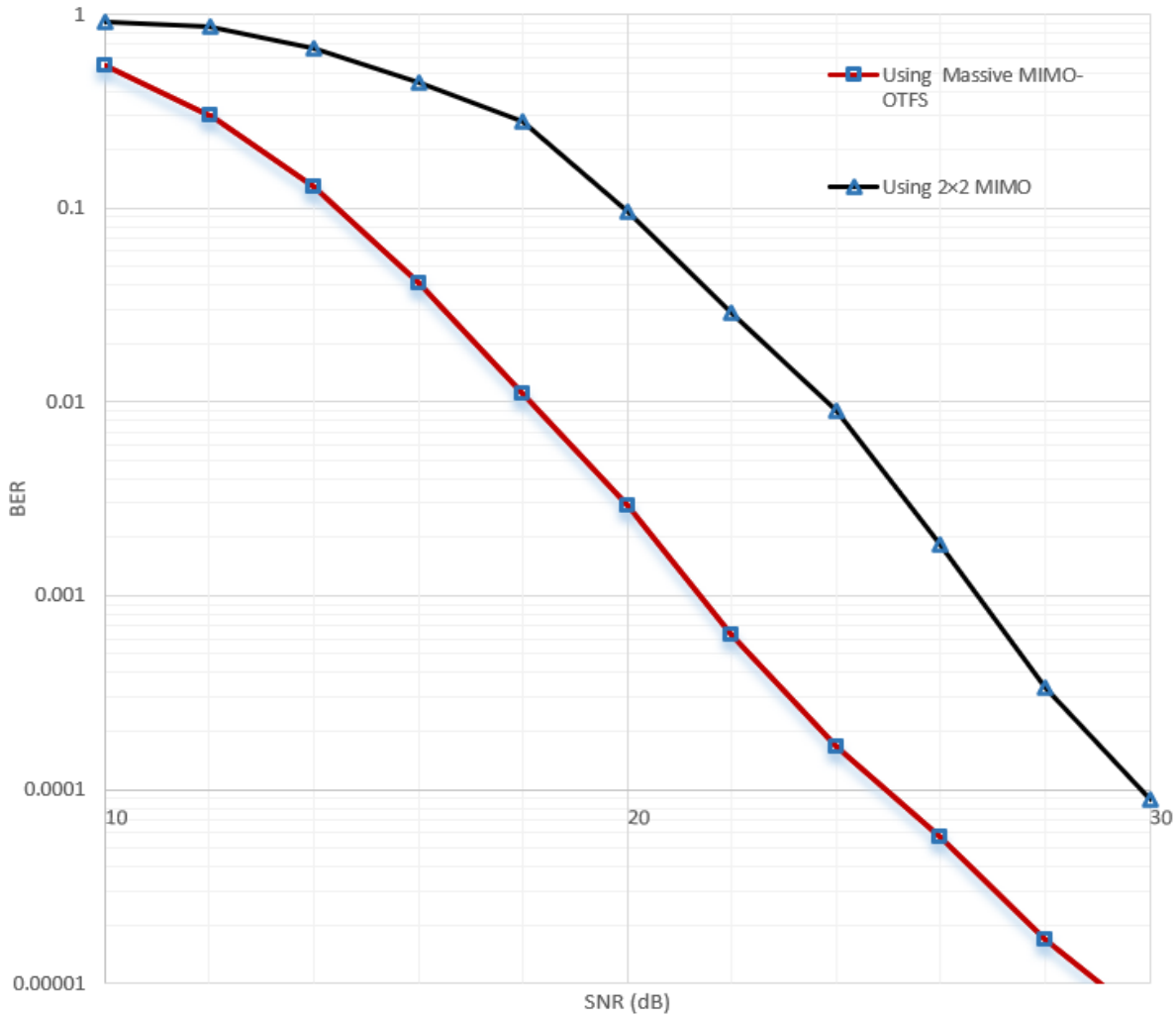

Fig.(4.14): SNR(dB) vs BER for downlink MIMO and massive MIMO-OTFS systems

Regarding the link budget of each MIMO and massive MIMO systems, we can see the difference in many parameters of each system. In the case of ordinary MIMO the input power is divided for only two antennas. In case of a Massive MIMO BS, the input power is divided over all the antennas of the BSs. From other side, in ordinary MIMO the carrier frequency is 2.5 GHz while the frequency of massive MIMO is 3.7 GHz. These link budget parameters must be taken into consideration in designing massive MIMO system.

4.3 Results of RoF-MMW - Multi-Carrier OFDM transmission Systems

In this section we are presenting the simulation results of Hybrid RoF-MMW based multi subcarrier OFDM backhaul transmission system using several QAM modulation formats and two OFDM subcarrier values to achieve best system performance and highest bit rate for the designed system.

4.3.1 Results Of MC-OFDM-MMW-RoF system using 16-QAM format

The following section illustrate the results and performance of 16-QAM system. At first, 16-subcarrier OFDM modulation used with a default bit rate of (40 GHz). The results show a successful transmission with acceptable SER value for all OFDM subcarriers as shown in figure (4.15).

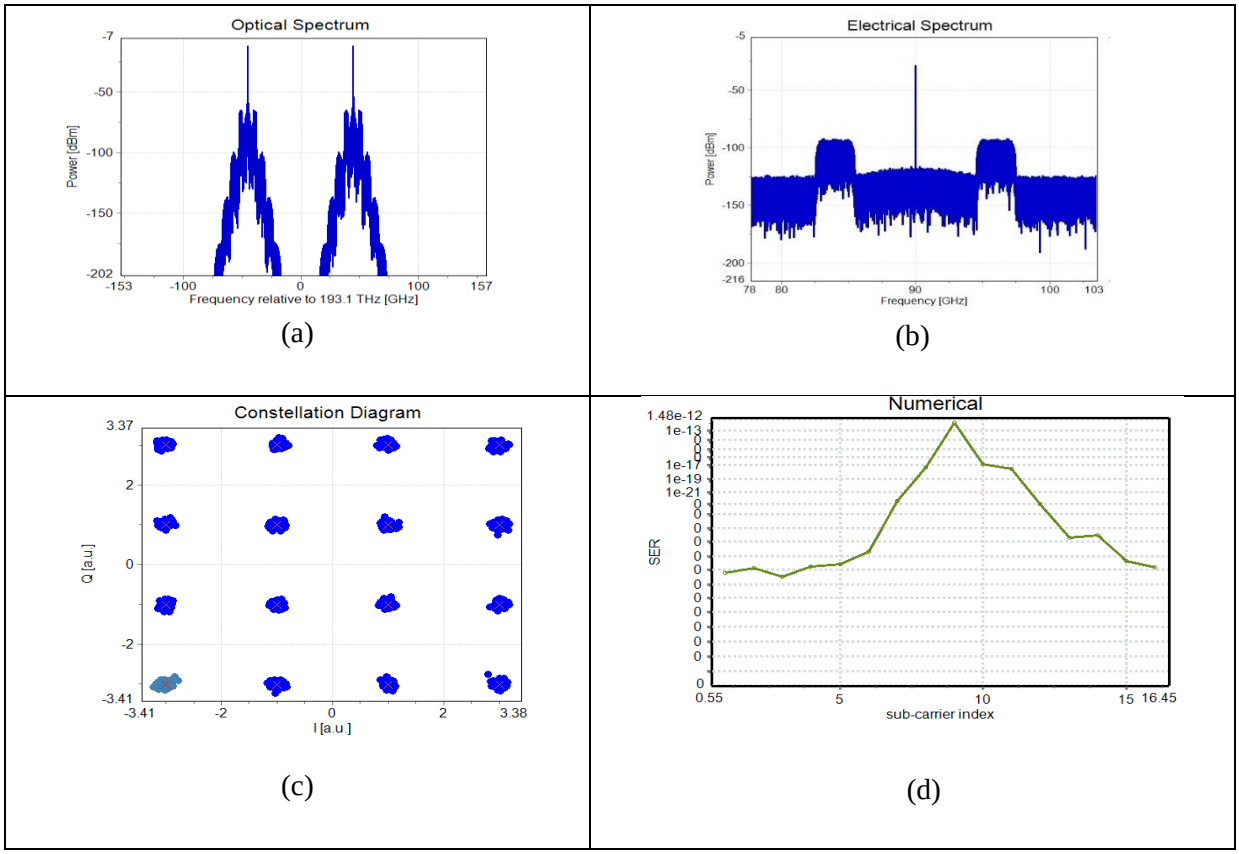

Fig. (4.15): 16 sub-carrier OFDM-RoF-MMW system: (a): Optical spectrum of OFDM on MMW, (b): Electrical spectrum for received 16 OFDM signals (c): Received constellation diagram for 8th subcarrier at 16 QAM format, (d): SER for each sub-carrier

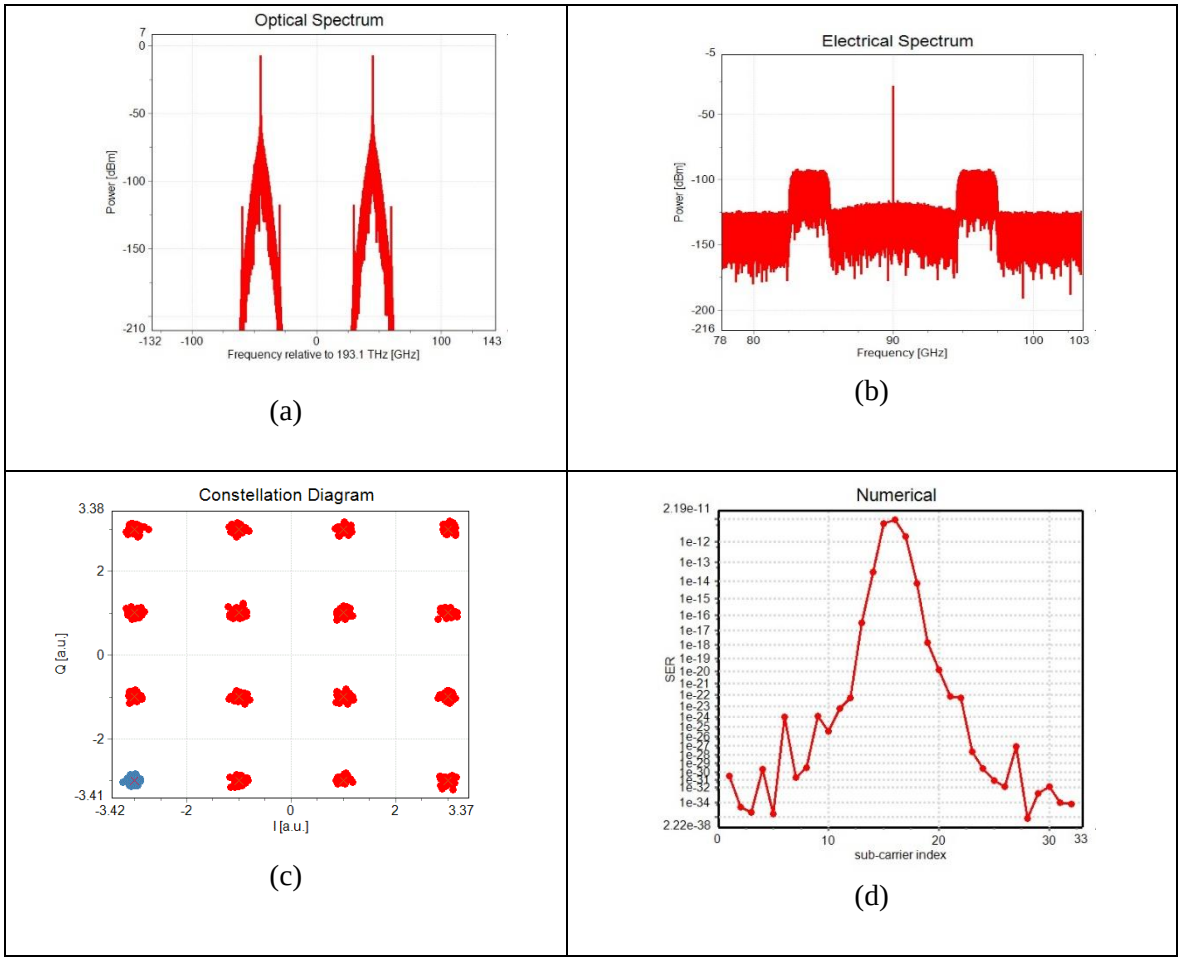

Fig. (4.16): 32 sub-carrier OFDM-RoF-MMW system: (a): Optical spectrum of OFDM on MMW, (b): Electrical spectrum for received 32 OFDM signals (c): Received constellation diagram for 16th subcarrier at 16 QAM format, (d): SER for each sub-carrier

Figure (4.16) shows the results of 32 sub-carrier OFDM-RoF-MMW system. As it difficult to show the spectrum of all subcarriers in VPI software, only two subcarriers used for example to show the optical and electrical spectrum representation for the designed system as shown at figure (4.14 a and b). As shown in figure (4.14c) a clear 16-QAM constellation for the worst case at 8th subcarrier achieved for the received data. By using our 32-OFDM-RoF-MMW system a higher transmission rate with acceptable SER for all subcarriers had been achieved as shown at figure (4.14d). Thanks to added python DSP different losses that resulted from PAPR and oscillator mismatch had been compensated.

Figure (4.17) presents the performance of BER vs SNR for hybrid RoF-MMW system with MC OFDM at 16QAM. The range of SNR was taken from 0 to 15 dB to express the BER for each SNR with a constant RoF link distance of 50 km. There is an increase in BER values of 32-OFDM among 16-OFDM due to increased number of transmitted subcarriers. From other side, an acceptable range of BER obtained at each subcarrier for 32 OFDM system for different SNR values.

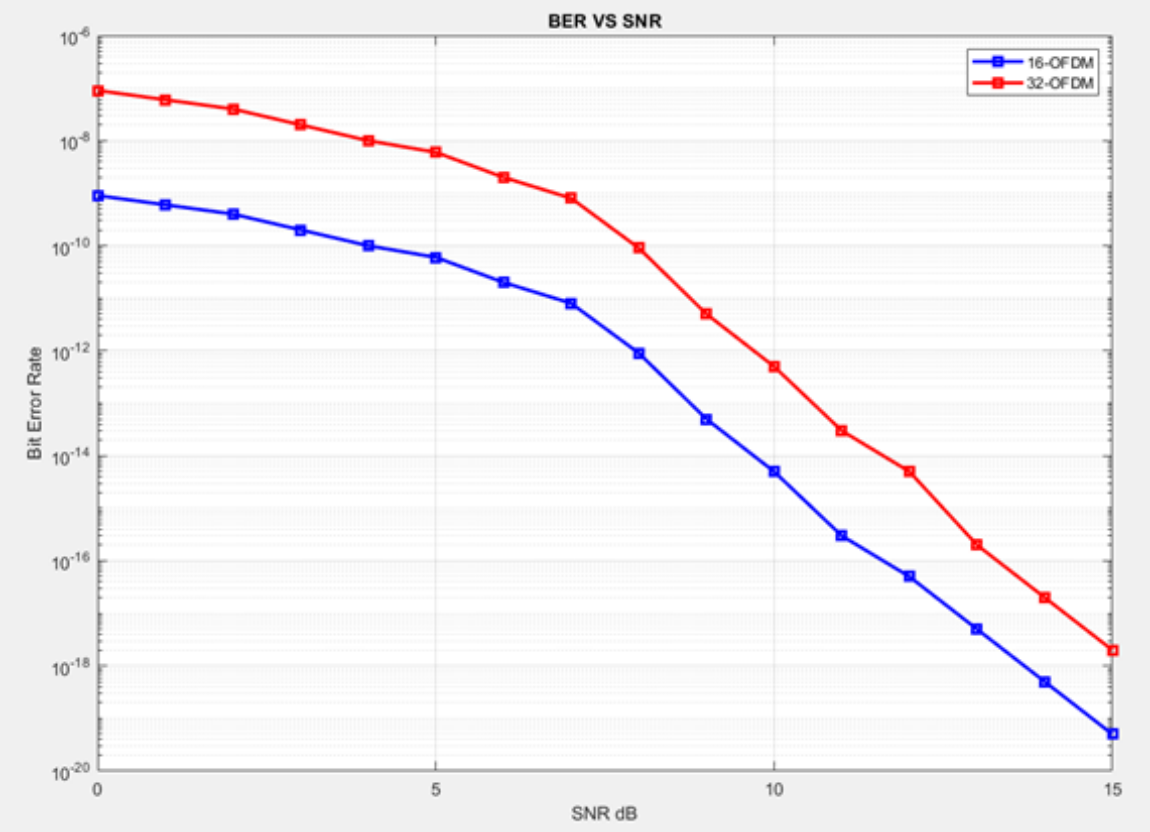

Fig.(4.17): Performance of BER vs SNR for hybrid RoF-MMW system with MC OFDM at 16QAM

Figure (4.18) explains the performance of BER for hybrid RoF-MMW system with 16-OFDM and 32-OFDM systems at 16QAM with different fiber distances. A range from 1km to 120 km fiber transmission distances used with a constant SNR of 10 dB and different BER values recorded. Its clear that increased transmission distance will lead to obtain higher BER values and the system performance will be degraded gradually due to linear dispersion losses

and nonlinear losses of RoF transmission channel. A successful transmission until 100 km obtained for our designed systems with acceptable BER for each type of subcarriers. A slight change at BER between 16-OFDM system and 32 OFDM system by increasing the BER value with increased number of subcarriers at different transmission distances.

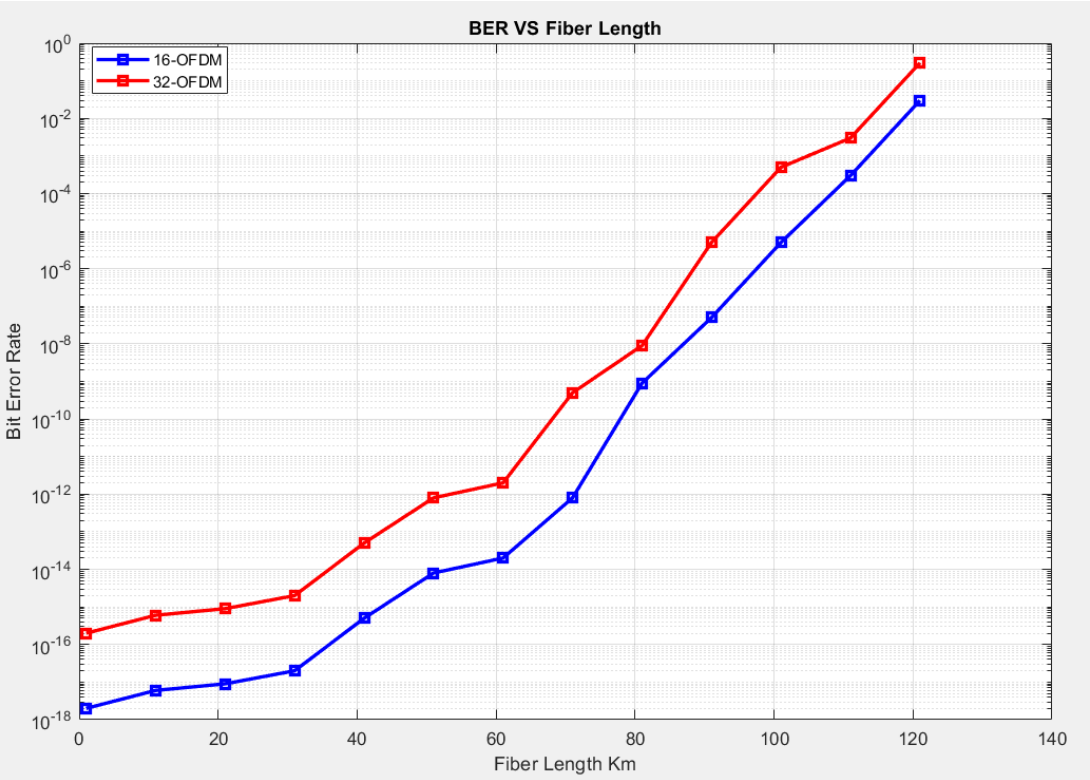

Fig.(4.18): Performance of BER vs fiber length for hybrid RoF-MMW system with MC OFDM at 16QAM

4.3.2 Results Of MC-OFDM-MMW-RoF system using 64-QAM format

The following results obtained for our hybrid OFDM-RoF-MMW system at 64-QAM system. Figure (4.19) illustrates different results of designed system at 16-OFDM system. As we can notice, there is a degradation in the performance by using higher order 64-QAM modulation format among 16-QAM system due to increased number of bits and data represented by using 64 QAM system.

Although, a successful transmission of our designed system with BER of less than 10^{-8} obtained using 16-OFDM system with achieved higher overall data rates as compared with 16-QAM.

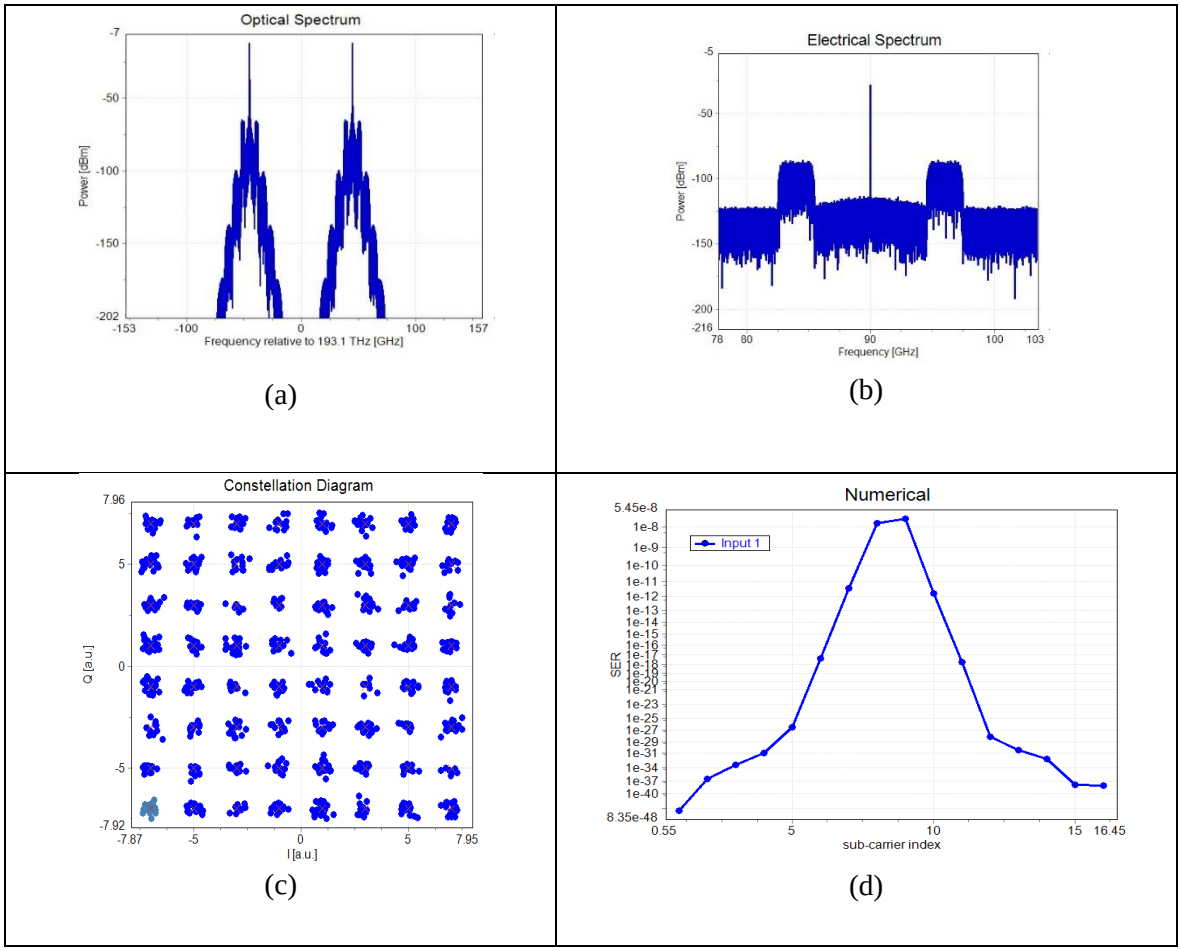

Fig. (4.19): 16 sub-carrier OFDM-RoF-MMW system: (a): Optical spectrum of OFDM on MMW, (b): Electrical spectrum for received 16 OFDM signals (c): Received constellation diagram for 8th subcarrier at 64 QAM format, (d): SER for each sub-carrier

Figure (4.20) shows the results of our designed OFDM-RoF-MMW system using 32-OFDM system. The achieved results also presenting acceptable range of SER for each subcarrier with a higher SER value of 10^{-3} at 16th subcarrier. The use of MMW technology offers very high-speed transmission link at (90 GHz) band. From other hand, using carrier frequency of (6GHz) obtains a promising transmission to be used in B5G systems.

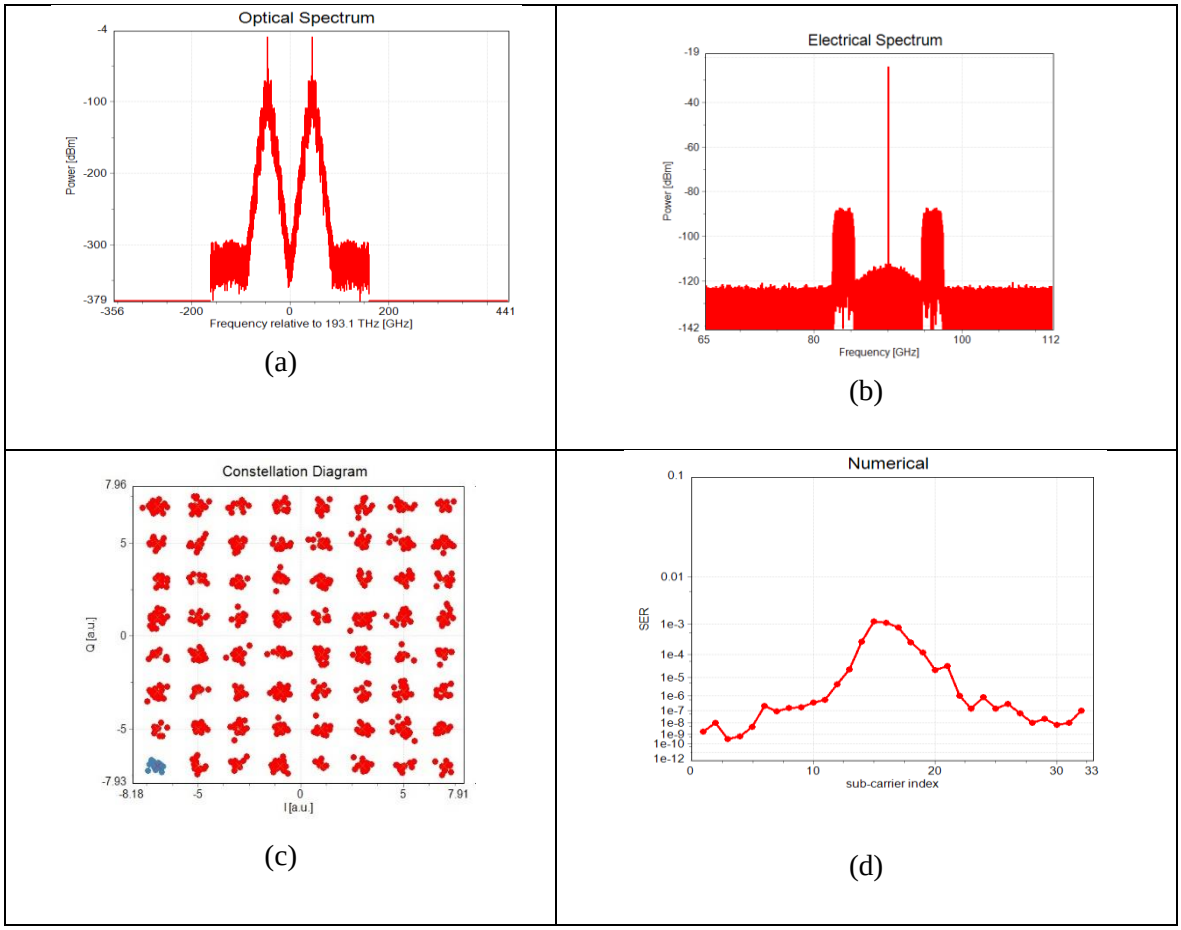

Fig. (4.20): 32 sub-carrier OFDM-RoF-MMW system: (a): Optical spectrum of OFDM on MMW, (b): Electrical spectrum for 32 OFDM signals (c): Received constellation diagram at 64 QAM format, (d): SER for each sub-carrier

Figure (4.21) illustrates the Performance of BER vs SNR for hybrid RoF-MMW system with MC OFDM at 64QAM format. The achieved BER is nearly 10^{-14} for 16-OFDM system and 10^{-12} for 32-OFDM system at maximum adjustable SNR of 15 dB. These are favorable values for BER to use our designed system for wireless backhaul transmission between main BS and RAU at B5G netwoks.

Figure (4.22) shows Performance of BER vs SNR for hybrid RoF-MMW system with MC OFDM at 64QAM. The use of seamless converged RoF transmission link enables the long transmission even for higher QAM modulation formats.

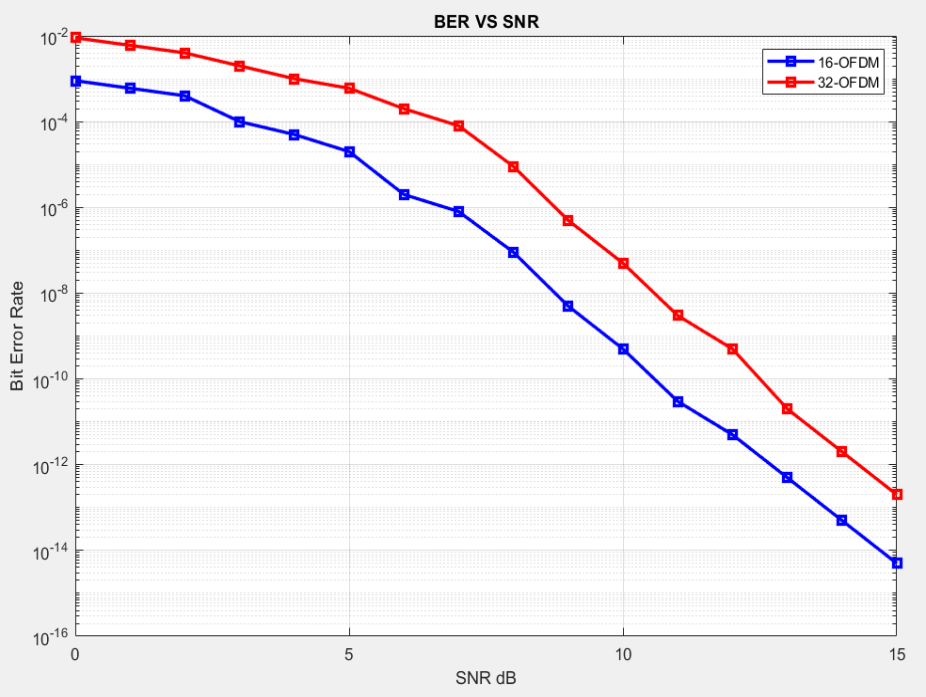

Fig.(4.21): Performance of BER vs SNR for hybrid RoF-MMW system with MC OFDM at 64QAM

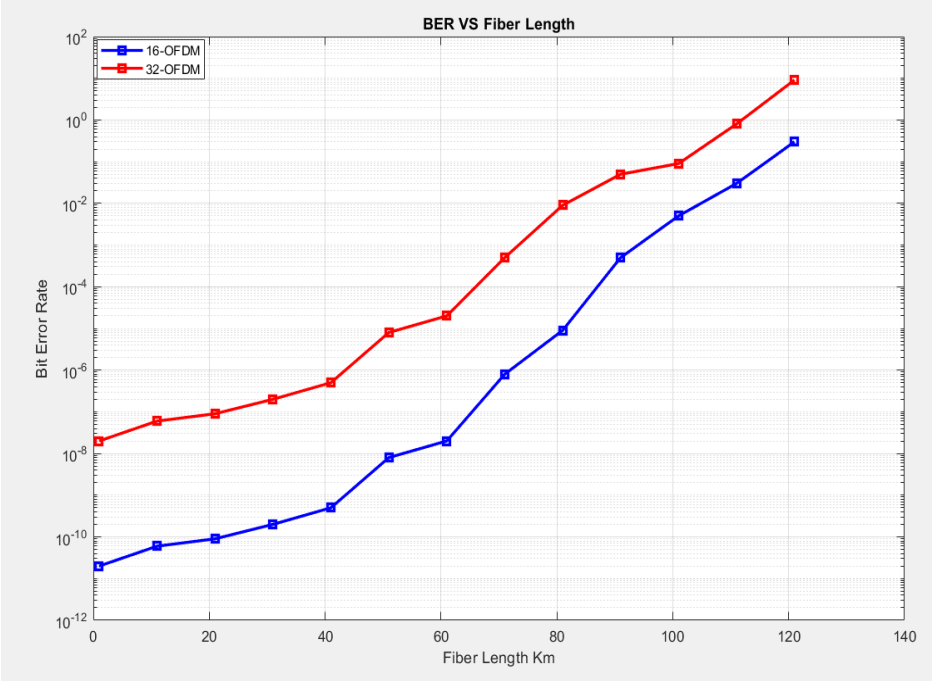

Fig.(4.22): Performance of BER vs fiber length for hybrid RoF-MMW system with MC OFDM at 64QAM

4.3.3 Results Of MC-OFDM-MMW-RoF system using 128-QAM format

Figure (4.23) presents the results of MC-OFDM-MMW-RoF system using 128-QAM format. Highest achievable 128 format can be obtained with nearly acceptable BER for this system to be the best choice of obtaining ultra-high-capacity transmission system among all designed systems.

The highest overall transmission system achieved by using 32-OFDM system with 128-QAM format. Figure (4.24) presents the results of MC-OFDM-MMW-RoF system using 128-QAM format.

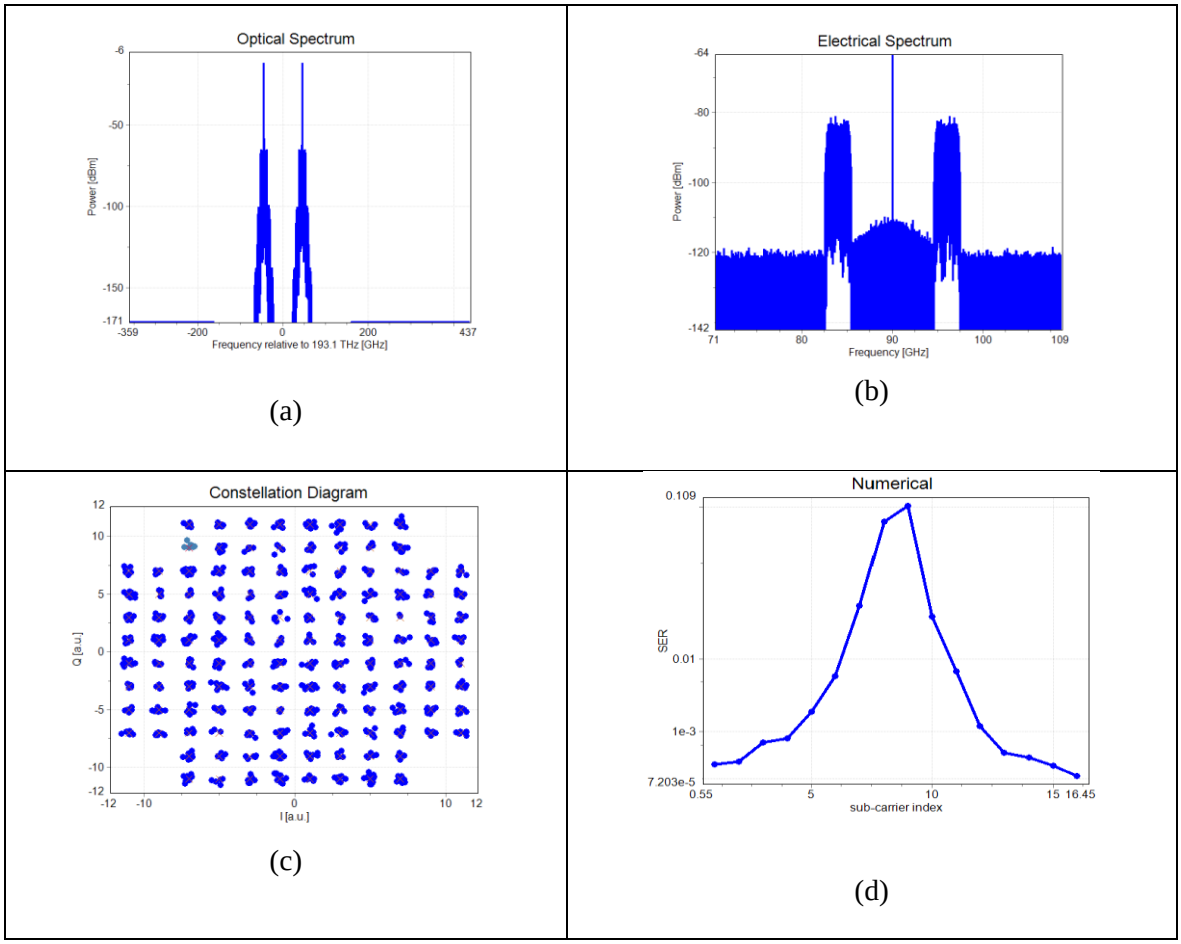

Fig. (4.23): 16 sub-carrier OFDM-RoF-MMW system: (a): Optical spectrum of OFDM on MMW, (b): Electrical spectrum for 16 OFDM signals (c): Received constellation diagram at 128 QAM format, (d): SER for each sub-carrier

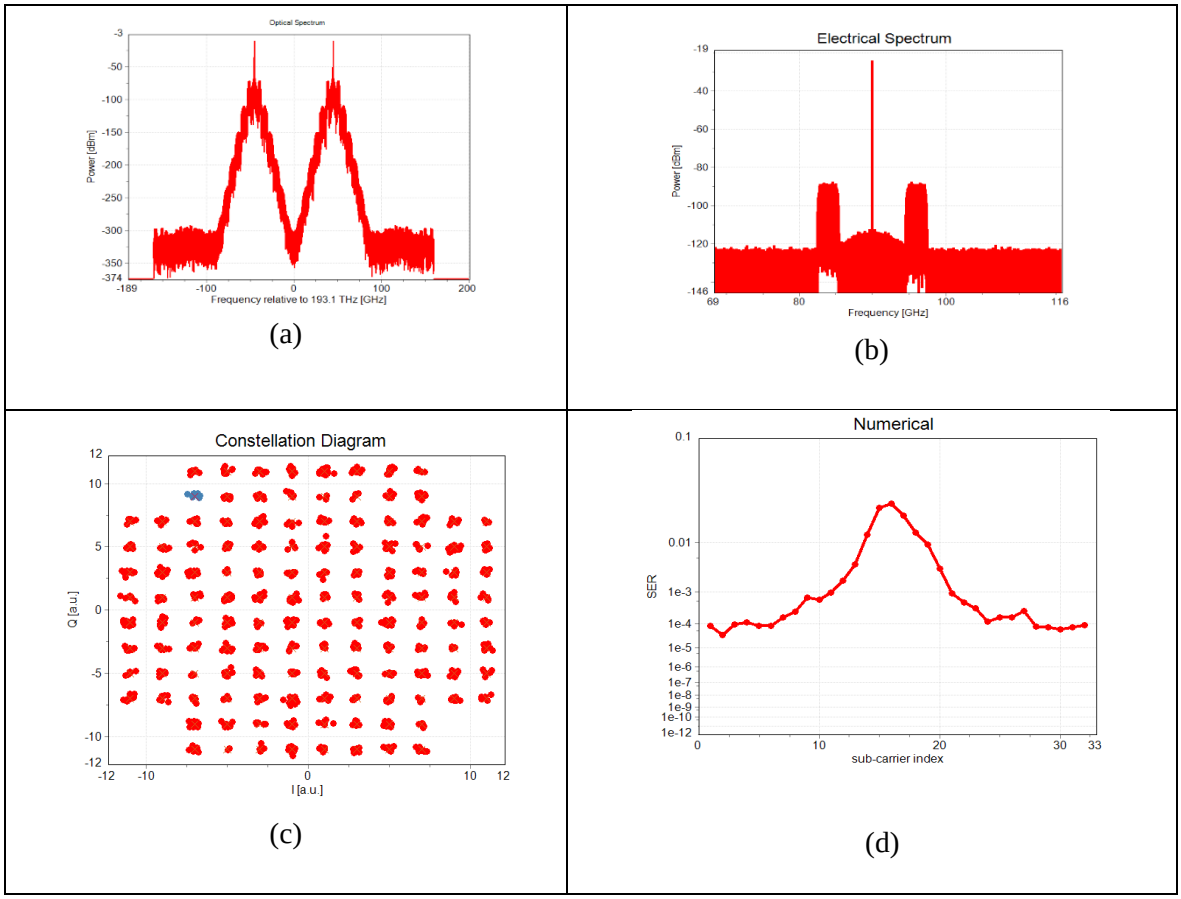

Fig. (4.24): 32 sub-carrier OFDM-RoF-MMW system: (a): Optical spectrum after AWG, (b): Electrical spectrum for 32 OFDM signals (c): Received constellation diagram at 128 QAM format, (d): SER for each sub-carrier

Figure (4.25) presents the performance of BER vs SNR for hybrid RoF-MMW system with MC OFDM at 128QAM. We can notice that even for high setting of SNR the value of BER still not favorable due to the susceptibility of 128 QAM to losses.

Figure (4.26) shows the performance of BER vs fiber length for hybrid RoF-MMW system with MC OFDM at 128QAM. Minimum acceptable BER and maximum distance of 80 km achieved for 16-OFDM system and minimum acceptable BER at maximum distance of 50 km achieved.

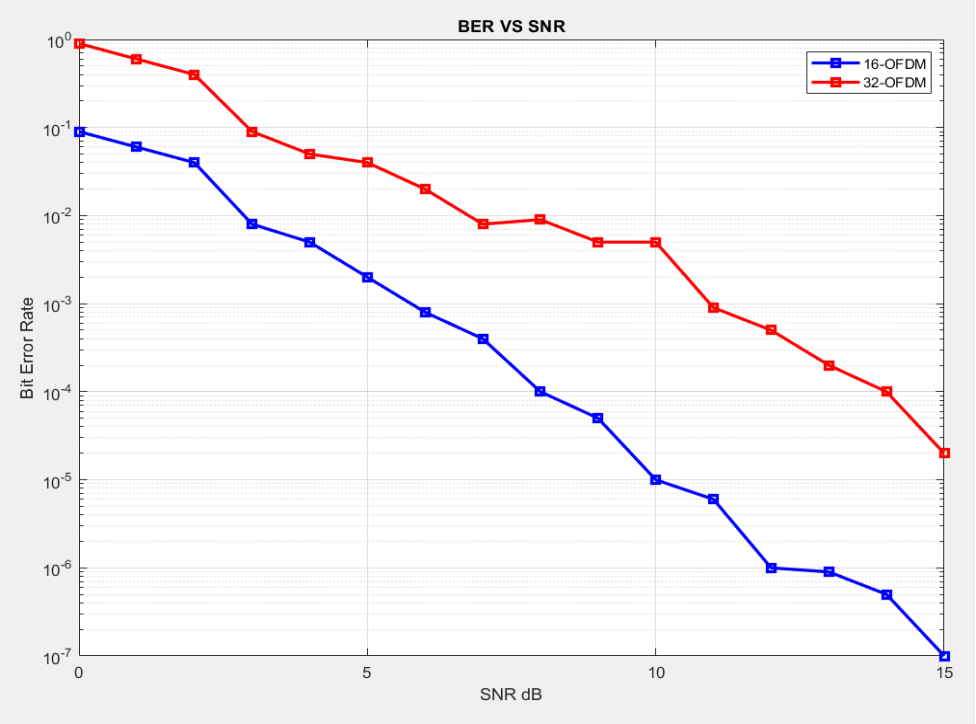

Fig.(4.25): Performance of BER vs SNR for hybrid RoF-MMW system with MC OFDM at 128QAM

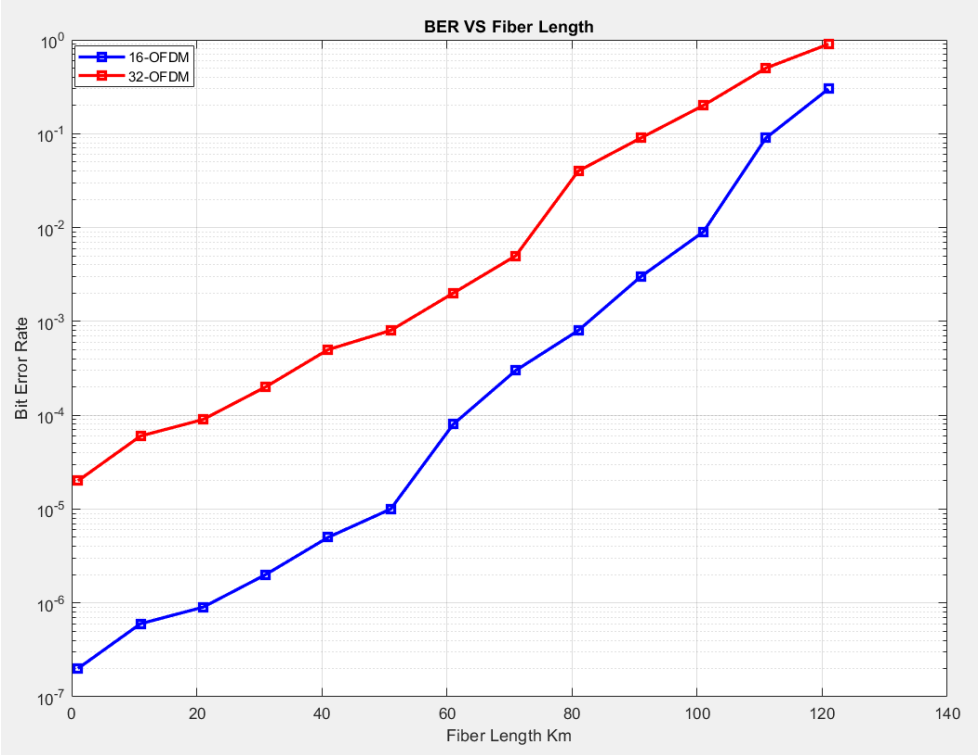

Fig.(4.26): Performance of BER vs fiber length for hybrid RoF-MMW system with MC OFDM at 128QAM

Figure (4.27) shows the electrical spectrum of OFDM carriers by using a carrier frequency of (6GHz) in 128-QAM system. The use of (6GHz) achieved best system performance and supports the transmission range of B5G networks to be the best carrier frequency value for our designed systems.

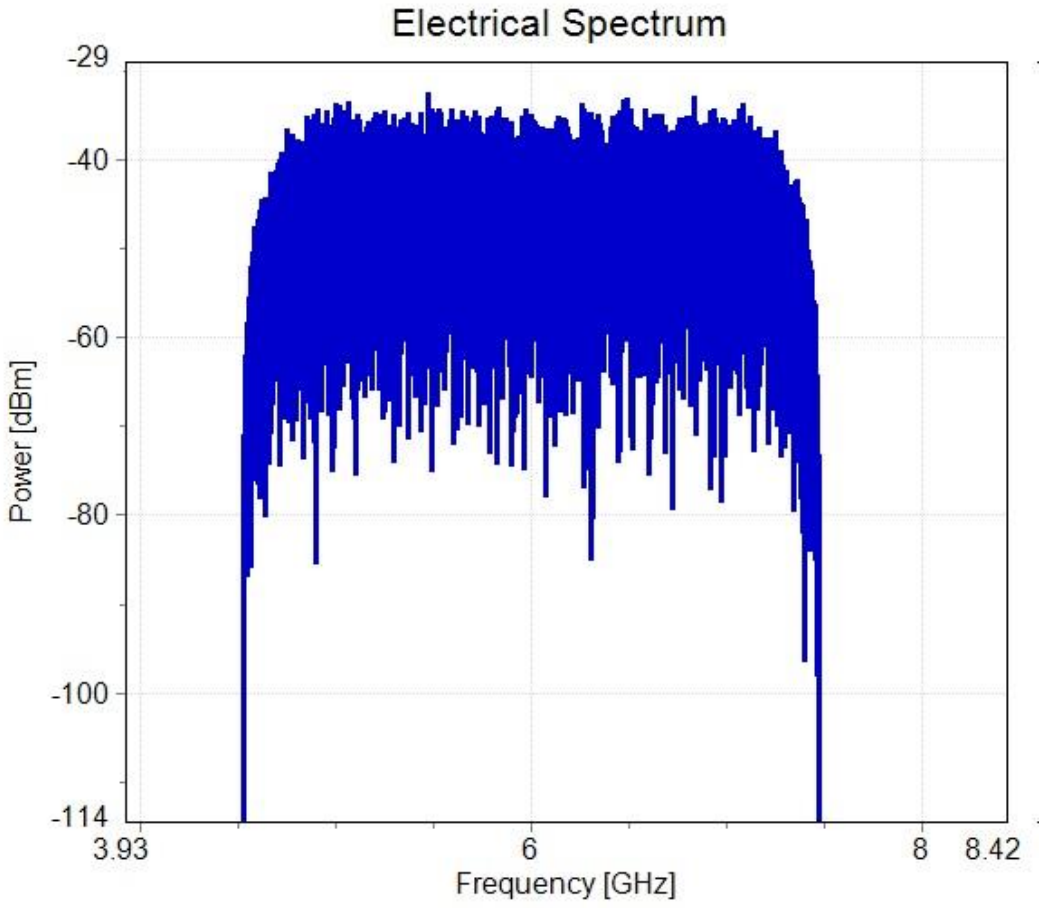

Fig. (4.27): Electrical spectrum of OFDM carriers by using a carrier frequency of (6GHz) at 128QAM format

The designed systems show a very promising performance to be involved in the next generation networks. By using default bit rate of 50 GHz, the best achieved results of OFDM-RoF-MMW system can be summarized using 32 subcarrier-OFDM system with 128 QAM format to obtain overall ultra-high-capacity system of nearly 11.2 THz (32-OFDM*7 bits/symbol*50GHz).

4.4 Results of All optical OFDM Transmission Systems

The following results obtained for All optical OFDM Transmission Systems. Two subcarriers of AO-OFDM will be achieved for ultra-high capacity transmission system.

4.4.1 Results of 16- All optical OFDM Transmission Systems

Figure (4.28) shows a successful transmission of 16-subcarrier all optical OFDM system by using QPSK modulation format. The QPSK designed method supported for long haul transmission.

The performance of 16 subcarriers of AO-OFDM based AWG is achieved by measuring BER as a function of the input power and the transmission length for QPSK modulation format.

Regarding the QPSK system, the performance is also evaluated by calculating BER as a function of input power and length of the fiber.

In the QPSK system, Fig. 2.28 displays the constellation diagrams as indicated in the QAM system at different input power at (-12, -8, 0) dBm for a specific DWDM channel (channel eight). Fig. 2.26 (a) shown the maximum and minimum amplitude of output constellation diagram of the OFDM signal that is 1.47 (a.u) and -1.47 (a.u) at -12 dBm input power. This amplitude value is increased to 1.14 (a.u) maximum value and -1.19 (a.u) minimum value in -8 dBm input power in Fig. 2.26 (b), while it becomes large again in 0 dBm input value as shown in Fig. 2.27 (c).

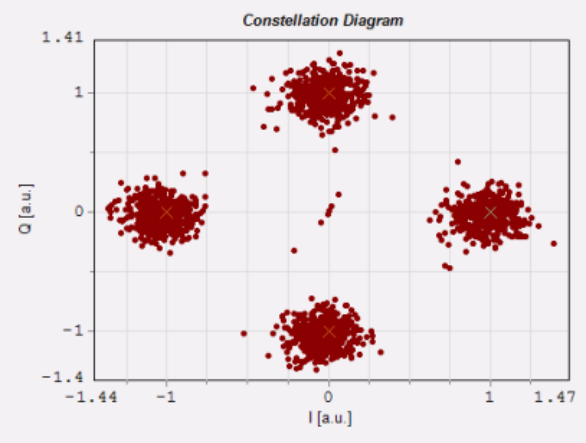

(a)

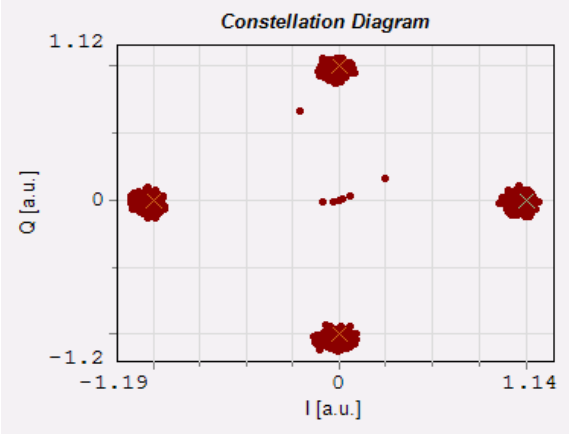

(b)

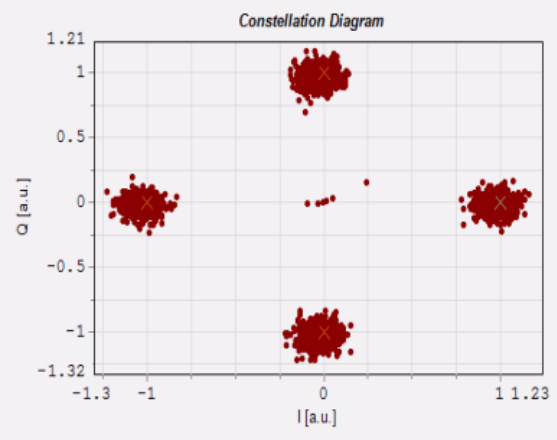

(c)

Figure (2.28): Received constellation diagrams for 16-AOOFDM-QPSK of channel 6 with: (a) -12 dBm, (b) -8 dBm, and (c) 0 dBm

The QPSK system obtained constellation diagrams of 16- All optical OFDM transmission systems with different length as shown in Fig. 4.29 (a) illustrated of constellation OFDM signal at 100 km transmission length. The amplitude value at maximum and minimum is 1.14 (a.u) and -1.23 (a.u), while at 500 km is 1.23 (a.u) and -1.37 (a.u). That is meaning the transmission length can be increased without effect on the output signal of OFDM at 0 dBm input power. For this, we can increase the transmission length to 1000 km to get maximum and minimum amplitude value 2.23 (a.u) and -2.35 (a.u) as shown in Fig. 4.29 (c).

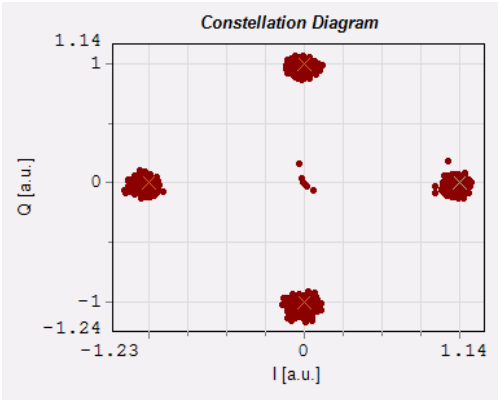

(a)

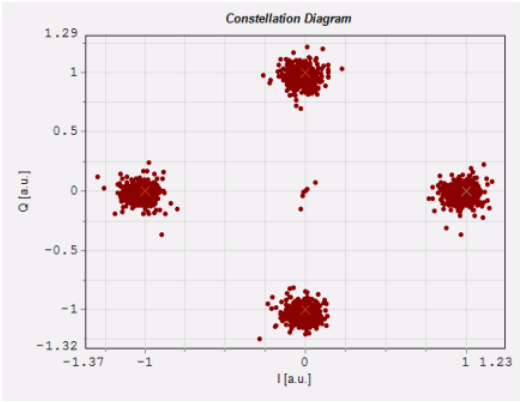

(b)

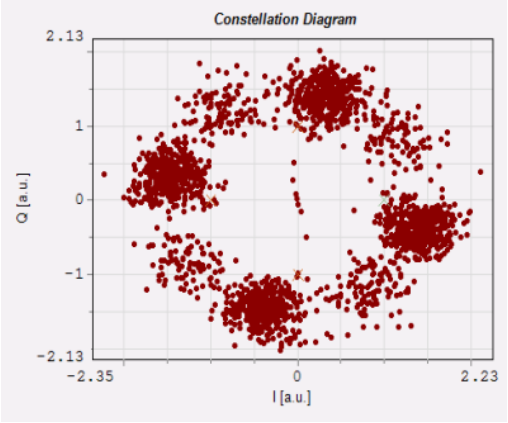

(c)

Figure (4.29): Received constellation diagrams for QPSK for channel 4 of 16 AO OFDM at: (a) 100 km, (b) 700 km, and (c) 1000 km

Digital signal processing for sliding window implementation of Viterbi & Viterbi phase estimator applied for dual-polarization mPSK to make better phase correction for received signals. A rectangular windowing filter is applied with the phase error estimated over (2*NPreSymbols+1) symbols. The NPreSymbols parameter gives the number of pre-symbols used for phase estimation. Figure (4.30) shows the effect of using mPSK DSP algorithm for phase correcting the required signal.

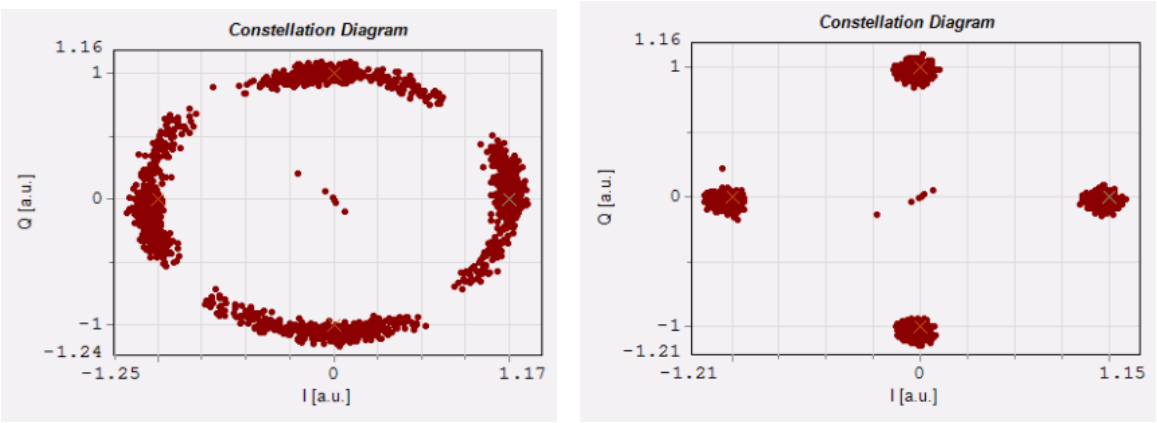

(a) (b)

Fig. (4.30): Received constellation diagram of 16 AO OFDM for QPSK signal: (a) without mPSK phase estimator, (b) with mPSK phase estimator

From other side, to increase the system capacity we performed 16-QAM for 16 AO OFDM system for al subcarriers. Other DSP algorithm improved for adaptive equalization of coherent 16-QAM signals as shown below.

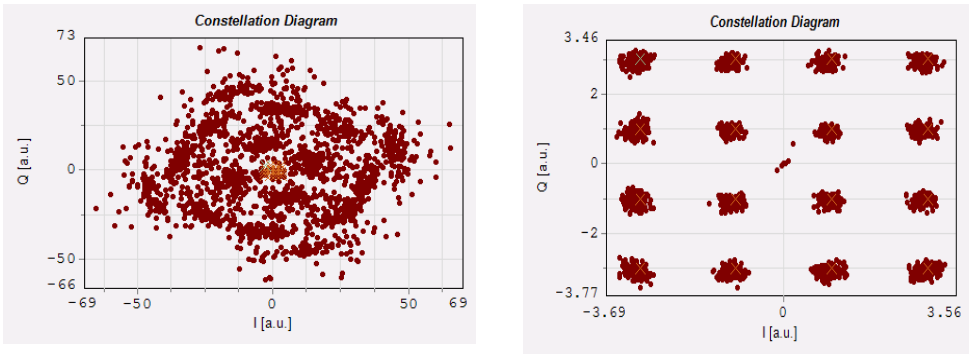

(a) (b)

Fig. (4.31): Constellation of 16 QAM for 16 AO OFDM (a) without, (b) with estimator

When we set low values for the input power high signal distortion occur. On other side, according to the self-phase modulation nonlinear effect (SPM), setting higher input power will lead to a larger nonlinearity distortion.

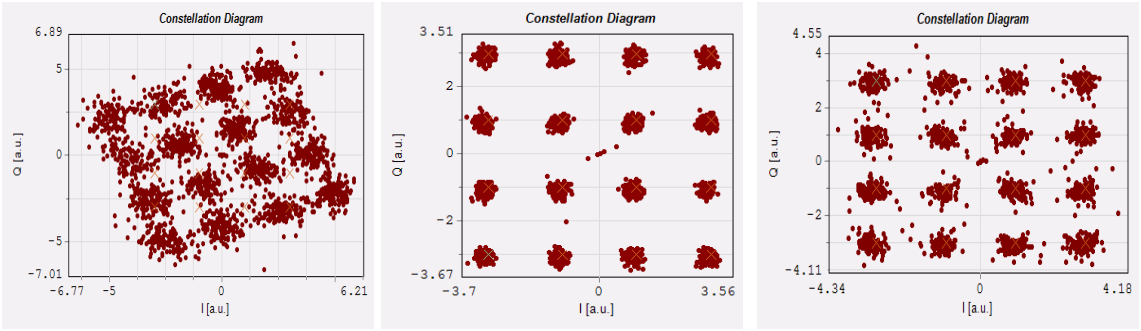

(a) (b) (c)

Fig. (4.32): Received constellation diagram of 16QAM for 16 all optical AO OFDM system channel 8 with a. -10dBm b. -6dBm c.0dBm at 300 Km

The received constellation diagrams for different input power values at 300Km transmission of 16QAM system for 16-AO OFDM system are shown in figures (4.32). On other side, according to the self-phase modulation nonlinear effect (SPM), setting higher input power will lead to a larger nonlinearity distortion. Also, there is restriction in the values of input power because of the damage threshold of optical fiber. As a result, there are only certain values suitable to get the required of our designed system as shown below:

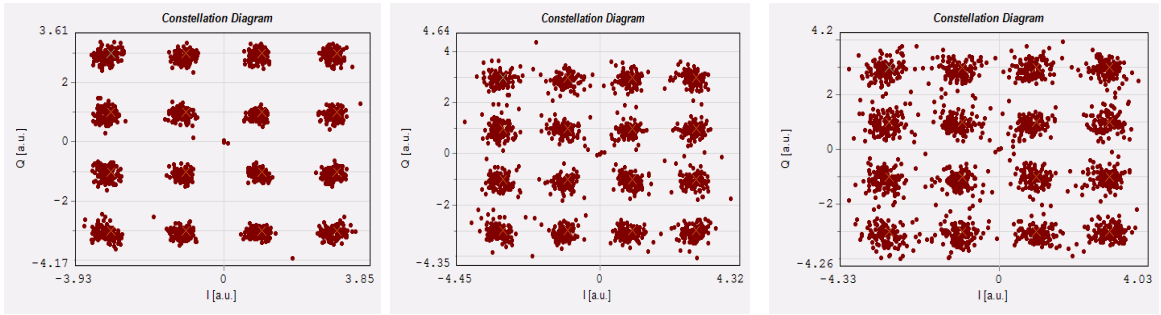

(a) (b) (c)

Fig. (4.33): The diagram of received constellation of 16QAM for channel 8 in 16-AO OFDM system with a. 100Km b. 500Km c.1000Km at -6 dBm input power

To test the 16-AO OFDM system performance in many conditions, several values of OSNR used against symbol error rate (SER) as shown in figure below:

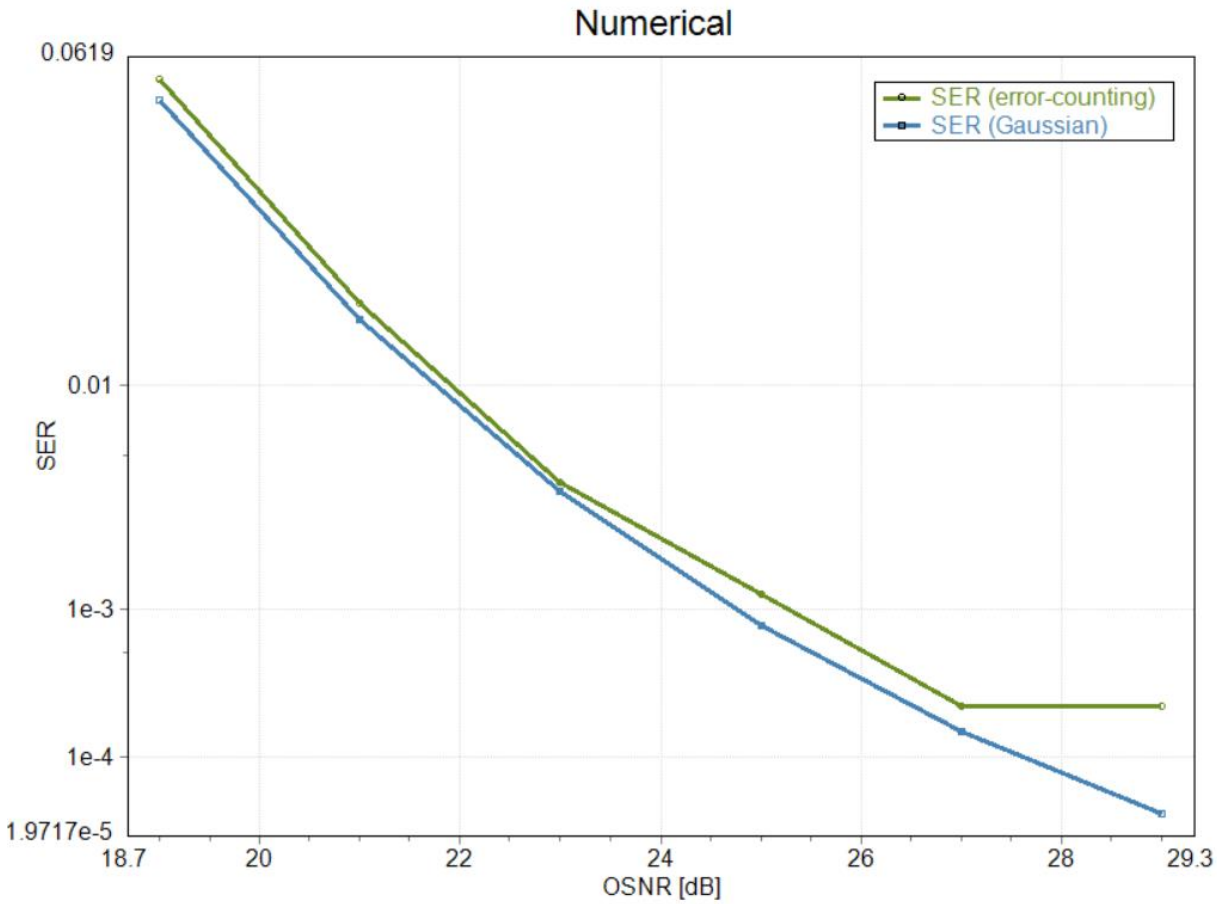

Fig.(4.34): BER vs SNR[dB] for 16 all optical AO OFDM system

Finally, eye diagram analyzer used for the received signal of channel 6 for example to express the performance of received data as shown in figure below:

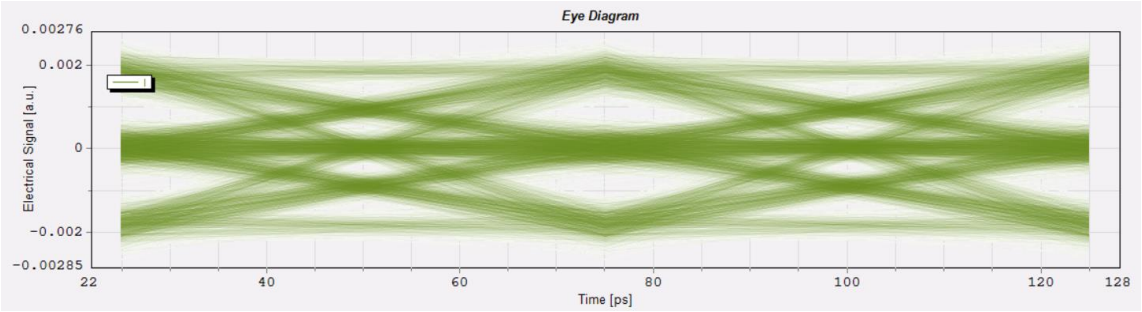

Fig.(4.35): Received eye diagram for channel 6 (In phase) of 16 all optical AO OFDM system

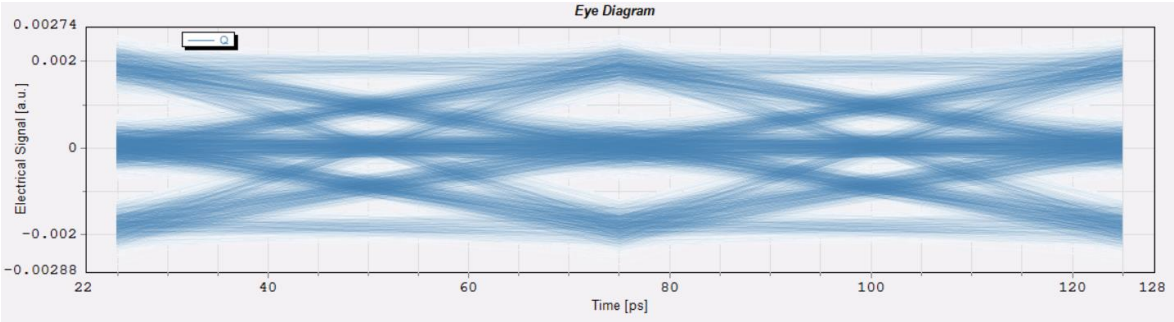

Fig.(4.36): Received eye diagram for ch.6 (Quadrature) of 16 all optical AO OFDM system

4.4.2 Results of 32- All optical OFDM Transmission Systems

In this section, the results of 32 AO OFDM system will be presented as a best choice of backhaul transmission system to offer highest capacity with long distances. The received constellation diagrams for different input power values at 100Km transmission of QPSK system for 32-AO OFDM system are shown in figures (4.37).

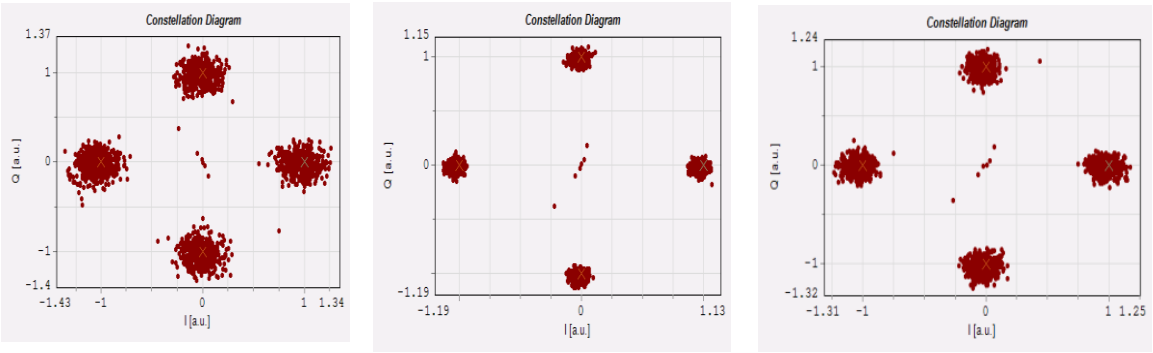

(a) (b) (c)

Fig. (4.37): Received constellation diagram of channel 6 in 32-AO OFDM system with a. -8dBm b.-4dBm c. 0dBm

Constellation diagrams for -4 dBm input power values at different distances of QPSK system for 32-AO OFDM system are shown in figure (4.38). Maximum reach for 32-AO OFDM system is (480 Km).

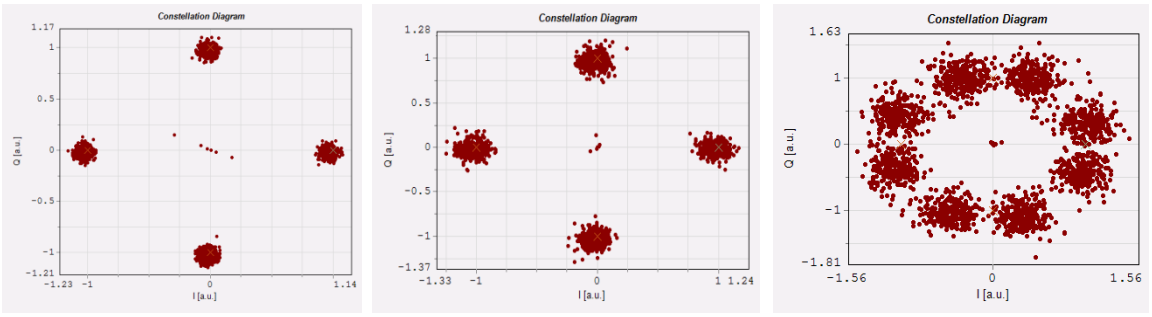

(a) (b) (c)

Fig. (4.38): Received constellation diagram of channel8X in 32-AO OFDM system with a. 100 Km b.300 Km c. 500 Km

The received constellation diagrams for different input power values at 100Km transmission of QPSK system for 32-AO OFDM system are shown in figures (4.39).

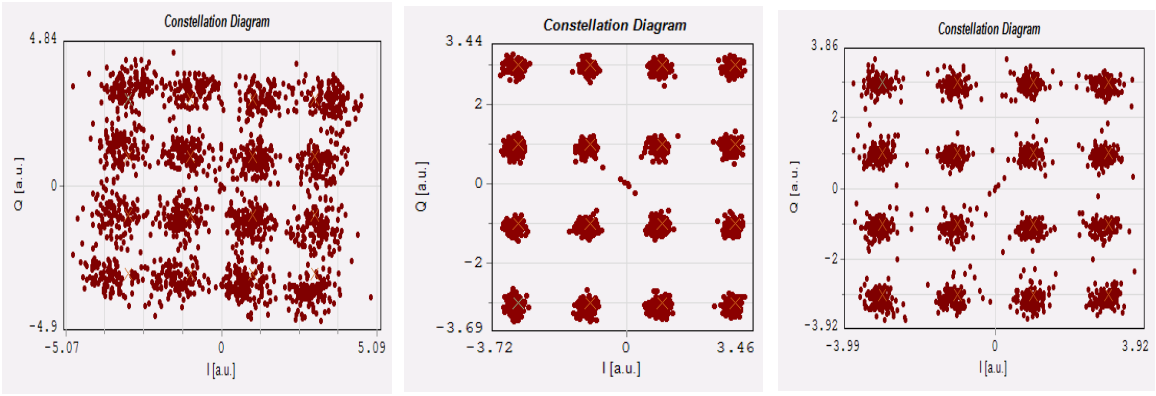

(a) (b) (c)

Fig. (4.39): Received constellation diagram of for 32 AO OFDM system channel 8 with a. -8 dBm b. -3dBm c.0dBm at 200 Km

The received constellation diagrams for different input power values at 100Km transmission of QPSK system for 32-AO OFDM system are shown in figures (4.40).

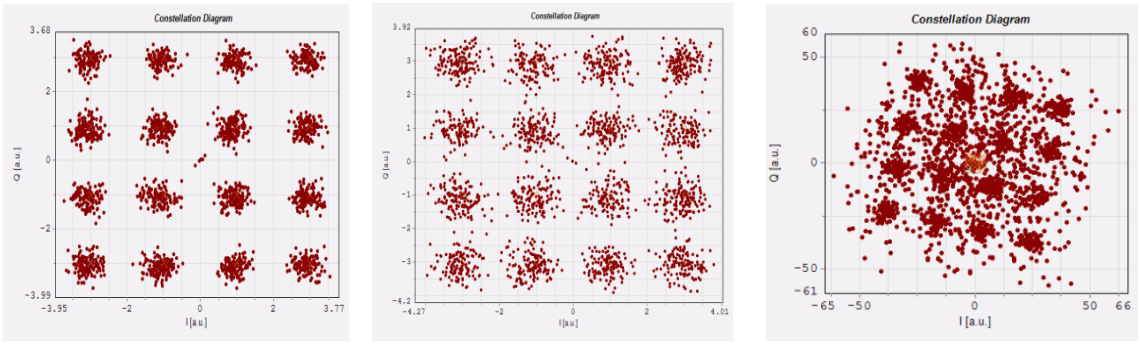

(a) (b) (c)

Fig. (4.40): The diagram of received constellation for channel 6 in 32AO OFDM system with a. 100Km b. 300Km c.500Km at -4 dBm input power

SER vs OSNR in [dB] for 32 AO OFDM system will be illustrated in figure (4.41).

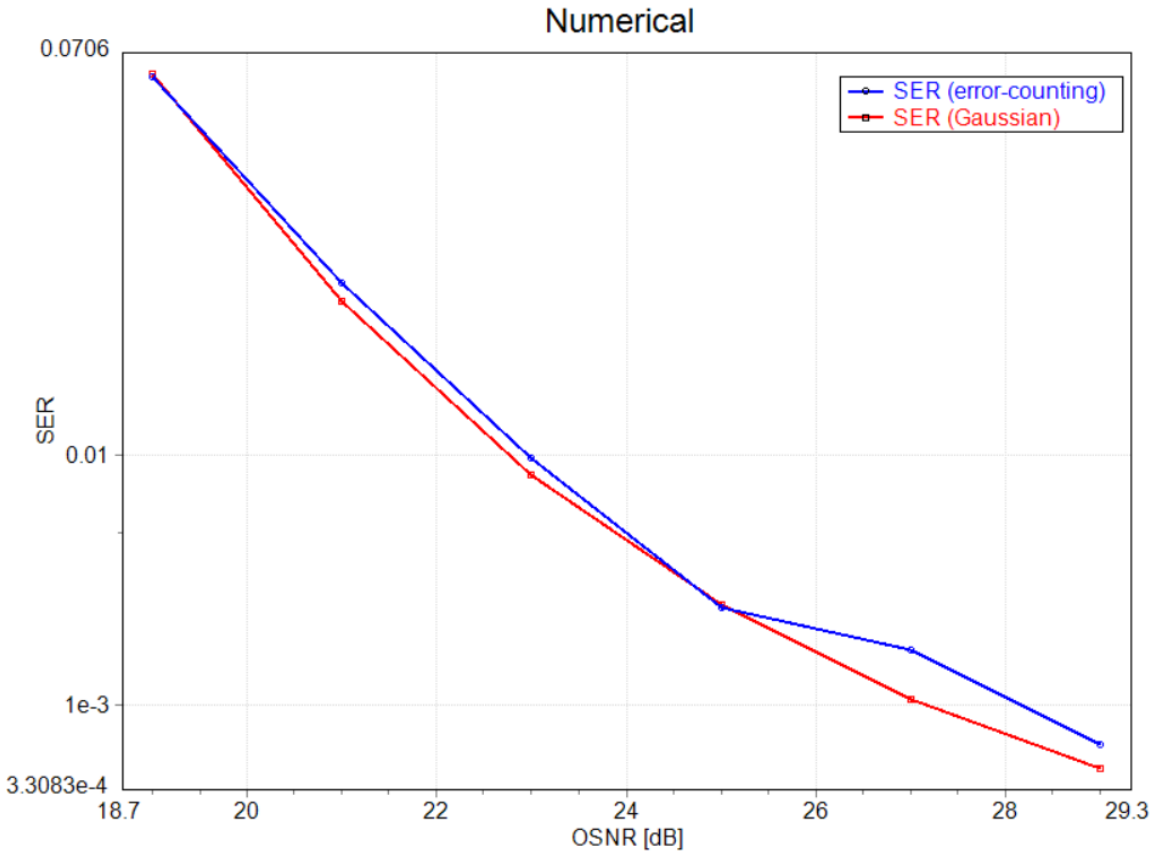

Fig. (4.41): SER vs OSNR [dB] for 32 AO OFDM system

As we can see from previous results, the optimum input power is varied for each system depending on the link budget of the system and other parameters. Figure (4.42) shows the adjusted input power for each AO OFDM system and the optimum input power for each system.

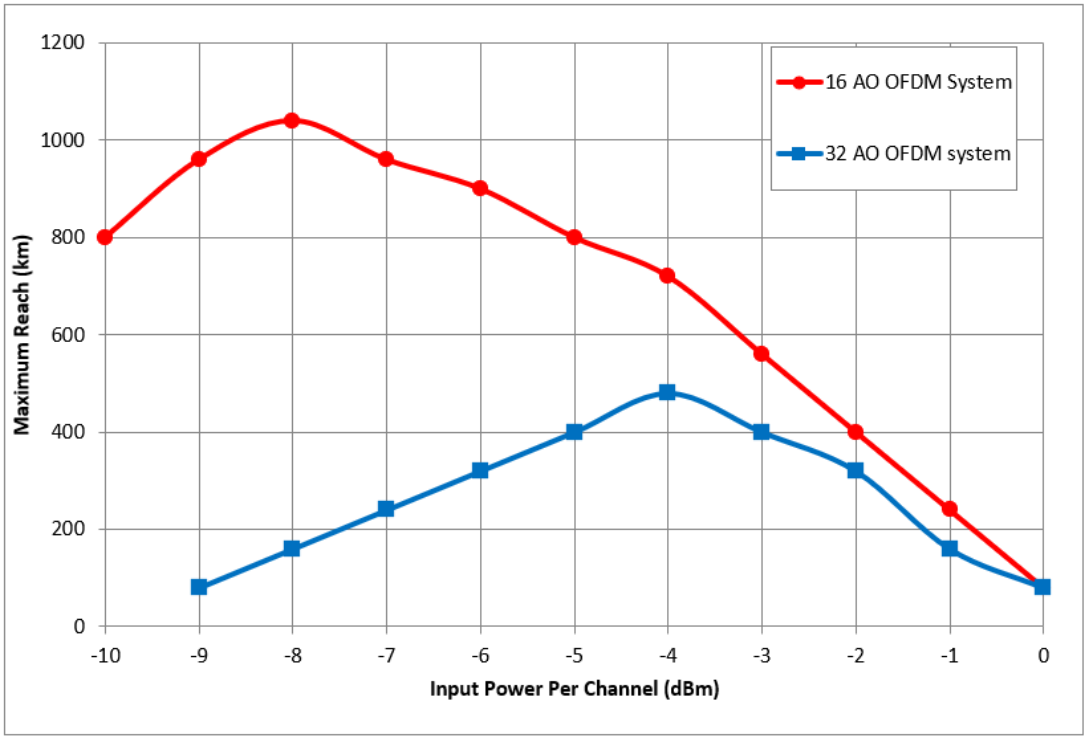

Fig.(4.42): SER vs OSNR[dB] for 32 AO OFDM system

From previous achievements, we can conclude that the total achieved data rate from 16 AO OFDM system is 32 Tb/s and the total achieved data rate from 32 AO OFDM is approximately 64 Tb/s which is considered as the best achieved transmission capacity system among all recent works.

Chapter Five

Conclusions and Future Work

5.1 Conclusion

We have many conclusions that can be presented and obtained from this thesis as shown below:

- In the presented thesis, three main complementary systems had been proposed. The first designed simulation is mMIMO OTFS system between user and base station based on massive MIMO techniques for both uplink and downlink scenarios. The second is a powerful simulation framework for a backhaul RoF-MMW transmission system between main base station and remote antenna unit based on multi-carrier OFDM modulation. Then, to integrate the overall system capabilities, all optical OFDM backhaul system with ultra high capacity achieved.
- By testing the system performance using BER vs SNR, OTFS modulation shows better results and performance among OFDM to be used with massive MIMO systems for both uplink and downlink transmission.
- The system performance for massive MIMO-OTFS system shows a great advantages among ordinary MIMO systems by achieving better spectral efficiency and energy efficiency of the designed systems.
- By using 256 subcarrier OTFS system, the best achieved transmission rate achieved for both uplink and downlink scenarios.
- By using python DSP and the losses compensators used in the simulation framework, the PAPR losses and drift in the receiver section had been compensated and many values of OFDM carriers (16, and 32 OFDM carriers) achieved for ultra-high-capacity transmission system.

- Also, a successful long transmission of up to 100 km obtained for RoF-MMW system under different bit rates and modulation formats
- By using 50 Gb/s default bit rate and 128 QAM modulation format, the best achievement of overall bit rate obtained with accepted BER to get 11.2 Tb/s ultra-high-capacity transmission system.
- The powerful simulation of next generation all optical-OFDM transmission system had been implemented by using optical FFT based on MMI couplers to achieve highest capacity transmission system.
- A successful transmission of 16 AO-OFDM had been achieved with an ultra-high capacity system with along distance reach to (1000 Km). While a distance reach to (700 Km) achieved for 32 OA OFDM.
- The optimum input power for 16 AO OFDM system to give less BER is (-8 dBm) and the optimum input power for 32 AO OFDM system is (-4 dBm).
- We can conclude that the total achieved data rate from 16 AO OFDM system is 32 Tb/s and the total achieved data rate from 32 AO OFDM is approximately 64 Tb/s which is considered as the best achieved transmission capacity system among all recent works.
- Massive MIMO-OTFS techniques and backhaul all optical OFDM systems presents a new generation for higher capacity communication systems with best performance as compared with the recent works.

5.2 Recommendation for Future Work

We suggest many works for development of future systems to enhance the operation of system as follows:

- Develop the exist OFDM-MMW systems to be transmitted over advanced multi core fiber systems to achieve higher bit rates.
- More advanced optimal algorithms can be presented to solve the channel estimation problem in hybrid field to get better performance.
- Massive MIMO systems can developed by using modern techniques to get higher number of antennas with less power consumption.
- Develop the use of all optical OFDM to use 64 subcarrier -AO OFDM.
- The demonstration of space division multiplexing (SDM) system to be involved in backhaul transmission system for achieving higher transmission bit rates

References

[1] S. Alavi, M. Soltanian, I. Amiri, M. Khalily, A. Supa'at, and H. Ahmad, "Towards 5G: a photonic based millimeter wave signal generation for applying in 5G access fronthaul," Sci. Rep. 6, 19891 (2016).

[2] Chengchao Liang, F. Richard Yu, and Xi Zhang, "Information-centric network function virtualization over 5g mobile wireless networks," IEEE Network, vol. 29, no. 3, pp. 68–74, 2015.

[3] Matias Richart, Javier Baliosian, Joan Serrat, and Juan-Luis Gorricho, "Resource Slicing in Virtual Wireless Networks: A Survey," IEEE Transactions on Network and Service Management, vol. 13, no. 3, pp. 462–476, 2016.

[4] Van-Giang Nguyen, Truong-Xuan Do, and YoungHan Kim, "SDN and Virtualization-Based LTE Mobile Network Architectures: A Comprehensive Survey," Wireless Personal Communications, vol. 86, pp. 1401–1438, 2016.

[5] Nikolaos Nomikos, Prodromos Makris, Dimitrios N. Skoutas, Demosthenes Vouyioukas, and Charalabos Skianis, "Enabling wireless prosuming in 5G networks," in 2014 International Conference on Telecommunications and Multimedia (TEMU), pp. 190–195, 2014.

[6] Mukundan Madhavan, Parul Gupta, and Malolan Chetlur, "Quantifying multiplexing gains in a Wireless Network Cloud," in 2012 IEEE International Conference on Communications (ICC), pp. 3212–3216, 2012.

[7] Mugen Peng, Yuan Li, Jiamo Jiang, Jian Li, and Chonggang Wang, "Heterogeneous cloud radio access networks: a new perspective for enhancing spectral and energy efficiencies," IEEE Wireless Communications, vol. 21, no. 6, pp. 126–135, 2014.

[8] Gunther Auer et al, “How much energy is needed to run a wireless network?,” IEEE Wireless Communications, vol. 18, no. 5, pp. 40–49, 2011.

[9] Eunsung Oh, Kyuho Son, and Bhaskar Krishnamachari, “Dynamic base station switching-on/off strategies for green cellular networks,” IEEE Transactions on Wireless Communications, vol. 12, no. 5, pp. 2126–2136, 2013.

[10] Sharifzadeh, M., & Ahmadirad, M., “Performance analysis of underwater wireless optical communication systems over a wide range of optical turbulence,” Optics Communications, no.427, pp. 609–616, 2018.

[11] Alsharif, M.H.; Nordin, R., “Evolution towards fifth generation (5G) wireless networks: Current trends and challenges in the deployment of millimetre wave, massive MIMO, and small cells,” Telecommun. Syst. 64, pp. 617–637, 2017.

[12] Ou Xie, “Image Retrieval of Tourism Landscape in Rural Revitalization Based on Wireless Communication Network,” Wireless Communications and Mobile Computing, Volume 2022, Article ID 7167611, pp. 1-13, 2022.

[13] Adarsh B. Narasimhamurthy, Mahesh K. Banavar, Cihan Tepedelenlioğlu, “OFDM Systems for Wireless Communications,” Synthesis Lectures on Algorithms and Software in Engineering, Chapter in book, 2010.

[14] H. F. Arrano and C. A. Azurdia-Meza, “OFDM: today and in the future of next generation wireless communications,” 2016 IEEE Central America and Panama Student Conference (CONESCAPAN), pp. 1-6, 2016.

[15] S. Hamidi, M. -R. Nezhad-Ahmadi and S. Safavi-Naeini, “TDM based Virtual FMCW MIMO Radar Imaging at 79GHz,” 2018 18th International Symposium on Antenna Technology and Applied Electromagnetics (ANTEM), pp. 1-2, 2018.

[16] Feng Hu, Bing Chen, and Kun Zhu, “Full spectrum sharing in cognitive radio networks toward 5g: A survey,” IEEE Access, vol. 6, pp. 15754–15776, 2018.

[17] W. S. H. M. W. Ahmad, N. A. M. Radzi, F. S. Samidi, A. Ismail, F. Abdullah, M. Z. Jamaludin, and M. N. Zakaria, “5g technology: Towards dynamic spectrum sharing using cognitive radio networks,” IEEE Access, vol. 8, pp. 14460–14488, 2020.

[18] Dario Sabella, Antonio de Domenico, Efstathios Katranaras, Muhammad Ali Imran, Marco di Girolamo, Umer Salim, Massinissa Lalam, Konstantinos Samdanis, and Andreas Maeder, “Energy Efficiency Benefits of RAN-as-aService Concept for a Cloud-Based 5G Mobile Network Infrastructure,” IEEE Access, vol. 2, pp. 1586–1597, 2014.

[19] August Betzler, Daniel Camps-Mur, Eduard Garcia-Villegas, Ilker Demirkol, and Joan Josep Aleixendri, “SODALITE: SDN Wireless Backhauling for Dense 4G/5G Small Cell Networks,” IEEE Transactions on Network and Service Management, vol. 16, no. 4, pp. 1709–1723, 2019.

[20] Ummy Habiba and Ekram Hossain, “Auction Mechanisms for Virtualization in 5G Cellular Networks: Basics, Trends, and Open Challenges,” IEEE Communications Surveys Tutorials, vol. 20, no. 3, pp. 2264–2293, 2018.

[21] Bin Han, Ji Lianghai, and Hans D. Schotten, “Slice as an Evolutionary Service: Genetic Optimization for Inter-Slice Resource Management in 5G Networks,” IEEE Access, vol. 6, pp. 33137–33147, 2018.

[22] Sihem Bakri, Bouziane Brik, and Adlen Ksentini, “On using reinforcement learning for network slice admission control in 5G: Offline vs. online,” International Journal of Communication Systems, vol. 34, no. 7, pp. e4757, 2021.

[23] J. Zhang, E. Bjornson, M. Matthaiou, D. W. K. Ng, H. Yang, and D. J. Love, “Prospective multiple antenna technologies for beyond 5G,” IEEE J. Sel. Areas Commun., vol. 38, no. 8, pp. 1637–1660, Aug. 2020.

[24] H. Q. Ngo, A. Ashikhmin, Y. Hong, E. G. Larsson, and T. L. Marzetta, “Cell-free massive MIMO versus small cells,” IEEE Trans. Wireless Commun., vol. 16, no. 3, pp. 1834–1850, Mar. 2017.

[25] W. Luo, X. Fang, M. Cheng, and Y. Zhao, “Efficient multiple-group multiple-antenna (MGMA) scheme for high-speed railway viaducts,” IEEE Trans. Veh. Technol., vol. 62, no. 6, pp. 2558–2569, Jul. 2013.

[26] Y. Dong, C. Zhang, P. Fan, and P. Fan, “Power-space functions in high speed railway wireless communications,” J. Commun. Netw., vol. 17, no. 3, pp. 231–240, Jun. 2015.

[27] . He, B. Ai, G. Wang, K. Guan, Z. Zhong, A. F. Molisch, C. BrisoRodriguez, and C. P. Oestges, “High-speed railway communications: From GSM-R to LTE-R,” IEEE Veh. Technol. Mag., vol. 11, no. 3, pp. 49–58, Sep. 2016.

[28] M. A. Albreem, M. Juntti and S. Shahabuddin, “Massive MIMO Detection Techniques: A Survey,” in *IEEE Communications Surveys & Tutorials*, vol. 21, no. 4, pp. 3109-3132, 2019.

[29] M. Abdullah et al., “Future Smartphone: MIMO Antenna System for 5G Mobile Terminals,” in IEEE Access, vol. 9, pp. 91593-91603, 2021.

[30] M. S. Sharawi, “Printed Multi-Band MIMO Antenna Systems and Their Performance Metrics,” in IEEE Antennas and Propagation Magazine, vol. 55, no. 5, pp. 218-232, Oct. 2013.

[31] S. Chen, J. Zhang, Y. Jin and B. Ai, “Wireless powered IoE for 6G: Massive access meets scalable cell-free massive MIMO,” in China Communications, vol. 17, no. 12, pp. 92-109, Dec. 2020.

[32] R. Kudo, S. M. D. Armour, J. P. McGeehan and M. Mizoguchi, “A channel state information feedback method for massive MIMO-OFDM,” in Journal of Communications and Networks, vol. 15, no. 4, pp. 352-361, Aug. 2013.

[33] X. Cheng, R. Zayani, H. Shaiek and D. Roviras, “Analysis and Cancellation of Mixed-Numerologies Interference for Massive MIMO-OFDM UL,” in IEEE Wireless Communications Letters, vol. 9, no. 4, pp. 470-474, April 2020.

[34] J. Fan et al., “Millimeter-wave Multimode Beamforming Network Based on Double-ridged Waveguides,” 2021 International Conference on Microwave and Millimeter Wave Technology (ICMMT), pp. 1-3, 2021.

[35] X. Ren, Q. -Y. Guo, S. Liao, W. He, Q. Xue and H. Wong, “A Millimeter-Wave Circularly Polarized Antenna for 5G Applications,” 14th UK-Europe-China Workshop on Millimetre-Waves and Terahertz Technologies (UCMMT), pp. 1-3, 2021.

[36] I. Ishteyaq, I. S. Masoodi and K. Muzaffar, "Wideband Printed Quasi-Yagi MIMO Antenna for Milli-meter Wave Applications," 2019 IEEE Indian Conference on Antennas and Propogation (InCAP), pp. 1-4, 2019.

[37] J. Vychodil, J. Blumenstein, T. Mikulasek, A. Prokes and V. Derbek, “Measurement of in-vehicle channel — Feasibility of ranging in UWB and MMW band,” 2014 International Conference on Connected Vehicles and Expo (ICCVE), pp. 695-698, 2014.

[38] R. Abdolee, R. Ngah, V. Vakilian and T. A. Rahman, “Application of radio-over-fiber (ROF) in mobile communication,” 2007 Asia-Pacific Conference on Applied Electromagnetics, pp. 1-5, 2007.

[39] M. Ali, L. E. García Muñoz and G. Carpintero, “E-band photonic transmitter with tapered slot antenna for RoF applications,” 2017 International Topical Meeting on Microwave Photonics (MWP), pp. 1-4, 2017.

[40] Y. Yan, H. Yuan, N. Zheng and S. Peter, “Performance of uplink multi-user MIMO in LTE-advanced networks,” 2012 International Symposium on Wireless Communication Systems (ISWCS), pp. 726-730, 2012.

[41] F. Rusek et al., “Scaling Up MIMO: Opportunities and Challenges with Very Large Arrays,” in IEEE Signal Processing Magazine, vol. 30, no. 1, pp. 40-60, Jan. 2013.

[42] Muhammet N. Seyman and Necmi Taspinar, “Channel estimation based on neural network in space time block coded MIMO–OFDM system,”, Digital Signal Processing, Volume 23, Issue 1, pp. 275-280, 2013.

[43] J. Lee, G. Gil, and Y. H. Lee, “Channel estimation via orthogonal matching pursuit for hybrid MIMO systems in millimeter wave communications,” IEEE Trans. Wireless Commun., vol. 64, no. 6, pp. 2370–2386, Jun. 2016.

[44] Y. Han, S. Jin, C. Wen, and X. Ma, “Channel estimation for extremely large-scale massive MIMO systems,” IEEE Wireless Commun. Lett., vol. 9, no. 5, pp. 633–637, May 2019.

[45] X. Wei, C. Hu and L. Dai, “Deep Learning for Beamspace Channel Estimation in Millimeter-Wave Massive MIMO Systems," in IEEE Transactions on Communications, vol. 69, no. 1, pp. 182-193, Jan. 2020.

[46] Mingyao Cui and Linglong Dai, M. Cui and L. Dai, “Channel estimation for extremely large-scale MIMO: Far-field or near-field?,” IEEE Transactions on Communications, vol.70, ID: 237142566, pp. 2663-2677, Aug. 2022.

[47] P. T. Dat, A. Kanno, K. Inagaki and T. Kawanishi, “High-Capacity Wireless Backhaul Network Using Seamless Convergence of Radio-over-Fiber and 90-GHz Millimeter-Wave,” in Journal of Lightwave Technology, vol. 32, no. 20, pp. 3910-3923, 15 Oct.15, 2014.

[48] Jaswinder Kaur1 and Vishal Sharma, “MIMO-OFDM-radio over fiber system incorporating higher order space-time block codes,” Microwave and Optical Technology Letters, vol.62. issue1, pp.1-9, 2019.

[49] Muhammad Usman Hadi, Hyun Jung, Salman Ghaffar, Pier Andrea Traverso, and Giovanni Tartarini, “Optimized digital radio over fiber system for medium range communication,” Optics Communications, Volume 443, pp. 177-185, 2019.

[50] Moussa El Yahyaoui, Ali El Moussati, Ghaïs El Zein, and Kamel Haddadi, “New millimeter wave generation scheme for MIMO-OFDM based Radio-over-Fiber system,” Optics Communications, Volume 442, Pages 101-105, 2019.

[51] Mehtab Singh, Sahil Nazir Pottoo, Jyoteesh Malhotra, Amit Grover, Moustafa H. Aly, “Millimeter-wave hybrid OFDM-MDM radio over free space optical transceiver for 5G services in desert environment,” Alexandria Engineering Journal, Volume 60, Issue 5, pp. 4275-4285, 2021.

[52] T. H. Dahawi, Z. Yusoff, M. S. Salleh, and J. M. Senior, “Low-cost MIMO-RoF-PON architecture for next-generation integrated wired and wireless access networks,” J. Opt. Commun. Netw. 13, pp. 41-52, 2021.

[53] M. Kollengode Ramachandran and A. Chockalingam, “MIMO-OTFS in High-Doppler Fading Channels: Signal Detection and Channel Estimation,” 2018 IEEE Global Communications Conference (GLOBECOM), pp. 206-212, 2018.

[54] Changyoung and Heung-Gyoon Ryu, “High Throughput Mobile Communication Based on OTFS System with the Delay-Doppler Compensation,” *Wireless Pers Commun*, vol. **106**, pp. 473–486, 2019.

[55] O. K. Rasheed, G. D. Surabhi and A. Chockalingam, “Sparse Delay-Doppler Channel Estimation in Rapidly Time-Varying Channels for

Multiuser OTFS on the Uplink," 2020 IEEE 91st Vehicular Technology Conference (VTC2020-Spring), pp.1-5, 2020.

[56] M. Mohammadi, H. Q. Ngo and M. Matthaiou, “When Cell-Free Massive MIMO Meets OTFS Modulation: The Downlink Case," ICC 2022 - IEEE International Conference on Communications, pp. 787-792, 2022.

[57] D. Shi et al., “Deterministic Pilot Design and Channel Estimation for Downlink Massive MIMO-OTFS Systems in Presence of the Fractional Doppler," in IEEE Transactions on Wireless Communications, vol. 20, no. 11, pp. 7151-7165, Nov. 2021.

[58] M. Sleiffer, “73.7 Tb/s (96 x 3 x 256-Gb/s) mode-divisionmultiplexed DP-16QAM transmission with inline MM-EDFA,” Opt. Express, vol. 20, no. 26, pp. B428–B438, Dec. 2012.

[59] N. H. Trung, “Multiplexing Techniques for Applications Based-on 5G Systems", in Multiplexing - Recent Advances and Novel Applications. London, United Kingdom: IntechOpen, 2022.

[60] S. B. Lande and A. A. Kadam, "Duty Cycle Based Digital Multiplexing Technique for Advanced Communication System," 2015 International Conference on Computational Intelligence and Communication Networks (CICN), pp. 523-528, 2015.

[61] A. Lord, L. C. Blank, J. M. Boggis, W. A. Stallard and E. Bryant, "Submerged optical multiplexing techniques for future transmission networks," IEE Colloquium on Submarine Optical Transmission Systems, 1988, pp. 1-15.

[62] H. K. Tsang, X. Wu and L. Liu, "Multiplexing and switching for mode division multiplexed optical interconnects," 2016 Progress in Electromagnetic Research Symposium (PIERS), pp. 3155-3155, 2016.

[63] Y. Zhao, Y. Zhang and W. Wang, "Research on condition monitoring of FDM equipment based on LSTM," 2021 IEEE International Conference on

Advances in Electrical Engineering and Computer Applications (AEECA), pp. 612-615,2021.

[64] K. R. Lakshmikumar, L. J. Loporcaro, M. J. Tompsett and J. C. Goetjen, "A CMOS analog front-end processor for an FDM system," IEEE Proceedings of the Custom Integrated Circuits Conference, pp. 1-12, 1990.

[65] N. Nadarajah, Elaine Wong and A. Nirmalathas, "Packet labeling technique using electronic code-division multiple-access for WDM packet-based access networks," in IEEE Photonics Technology Letters, vol. 18, no. 4, pp. 607-609, Feb. 15, 2006.

[66] S. Kawanishi, "Optical TDM transmission techniques toward Tbit/s," Conference Proceedings. LEOS '97. 10th Annual Meeting IEEE Lasers and Electro-Optics Society 1997 Annual Meeting, pp. 287-288 vol.1, 1997.

[67] H. Jiang, D. Li and W. Li, "Performance Analysis of Overlapped Multiplexing Techniques," 2007 3rd International Workshop on Signal Design and Its Applications in Communications, pp. 233-237, 2007.

[68] Lajos L. Hanzo; L-L. Yang; E-L. Kuan; K. Yen, "CDMA Overview," in Single and Multi-Carrier DS-CDMA: Multi-User Detection, Space-Time Spreading, Synchronisation, Networking and Standards , IEEE, pp.35-80, 2004.

[69] Z. Luo and X. Xiong, "Performance comparison of SC-FDMA-CDMA and OFDM-CDMA systems for uplink," 2011 International Conference on Consumer Electronics, Communications and Networks (CECNet), pp. 1475-1479, 2011.

[70] N. Karelin, H. Louchet, I. Koltchanov, and A. Richter, “Modeling and design framework for SDM transmission systems,” VPI Development Center, ul. Filimonova 15-50831, 220037 Minsk, Belarus, 2015.

[71] C. Xia, “Optical fibers for Space division multiplexed transmission and networking,” Master thesis, B.S. Zhejiang University, China, 2015.

[72] A. Pandharipande, "Principles of OFDM," in IEEE Potentials, vol. 21, no. 2, pp. 16-19, April-May 2002.

[73] D. Rajeswaran and A. K. Nair, "A novel approach for reduction of PAPR in OFDM communication," 2016 International Conference on Communication and Signal Processing (ICCSP), pp. 1978-1981, 2016.

[74] M. Bogdanović, "Power line communication system modeling based on coded OFDM," 2012 Proceedings of the 35th International Convention MIPRO, pp. 760-764,2012.

[75] B. Ban, G. Zhu, Y. Jiang and H. Li, "A modified channel estimation algorithm for MB-OFDM system based on UWB channel model," 2010 2nd IEEE InternationalConference on Network Infrastructure and Digital Content, pp. 584-588, 2010.

[76] M. Kyryk and V. Yanyshyn, "OFDM-based cognitive radio system capacity evaluation model," The Experience of Designing and Application of CAD Systems in Microelectronics, pp. 137-139, 2015.

[77] L. C. Vieira and N. J. Gomes, "Baseband behavioral modeling of OFDM-Radio over fiber link distortion," 2012 IEEE International Topical Meeting on Microwave Photonics, pp. 188-191, 2012.

[78] M. Bogdanović, "Computer based simulation model realization of OFDM communication over power lines," 2012 20th Telecommunications Forum (TELFOR), pp. 249-252, 2012.

[79] P. J. Winzer and R. J. Essiambre. “Advanced modulation formats for high-capacity optical transport networks”. J. Lightwave Technol., 24(12):4711–4728, Dec 2006.

[80] T. A. Eriksson, “Multidimensional Modulation Formats for Coherent Optical Communication Systems”, Thesis for the degree of Licentiate of Engineering, Göteborg, Sweden, 2014.

[81] Qun Shi, “Error performance of OFDM-QAM in subcarrier multiplexed fiber-optic transmission,” in IEEE Photonics Technology Letters, vol. 9, no. 6, pp. 845-847, June 1997.

[82] Y. Feng, S. Liu, N. Li and Y. Chen, “A new OFDM synchronization algorithm using training cyclic prefix,” 2011 International Conference on Mechatronic Science, Electric Engineering and Computer (MEC), pp. 1489-1491,2011.

[83] P. Sudheesh et al., “Cyclic prefix assisted sparse channel estimation for OFDM systems,” 2012 International Conference on Computing, Communication and Applications, pp. 1-4, 2012.

[84] M. Kyryk and V. Yanyshyn, “OFDM-based cognitive radio system capacity evaluation model,” The Experience of Designing and Application of CAD Systems in Microelectronics, pp. 137-139, 2015.

[85] S. Vukotić and D. Vućić, “Detection and clasiffication of OFDM/QAM and OFDM/OQAM signals based on cyclostationary features,” 2015 23rd Telecommunications Forum Telfor (TELFOR), pp. 232-235, 2015.

[86] Y. A. Jung, S. -B. Byun, H. -J. Shin, D. -C. Han, S. -H. Cho and S. -H. Lee, “Frequency and Symbol Timing offset Estimation Method for CP-OFDM based System,” 2021 International Conference on Information and Communication Technology Convergence (ICTC), pp. 599-601, 2021.

[87] J. Wang, Z. Xie and J. Jiao, “Doppler Compensation of Underwater Acoustic OFDM Based on Parallel Search in Time and Frequency Domain and FPGA Implementation,” 2018 IEEE 18th International Conference on Communication Technology (ICCT), 2018, pp. 387-391, 2018.

[88] K. R. Murali and A. Chockalingam, “On OTFS Modulation for High-Doppler Fading Channels,” 2018 Information Theory and Applications Workshop (ITA), pp. 1-10, 2018.

[89] S. S. Das, V. Rangamgari, S. Tiwari and S. C. Mondal, “Time Domain Channel Estimation and Equalization of CP-OTFS Under Multiple Fractional Dopplers and Residual Synchronization Errors,” in IEEE Access, vol. 9, pp. 10561-10576, 2021.

[90] M. S. Khan, Y. J. Kim, Q. Sultan, J. Joung and Y. S. Cho, “Downlink Synchronization for OTFS-Based Cellular Systems in High Doppler Environments,” in IEEE Access, vol. 9, pp. 73575-73589, 2021.

[91] S. K. Mohammed, “Time-Domain to Delay-Doppler Domain Conversion of OTFS Signals in Very High Mobility Scenarios,” in IEEE Transactions on Vehicular Technology, vol. 70, no. 6, pp. 6178-6183, June 2021.

[92] A. Naikoti and A. Chockalingam, “Low-complexity Delay-Doppler Symbol DNN for OTFS Signal Detection,” 2021 IEEE 93rd Vehicular Technology Conference (VTC2021-Spring), pp. 1-6, 2021.

[93] S. Srivastava, R. K. Singh, A. K. Jagannatham and L. Hanzo, “Delay-Doppler and Angular Domain 4D-Sparse CSI Estimation in OTFS Aided MIMO Systems,” in IEEE Transactions on Vehicular Technology, 2022.

[94] P. Raviteja, K. T. Phan, Y. Hong and E. Viterbo, “Orthogonal Time Frequency Space (OTFS) Modulation Based Radar System,” 2019 IEEE Radar Conference (RadarConf), pp. 1-6, 2019.

[95] D. Wang, B. Sun, F. Wang, X. Li, P. Yuan and D. Jiang, “Transmit diversity scheme design for rectangular pulse shaping based OTFS,” in China Communications, vol. 19, no. 3, pp. 116-128, March 2022.

[96] C. Naveen and V. Sudha, “Peak-to-Average Power Ratio reduction in OTFS modulation using companding technique,” 2020 5th International Conference on Devices, Circuits and Systems (ICDCS), pp. 140-143,2020.

[97] Y. Yang et al., “Design and analysis of spatial modulation based orthogonal time frequency space system,” in China Communications, vol. 18, no. 8, pp. 209-223, Aug. 2021.

[98] R. M. Augustine, G. D. Surabhi and A. Chockalingam, “Space-Time Coded OTFS Modulation in High-Doppler Channels,” 2019 IEEE 89th Vehicular Technology Conference (VTC2019-Spring), pp. 1-6, 2019.

[99] P. P. Vaidyanathan, “On the degree of MIMO systems," 2007 IEEE International Symposium on Circuits and Systems, pp. 661-664,2007.

[100] A. K. Sarangi and A. Datta, “Capacity Comparison of SISO, SIMO, MISO & MIMO Systems,” 2018 Second International Conference on Computing Methodologies and Communication (ICCMC), pp. 798-801, 2018.

[101] S. Takahashi, I. Watanabe, K. Nishimori, R. Taniguchi and T. Murakami, “Blind-based demodulation scheme for virtual massive MIMO systems,” 2020 International Symposium on Antennas and Propagation (ISAP), pp. 511-512, 2021.

[102] K. Gunaseelan, P. Reba and A. Kandaswamy, “Adaptive Resource Allocation with Multiuser Interference Cancellation for MIMO OFDM Systems,” 2009 International Conference on Signal Processing Systems, pp. 239-243, 2009.

[103] M. Sharf and D. Zelazo, “Analysis and Synthesis of MIMO Multi-Agent Systems Using Network Optimization,” in IEEE Transactions on Automatic Control, vol. 64, no. 11, pp. 4512-4524, Nov. 2019.

[104] S. P. Jiménez, F. M. Maciel, L. Soriano-Equigua, V. H. Castillo and J. L. Álvarez, “A differential evolution-based algorithm for calculating beamformers in MIMO systems,” 2015 10th Iberian Conference on Information Systems and Technologies (CISTI), pp. 1-5, 2015.

[105] F. Yassin, A. Asma, Z. Ali and B. A. Ridha, “A Learning Rate For MIMO Nonlinear System Emulation,” 2021 IEEE 2nd International Conference on Signal, Control and Communication (SCC), pp. 37-42, 2021.

[106] De-xin Gao, Xiu-hua Dou and Qing Yang, “Singular optimal control for MIMO systems with persistent disturbances,” 2009 Chinese Control and Decision Conference, pp. 746-750, 2009.

[107] L. -s. Wei, M. Jiang, Y. Song and M. -r. Fei, “Scheduling methodology and stability of mimo networked control systems,” 2009 Chinese Control and Decision Conference, 2009, pp. 533-537, 2009.

[108] W. Cuiqin, Li Aihua and Z. Zhenren, "Analysis and Modeling of MIMO Networked Control Systems,” 2007 Chinese Control Conference, pp. 235-238, 2007.

[109] T. Hossain, M. Y. Ali and M. Munjure Mowla, “Energy Efficient Massive MIMO 5G System with ZF Receiver,” 2019 3rd International Conference on Electrical, Computer & Telecommunication Engineering (ICECTE), pp. 133-136, 2019.

[110] Tabassum, A. H. Sakr, and E. Hossain, “Analysis of Massive MIMO-Enabled Downlink Wireless Backhauling for Full-Duplex Small Cells,” IEEE Transactions on Communications, vol. 64, pp. 2354–2369, June 2016.

[111] Björnson, M. Kountouris, and M. Debbah, “Massive MIMO and small cells: Improving energy efficiency by optimal soft-cell coordination,” in ICT 2013, pp. 1–5, May 2013.

[112] I. Shubhi and H. Murata, “Dynamic Precoder for Massive MIMO in the Presence of Large Doppler Spread,” in 2017 IEEE 85th Vehicular Technology Conference (VTC Spring), pp. 1–5, June 2017.

[113] P. Paul and M. M. Mowla, "A Novel Beamspace Channel Estimation Technique for Millimeter Wave Massive MIMO Systems," 2019 3rd International Conference on Electrical, Computer & Telecommunication Engineering (ICECTE), pp. 185-188, 2019.

[114] Y. Zhao, W. Zhao, G. Wang, B. Ai, H. H. Putra and B. Juliyanto, "AoA-based channel estimation for massive MIMO OFDM communication

systems on high speed rails," in China Communications, vol. 17, no. 3, pp. 90-100, March 2020.

[115] J. AMADID, M. BOULOUIRD and M. M. HASSANI, "Channel Estimation with Pilot Contamination in Mutli-Cell Massive MIMO systems," 2020 IEEE 2nd International Conference on Electronics, Control, Optimization and Computer Science (ICECOCS), pp. 1-4, 2020.

[116] A. Alshammari, S. Albdran, M. A. R. Ahad and M. Matin, "Impact of angular spread on massive MIMO channel estimation," 2016 19th International Conference on Computer and Information Technology (ICCIT), pp. 84-87, 2016.

[117] M. A. Albreem, A. H. A. Habbash, A. M. Abu-Hudrouss and S. S. Ikki, "Overview of Precoding Techniques for Massive MIMO," in IEEE Access, vol. 9, pp. 60764-60801, 2021.

[118] S. Berra, M. A. M. Albreem and M. S. Abed, "A Low Complexity Linear Precoding Method for Massive MIMO," 2020 International Conference on UK-China Emerging Technologies (UCET), pp. 1-4, 2020.

[119] V. -F. Crâşmariu, M. -O. Arvinte, A. -A. Enescu and S. Ciochină, "A reduced complexity multi-user massive MIMO precoding method," 2017 40th International Conference on Telecommunications and Signal Processing (TSP), pp. 178-181, 2017.

[120] V. Angeline Beulah and S. Markkandan, "Performance analysis of precoding techniques for Massive MU-MIMO systems," 2015 International Conference on Innovations in Information, Embedded and Communication Systems (ICIIECS), pp. 1-5, 2015.

[121] T. Tlili, N. Rebhi and H. Amiri, "Massive MIMO approach for interference reduction using precoding," 2017 International Conference on Smart, Monitored and Controlled Cities (SM2C), pp. 32-35, 2017.

[122] C. -C. Hu, W. -C. Lin and W. -S. Liao, "Hybrid Precoding MmWave Massive MIMO Systems with Dynamic-Resolution DAC," 2018 IEEE 7th Global Conference on Consumer Electronics (GCCE), pp. 134-135, 2018.

[123] Hongtao Lin, Okechukwu Ogbuu, Jifeng Liu, Lin Zhang, Jurgen Michel, and Juejun Hu, “Breaking the energy-bandwidth limit of electro-optic modulators: Theory and a device proposal,” Journal Of Lightwave Technology, vol. 31, no. 24, December 15, 2013.

Acknowledgement

The accomplishment of this thesis benefits of the help and direction from my dear supervisor Prof. Laith Ali Abdul Rahaim is always happy and willing to help me solve the confusions and direct me approach to the final result of the thesis.

Finally, I would like to express my special thanks to VPI photonics software managers for their valuable support and very helpful communication packages to produce the work of project in the best form.

Appendix A

VPI Graphics User Interface[A.1]

Figure below shows the main GUI of VPI v.9.8 powerful simulation software.

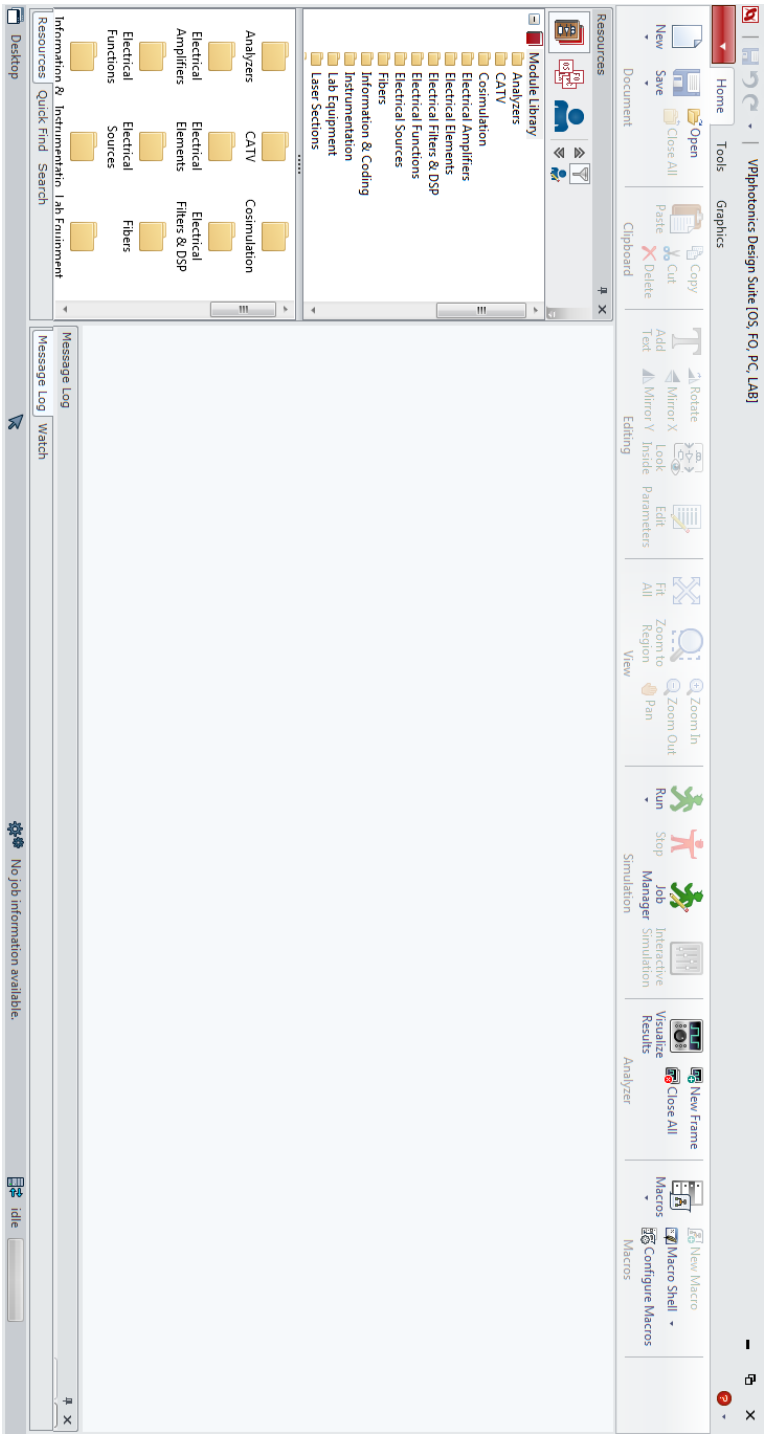

Figure(A.1): VPI Photonics V.9.8 Graphics Screen

Parameters Used in Simulation

In this appendix the description of the components used in the simulation are illustrated as shown in table (A.1).

Table (A.1): of components used in simulation [A-1]

Parameter	Description
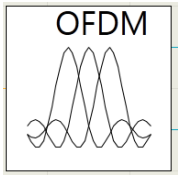	The Coder_OFDM module generates electrical signals corresponding to the real and imaginary parts of an orthogonal frequency-division multiplexed (OFDM) signal. The generated signal can be processed before and after iFFT by custom DSP with a predefined interface. Various bit and power loading schemes are supported.
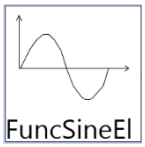	The FuncSineEl module generates an electrical sine waveform superimposed on a constant bias.
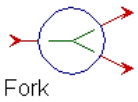	The Fork_2 module divides data into two identical paths. Often required for correct scheduling.
	The AWG M*N module simulates an M to N multiplexer based on an arrayed waveguide grating.
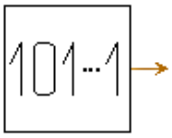	The PRBS module generates many types of pseudo random data sequences,
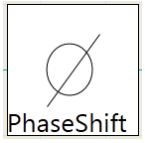	The PhaseShiftEl module applies a constant phase shift (advance) to a signal. It requires Periodic Boundary conditions, as a non-causal Hilbert transform is used.

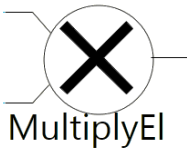	The Multiply_El module multiplies two electrical waveforms together. It can be used as a loss-less mixer, a modulator, or a switch.
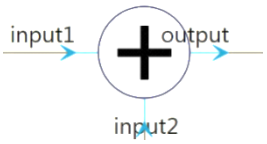	The AddSignalsEl module adds two electrical signals.
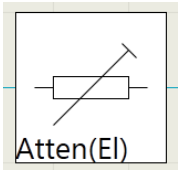	The AttenuatorEl module is an electrical attenuator. The attenuator is assumed to create no thermal noise. Thermal noise should be included as an equivalent noise elsewhere in the circuit.
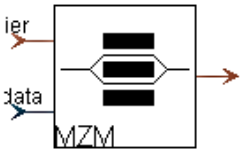	The ModulatorMZ module simulates a Mach-Zehnder modulator and can take into account a frequency chirp resulting from the modulator asymmetry.
	When used with sampled-mode signals, the module Nonlinear Dispersive Fiber (NLS) solves the nonlinear Schroedinger (NLS) equation describing the propagation of linearly-polarized optical waves in fibers using the split-step Fourier method. Depending on the signal representation, different effects are represented: if the signals are in a Single Frequency Band (SFB), or JoinSampledBands = ON, the model takes into account stimulated Raman scattering (SRS), four-wave mixing (FWM), self-phase modulation (SPM), cross-phase modulation (XPM), first order group-velocity dispersion (GVD), second order GVD and attenuation of the fiber.
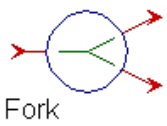	The Fork_2 module divides data into two identical paths. Often required for correct scheduling. See Advanced Wiring Tools and Scheduling.

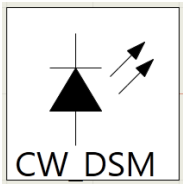	The LaserCW_DSM module is a 'Data Sheet Model' of a CW laser. Its parameters are those commonly found on a manufacturer's data sheet. By implication, they are also parameters that are easy to measure. The laser has a side mode, intensity noise, wavelength drift with temperature and linewidth.
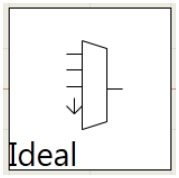	The WDM_MUX_N_1_Ideal module multiplexes N optical WDM channels with an adjustable insertion losses.
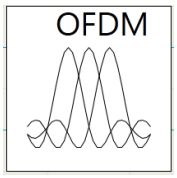	This module decodes an OFDM signal (such as that generated by the Coder_OFDM module). It performs demodulation, cyclic prefix removal and pre- and post- FFT DSP processing. The returned stream of samples is padded with zeros to compensate for any differences between the effective and transmitted data rates (see Coder_OFDM).
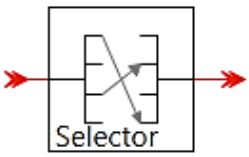	The BusSelector module allows selecting the path for data traveling between two buses. Alternatively, the module can be used to easily send a signal to the desired wire of an AWG or to excite the desired modes of a multi-mode fiber.
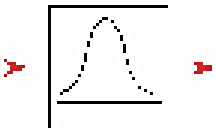	The FilterOpt module is a universal optical filter model for simulations of band pass, band stop and comb filters with the standard transfer functions: Butterworth, Bessel, Chebyshev, Elliptic, Gaussian, Rectangular, Trapezoid and Integrator. The model can also be used to simulate a measured filter whose transfer function is supplied in an input file.

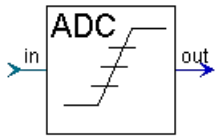	The ADC module emulates an array of realistic electrical analog-to-digital converters (ADC), whose transfer function can be defined via parameters or read from a file. Limited resolution, offset and gain errors, differential nonlinearities as well as timing jitter can be modeled. The module accepts multiple inputs. An n-th column of the output matrix corresponds to the n-th input.
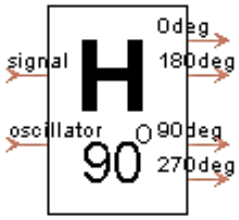	The Hybrid90deg module represents a generic 2x4 quadrature optical hybrid. It combines two input signals and generates four optical signals with a 90-degree phase difference. A typical application is coherent signal demodulation.
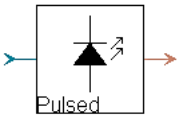	The LaserPulsed module models a DFB laser with adiabatic and dynamic chirp. It uses behavioral parameters to describe the laser's operation.
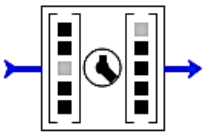	The synch DSP module recovers the time offset of the sampled signals represented by a matrix by performing correlations between them and the reference regenerated from the data carried by the specified logical channel(s). If the computed cross-correlations indicate that in the input matrix the polarization components are swapped - [Iy, Qy, Ix, Qx], then the module swaps the matrix column pairs so that in the output they are [Ix, Qx, Iy, Qy].

	The FilterEl module is a universal electric filter model for simulations of low pass, high pass, band pass, band stop and comb filters with the standard transfer functions: Butterworth, Bessel, Chebyshev, Elliptic, Gaussian, Trapezoid and Integrator.
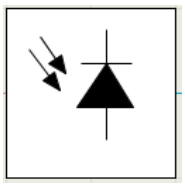	The Photodiode module is a model of PIN and APD photodiodes. These can be simulated on base of predefined responsivity, avalanche multiplication, dark current and noise. Alternatively, the voltage and temperature dependence is considered by using an equivalent RC circuit.
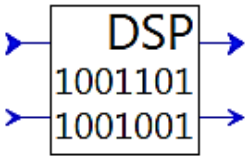	Python-based DSP library for single-carrier coherent transmission. The module processes signal samples represented as a float matrix. A row of the matrix contains samples of [I Q] signal components for 2D, and [Ix, Qx, Iy, Qy] signal components for 4D modulations. The module receives the input sampling rate and outputs the post-processing sampling rate as a float numbers. Following DSP algorithms are implemented: Carrier Frequency Recovery; CD Compensation; Delay; FIR Filter; 16QAM Phase Estimation.
Analyzers	
	The NumericalAnalyzer1D module works as an interface to the VPIphotonicsAnalyzer tool for one-dimensional numerical data.

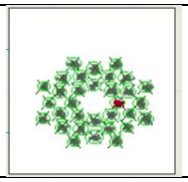	The OFDM_SC_Analyzer module estimates SER of an OFDM signal for selected sub-carriers.
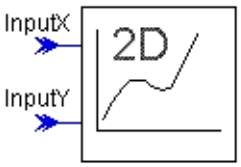	The NumericalAnalyzer2D module works as an interface to the VPIphotonicsAnalyzer tool for two-dimensional numerical data.
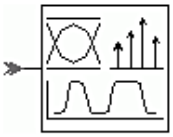	The SignalAnalyzer module works as an interface to the VPIphotonicsAnalyzer tool that is used to display and analyze electrical and optical signals.

Reference:

[A.1] VPI Optical Components Help.

Appendix B

Python DSP Commands at receiver side of OFDM-RoF-MMW system

PostFFTPhaseCorrection.py: This python code used as DSP to remove the drift effect of the mismatched oscillator at the receiver side and reduce the effect of PAPR in OFDM.

The procedure of work is as follows:

1. Set the drift parameter in physical parameters to 1 MHz and run the schematic to see

   the effect of the mismatched oscillator at the receiver side.

2. Remove the drift effect by activating "PostFFTDSP_Type" at the receiver side and set the value of the global parameter PilotTones to 1 (central subcarrier is used as a pilot tone). As a result the drift and PAPR will be compensated.

The python DSP code is:

```
import vpi_tc_ptcl
from numpy import *
# DSP procedure for Decoder_OFDM module
def PostFFTPhaseCorrection(S_symbolsRx,PT,UserParams):
#This procedure implements pilot tones based equalization of OFDM signal.
#Required Inputs:
#Pilot Tone index + pilot tone word
#The real and imaginary parts of PTWord are passed in UserParams as follows:
#index Re(w1) Re(w2) ... Re(wN) Im(w1) Im(w2) ... Im(wN)
[NFrames,NCarriers]=S_symbolsRx.shape;
   n=len(UserParams);
   if (n%2)==0:
vpi_tc_ptcl.message('An even number of user parameters is expected for equalization procedure. Equalization will not be performed.')
```

```
index=UserParams[0]

PTWord=UserParams[1:n/2]+1j*UserParams[n/2+1:n-1];

   xi=arange(NCarriers)

   if len(PT)>0:

 #Track mean amplitude and phase error of the pilot tones along the frames

        for k in range (0,NFrames):

        coeff=PTWord[mod(k,len(PTWord))]/S_symbolsRx[k,index-1];

        S_symbolsRx[k,:]=S_symbolsRx[k,:]*coeff;

        else:

      vpi_tc_ptcl.message('There are no pilot tones available for dynamic equalization. Equalization will not be performed.');

      return S_symbolsRx
```

وزارة التعليم العالي والبحث العلمي

جامعة بابـل / كلية الهندسة

قسم الهندسة الكهربائية

تصميم وتحليل الأداء لمساحة التردد الزمني المتعامد في شبكات الاتصالات

أطروحة

مقدمة الى كلية الهندسة في جامعة بابل

كجزء من متطلبات نيل درجة الدكتوراه في علوم الهندسة الكهربائية /الالكترونيك والاتصالات

من قبل

مصدق ماهر عبد الزهرة

اشراف

الأستاذ الدكتور ليث علي عبد الرحيم

1444 هجري

2023 ميلادي

الملخص

يدعى نظام الاتصالات اللاسلكية بجوهر شبكات إدارة الإنترنت للاتصالات التليفونية. لتنمية قدرة الإرسال عبر عرض النطاق الترددي الثابت، هناك العديد من التقنيات المحتملة التي تم تطويرها في السنوات الأخيرة.

هناك عدة طرق ممكنة لزيادة سعة الإرسال عبر عرض النطاق الترددي الثابت. يعد تعدد الإرسال بتقسيم التردد المتعامد (OFDM) من أكثر الطرق فعالية التي يمكن أن توفر تحقيق المزيد من المعلومات. من ناحية أخرى، فإن استخدام تقنية المرسلات المكثفة للإدخال المتعدد والأخراج المتعدد (massive MIMO) في أنظمة الإرسال اللاسلكي الحديثة توفر أعلى أداء وأفضل كفاءة طيفية بين جميع التقنيات الحديثة.

يُظهر أداء النظام (*Massive MIMO-OTFS*) مزايا كبيرة بين أنظمة (MIMO) العادية من خلال تحقيق كفاءة طيفية أفضل وكفاءة طاقة للأنظمة المصممة. باستخدام 256 نظام(OTFS) للناقل الفرعي، تحقق أفضل معدل إرسال تم تحقيقه لكل من سيناريوهات الوصلة الصاعدة والهابطة مع معدل (*BER*) مقبول يبلغ حوالي (10^{-5})

من ناحية أخرى، فإن إحدى تقنيات التضمين الحديثة الأكثر أهمية هي تقنية تعامد فضاء التردد والزمن (OTFS) والتي تعتبر جيل تضمين جديد يتغلب على تحديات الجيل الخامس (5G)

يعتبر نظام الانتشار المزدوج الذي تم تصميمه أفضل نظام بين جميع الأنظمة ذات الصلة. ثاني الأنظمة المصممة هو هيكل محاكاة بتصميم قوي لنظام النقل البصري (RoF-MMW) بين محطة الاتصالات الرئيسية ومحطة البث البعيدة بالاعتماد على تقنية (OFDM). الهيكل المصمم بقوة والخاص بأنظمة الارسال لمسافات بعيدة ضمن الجيل القادم لنقل بيانات تقنية (OFDM) عبر (RoF-MMW) تم تنفيذه بنجاح.

باستخدام معدل نقل بيانات افتراضي (50 كيكا بت/ثانية) للإشارة المرسلة وباستخدام نوع التضمين (128- QAM) لنظام (*OFDM-RoF-MMW*) لمسافة (50 كم) تم الحصول على اعلى معدل لنقل البيانات الكلية بمقدار (11.2 تيرا بت/ثانية) ضمن قيمة مقبولة ل (*BER*) وبالتالي تم الحصول على نظام نقل فائق السرعة.

باستخدام (*python DSP*) ومعوضات الخسائر المستخدمة في نظام المحاكاة المصمم في تعويض الخسائر الناجمة عن (*PAPR*) وتعويض الخسائر الناتجة من انحراف الإشارة في جزء استلام الإشارة كما تم استخدام عدة قيم للحوامل الثانوية لنظام OFDM بقيم 16 و32 لتحقيق نظام نقل فائق السرعة.

تم تنفيذ نظام محاكاة للجيل التالي ذات كفاءة عالية عن طريق استخدام أنظمة الإرسال البصري (*AO OFDM*) باستخدام تقنية (OFFT) بالاعتماد على جهاز المحاكاة (MMI) لتحقيق أعلى نظام نقل سعة. تم تحقيق إرسال ناجح لـ (*AO-OFDM* 16) باستخدام نظام فائق السعة مع مسافة تصل إلى (1000 كم). بينما وصلت المسافة إلى (700 كم) لـنظام (*AO-OFDM* 32).

قدرة الإدخال المثلى لنظام (*AO-OFDM* 16) لإعطاء أقل قيمة ل *BER* هي (*-8 dBm*) وقدرة الإدخال المثلى لنظام (*AO-OFDM* 32) هي (*-4 dBm*).

إجمالي معدل البيانات المحقق من نظام (*AO-OFDM* 16) هو 32 تيرا بت/ ثانية ومعدل البيانات الإجمالي المحقق من نظام (*AO-OFDM* 32) حوالي 64 تيرا بت/ ثانية والذي يعتبر أفضل نظام قدرة إرسال تم تحقيقه بين جميع الأعمال الحديثة.

يوفر الجمع بين تقنيات (massive MIMO) وأنظمة النقل (AO OFDM) جيلًا جديدًا لأنظمة الاتصالات فائقة السعة مع أفضل أداء بين الأنظمة المتطورة حاليا.